UNIVERSITY OF CALIFORNIA
RIVERSIDE

Zika Virus NS5-Mediated Innate Immune Suppression

A Dissertation submitted in partial satisfaction
of the requirements for the degree of

Doctor of Philosophy

in

Cell, Molecular & Developmental Biology

by

Stephanie Thurmond

September 2020

Dissertation Committee:
Dr. Rong Hai, Chairperson
Dr. Shou-wei Ding
Dr. Weifeng Gu

The Dissertation of Stephanie Thurmond is approved:

_____

_____

_____

Committee Chairperson

University of California, Riverside

Acknowledgements

The text of this dissertation, in part, is a reprint of the material as it appears in *Viruses*, 2018; *Nature Communications*, 2017; and *Nature Structural & Molecular Biology*, 2020. In accordance with department guidelines, I have obtained permission from the publishers to re-print this material. The coauthors Rong Hai and Jikui Song listed in these publications directed and supervised the research which forms the basis of this dissertation.

The citations are as follows:

1. Thurmond, S., Wang, B., Song, J. & Hai, R. Suppression of type I Interferon signaling by flavivirus NS5. *Viruses* **10,** 712–16 (2018).

2. Wang, B., Tan, X.F., Thurmond, S., Zhang, Z.M., Lin, A., Hai, R., Song, J. The structure of Zika virus NS5 reveals a conserved domain conformation. *Nat. Commun.* **8,** 1–6 (2017).

3. Wang, B.*, Thurmond, S.*, Zhou, K.*, Sánchez-Aparicio, M.T.*, Fang J., Lu, J., Gao, L., Ren, W., Cui, Y., Veit, E.C., Hong, H., Evans, M., O'Leary, S., García-Sastre, A., Zhou, Z.H., Hai, R., Song, J. Structural basis for STAT2 suppression by flavivirus NS5. *Nat. Struct. Mol. Biol.* **36,** 124–11 (2020).

Author Contributions

Chapter 1

S.T. wrote the manuscript.

Chapter 2

B.W., S.T. and R.H. cloned ZIKV NS5. B.W., A.L. and J.S. purified the protein sample. B.W. and X.-F.T. crystallized ZIKV NS5 and collected the X-ray data set. X.-F.T. and Z.-M.Z. determined the crystal structure. R.H. and S.T. performed enzymatic assay. R.H. and J.S. organized the study. S.T., R.H. and J.S. wrote the manuscript.

Chapter 3

B.W., S.T., K.Z., M.S., J.F., J.L., L.G., W.R., Y.C., H.H., S.O'L., R.H. and J.S. performed experiments and data analysis. E.V. and M.E. provided technical support. R.H. and J.S. conceived the project, A.G.S., Z. H.Z., R.H. and J.S. supervised the study. B.W., S.T., K.Z., Z.H.Z., R.H. and J.S. wrote the manuscript.

Chapter 4

S.T., M.S. and R.H. performed experiments and data analysis. R.H. and J.S. conceived the project, A.G.S., Z. H.Z., R.H. and J.S. supervised the study. B.W., S.T., K.Z., Z.H.Z., R.H. and J.S. wrote the manuscript.

ABSTRACT OF THE DISSERTATION

Zika Virus NS5-Mediated Innate Immune Suppression

by

Stephanie Thurmond

Doctor of Philosophy, Graduate Program in Cell, Molecular & Developmental Biology
University of California, Riverside, September 2020
Dr. Rong Hai, Chairperson

The *Flavivirus* genus consists of over 70 vector-borne, single-stranded RNA-containing viruses, including dengue virus (DENV) and Zika virus (ZIKV), which cause major epidemics among humans and pose a serious threat to global public health. No vaccines or antivirals exist to prevent or treat infections caused by DENV and ZIKV. To establish infection, it is vital for flaviviruses to overcome the antiviral state induced by type 1 interferon. ZIKV and DENV NS5 proteins can bind to human signal transducer and activator of transcription 2 (hSTAT2) protein, a key signaling intermediary for interferon (IFN) responses, which triggers the subsequent proteasome-dependent degradation of hSTAT2. NS5 does not have a host counterpart; thus, NS5 or the NS5-hSTAT2 interaction are logical antiviral targets. However, the underlying mechanism of the *Flavivirus* NS5-hSTAT2 interaction remains elusive. Here, we have elucidated the structure of the ZIKV NS5 protein and re-purposed a small molecule inhibitor against DENV for the inhibition of ZIKV RdRp activity. We have also delineated the

biochemical and structural basis of the DENV and ZIKV NS5-hSTAT2 interactions and used the knowledge gained from those studies to generate hSTAT2 and NS5 mutants deficient in interaction. We discovered that the mechanism of hSTAT2 interaction is conserved among the DENV2 and ZIKV NS5 proteins. In addition to hSTAT2 degradation, we found that ZIKV NS5 also competes with IRF9 for hSTAT2 binding, resulting in a two-pronged ISGF3 suppression mechanism. Finally, the hSTAT2-interaction deficient NS5 mutants were used as tools to interrogate the functional consequences of the hSTAT2-NS5 interaction during ZIKV infection. Disruption of the ZIKV NS5-hSTAT2 interaction resulted in loss of NS5-mediated hSTAT2 degradation and IFN suppression. Importantly, during infection, this interaction is critical for efficient ZIKV propagation. The work described here provides critical insights into DENV2 and ZIKV NS5-mediated hSTAT2 degradation and suppression of the IFN response and will facilitate the development of novel vaccines and inhibitors of *Flavivirus* infections.

Table of Contents

Appendices

List of Figures

Chapter 1

Chapter 2

Chapter 3

Chapter 4

Appendix A

Appendix B

List of Tables

Chapter 1: Introduction

Introduction

Flaviviruses are globally significant arthropod-borne viruses that cause disease in hundreds of millions of people each year. The *Flavivirus* genus is part of the *Flaviviridae* family and comprises over 70 species, including dengue and Zika viruses. Facilitated by the warming climate, urbanization and increasing travel to endemic areas, many of these pathogens have expanded into new territories, and flaviviral infections have increased worldwide[1]. Despite the enormous burden on public health posed by flaviviruses, there are currently no antiviral therapies available and limited vaccines.

Zika virus (ZIKV) was originally discovered in 1947 from a sentinel rhesus monkey in Uganda and has recently re-emerged in several major epidemics in Asia and the Americas[2]. ZIKV is classified phylogenetically into two distinct lineages, African and Asian with the Asian lineage ZIKV being responsible for the recent epidemics[2]. Infection with ZIKV is often asymptomatic but can cause fever, rash and arthralgia, and has additionally been causally linked to congential microcephaly and Guillain-Barré syndrome[3]. ZIKV pathogenesis has exhibited some features unique among the flaviviruses, such as persistence in immune-privileged sites and sexual transmission, presenting new challenges in the development of countermeasures[3]. Dengue virus (DENV) is responsible for the highest incidence of disease among the flaviviruses (~400 million annually[4]). There are four genetically distinct serotypes of DENV and infection with one serotype confers long-lasting immunity against only the infecting serotype, complicating the development of an effective pan-serotype vaccine. Primary DENV infections are frequently asymptomatic but can result in fever and rash. Secondary

infections, especially with a heterologous serotype, can cause the lethal dengue hemorrhagic fever and shock syndrome[5].

Flavivirus genome replication and life cycle

Flavivirus genomes are 10-11 kb single-stranded positive-sense RNA molecules flanked by structured 5' and 3' untranslated regions (UTRs). A virally encoded methyltransferase provides a $m^7GpppAm_{2'\text{-}O}$ cap structure to the 5' end of the genome similar to mammalian mRNA caps[6], but the flaviviral genome lacks a 3' polyadenylation tail. The genome is translated as a single polyprotein which is proteolytically processed by host and viral proteases to generate three structural proteins (capsid (C), pre-membrane (prM) and envelope (E)) and seven non-structural proteins (NS1, NS2A, NS2B, NS3, NS4A, NS4B and NS5). The non-structural proteins are responsible for replication of the viral genome, polyprotein processing and host immune response antagonism. Mature virions are ~50 um in diameter and consist of the RNA genome encapsulated by a lipid envelope and the three structural proteins C, prM and E[7].

Flaviviruses enter the cell via endocytosis and traffic to endosomes where the envelope protein undergoes a low pH-induced conformational change resulting in fusion of the endosomal membrane with the viral membrane. This fusion event allows the nucleocapsid to be released from the endosome, and the genome is rapidly translated at the surface of the endoplasmic reticulum (ER). The viral non-structural proteins facilitate the formation of replication complexes by hijacking host cytoplasmic membranes. These compartments coordinate the replication and translation of the viral genome and help to

shield viral components from host recognition. The NS proteins form a replication complex that generates negative-sense RNAs that function as templates for positive-sense genome RNA. Newly synthesized viral RNA is packaged, and the immature virion is transported through the host secretory pathway where it is further processed by host proteases to generate a mature virion which is released from the infected cell by exocytosis[7].

NS5 structure and enzymatic roles

NS5 is the most conserved flavivirus protein, with less than 45% amino acid difference reported among the vector-borne flaviviruses[8]. The N-terminus encodes the viral methyltransferase (MTase), while the C-terminus encodes the RNA-dependent RNA polymerase (RdRp)[9]. The MTase domain caps the RNA genome via a two-step reaction and also serves as the guanylyltransferase[6]. The MTase connects a guanosine to the first adenosine nucleotide of the viral RNA through a 5'-5' triphosphate bridge. The GpppA cap is then methylated at the guanine N-7 position, and the first adenosine nucleotide is methylated at the ribose 2'-O position[22]. Capping of the genome protects it from cellular exoribonucleases, ensures efficient translation and allows escape from host pathogen-associated molecular pattern (PAMP) sensors.

The RdRp transcribes RNA from the RNA genome *de novo*[10,11], and the replication process is thought to involve three different conformational states: pre-initiation, initiation and elongation[12,13]. In the pre-initiation state, NS5 is poised to receive initial NTPs, but the RNA exit tunnel is blocked. In the second state, initiation, NS5

binds to the 3′ and 5′ UTRs of the cyclized viral RNA template. Meanwhile, ATP and GTP molecules enter the active site within the NS5 RdRp domain to base-pair with the conserved C and U bases at the 3′ end of the RNA genome. Subsequently, a ribose-phosphate bond is generated between the adenine ribose and the guanine phosphate, forming the initial dinucleotide primer[14]. In the third state, elongation, the RNA exit tunnel of NS5 opens up, allowing for processive RNA polymerization. As observed in other flaviviruses, it is probable that additional viral factors are involved in facilitating ZIKV RNA replication. For example, ZIKV NS3, the viral helicase, is essential for unwinding the double-stranded RNA intermediate formed during genome synthesis[15-19]. Additionally, the NS4B protein is involved in altering the host ER membrane to facilitate anchoring of the viral replication complex[20].

To date, structures of full-length NS5 from Japanese encephalitis virus (JEV)[21], DENV3[22] and ZIKV[9,23,24] have been reported. The ZIKV and JEV NS5 conformations exhibit a high degree of similarity, suggesting structural conservation among the flaviviruses[9]. In contrast, the domain orientations of ZIKV and DENV NS5s differ significantly, although the residues at the domain interface are highly conserved among ZIKV, DENV and JEV[9]. These observations support an earlier observation that the flavivirus NS5 exhibits a high degree of flexibility in solution and can adopt a compact or extended conformation[25], which may have an impact on the diverse functions of NS5. Indeed, mutagenesis of the conserved interface residues of the DENV3 NS5 caused enhanced RdRp activity, but inhibited viral infectivity[22]. Furthermore, recent structural evidence suggests that the two subdomains cooperate in the execution of the sequential

replication and capping functions, although the mechanism remains unknown[21,26]. Taken together, these reports suggest that the flexibility and distinct conformations of the flavivirus NS5 may be linked to the various steps involved in RNA capping and replication. More experiments are needed to clarify the potential role of the conformational changes in regulating NS5 activities.

NS5 is essential for viral replication but lacks a human counterpart, making NS5 an ideal drug target for potential therapeutics. In fact, the concept of NS5 as a drug target has been validated by the success of commercially available drugs targeting the RdRp of hepatitis C, which belongs to the same viral family as ZIKV[27]. Multiple strategies have been devised to develop inhibitors targeting ZIKV NS5 and its flavivirus homologues. To date, several drugs have been synthesized and evaluated as potential therapeutics, and re-purposing of some patented drugs has been attempted with some success[28-38].

Flavivirus NS5 post-translational modifications

The limited size of *Flavivirus* genomes necessitates the evolution of viral proteins to develop multiple functions. One strategy for modulation of protein activity is via post-translational modifications (PTMs), which can impact the function, subcellular localization, protein-protein interaction or stability of the modified protein[39]. Several PTMs of flavivirus NS5s have been documented with potential regulatory roles. Serine/threonine phosphorylation appears to be conserved throughout the *Flaviviridae* family[40,41], but the function of this modification and the identity of the host kinases involved are largely unknown. The DENV NS5 protein is phosphorylated by both

mammalian and mosquito protein kinase G at a conserved Thr449 in the RdRp domain[42,43]. The differential phosphorylation of DENV NS5 was shown to affect its interaction with the viral helicase, NS3, which is required for genome replication[44]. The West Nile virus (WNV) NS5 MTase domain is also phosphorylated by, and interacts with, protein kinase G, and abolishing this interaction inhibits viral replication[45]. Glutathionylation of the DENV and ZIKV NS5s has also been reported but has no known function[46].

Bioinformatic analysis reveals putative SUMO-interacting motifs (SIMs) in ~92% of flavivirus NS5s[47]. This motif is highly conserved among African and Asian lineage ZIKV strains and the SUMO inhibitor 2-D08 is protective against flaviviruses *in vitro*[47]. SUMOylation of the DENV NS5 was shown to be important for DENV replication[48] and SIM-mutated ZIKV NS5 cannot efficiently suppress type I IFN signaling[47]. Finally, ubiquitination of viral proteins is increasingly being recognized as important for efficient viral replication[49-55]. Among the flaviviruses, ubiquitination of NS5 has been demonstrated for Langat virus (LGTV)[39] and yellow fever virus (YFV)[55]. Ubiquitination of YFV NS5 is dependent on type I IFN production and enables NS5 interaction with human STAT2[55]. Several other flavivirus NS5s, including tick-borne encephalitis virus (TBEV), DENV and ZIKV NS5, are known to interact with host cell ubiquitination pathways to facilitate evasion of the host immune response[8,56,57]. Ubiquitination of these NS5 proteins may be involved in the evasion strategies but direct experimental evidence for this modification is currently lacking[58].

Flavivirus NS5 nuclear localization

Replication of the flavivirus genome occurs exclusively in the cytoplasm[59,60]. However, a significant portion of the NS5 protein is observed within the nucleus during YFV[61], JEV[62], ZIKV[8], WNV[63] and DENV[64] infections. Inhibiting the nuclear localization of DENV and WNV NS5 significantly decreases viral titers[63,65]. Inversely, inhibiting the nuclear export of DENV NS5 decreased the induction of IL-8, which plays a role in induction of inflammation[66], suggesting nuclear localization of NS5 may be important for immune modulation[67]. This observation is further supported by a study showing that interaction of NS5 with host spliceosome components leads to changes in mRNA isoform abundance of antiviral factors[68]. ZIKV and JEV NS5 were similarly reported to interact with host cell spliceosome machinery[69]. There are differences, however, in the level of NS5 nuclear localization among the different DENV serotypes. NS5 from serotypes 2 and 3 accumulate in the nucleus, while DENV1 and 4 NS5 reside in the cytoplasm[70]. For serotype 4, cytoplasmic localization is likely due to the lack of a functional nuclear localization signal (NLS)[70]. Levels of IL-8 did not change with the different serotypes, and the function of the differential localization is still unknown[70].

Several recent reports have demonstrated that ZIKV NS5 nuclear localization is important for disease pathogenesis and modulation of the host immune response[71-75]. ZIKV NS5, like DENV, contains a bipartite nuclear localization signal (NLS) in the interdomain region[71-74], although one group reported an additional NLS in the N-terminal region of NS5[74]. NS5 nuclear translocation is mediated by interaction with importin-α, and NS5 sequesters and co-localizes with importin-α within the nucleus[72]. Interestingly,

in contrast with DENV NS5, ZIKV NS5 proteins form spherical, punctate nuclear bodies that exclude DNA during infection[72,75]. Importin-α is also localized to these discrete nuclear structures, which may function to inhibit the nuclear translocation of antiviral host factors[72].

ZIKV encoding NS5 NLS mutants are attenuated in viral RNA replication and virus production[73]. It was suggested that the observed attenuation was due to increased cytoplasmic degradation of NS5 when nuclear accumulation is inhibited[73]. The mechanism of NS5 degradation is unknown, as inhibitors of several protein degradation pathways did not restore NS5 stability[73]. ZIKV NS5 is a potent type I IFN suppressor (discussed in more detail below) and evidence has recently emerged linking NS5 nuclear localization and type I IFN suppression[71,74,75]. This research will be described below following a discussion of NS5-mediated type I IFN suppression.

Host innate immune response to flavivirus infection

The type I IFN signaling pathway is one of the first lines of defense against flavivirus infection of mammals. Type I IFNs are produced by mammalian cells in response to viral infection and play a pivotal role in counteracting viral pathogenesis[76]. Flavivirus-infected individuals have elevated levels of immune-related gene transcripts and serum IFN[77-81]. In mouse and cell models, similar elevations have been reported[82-84] and production has been shown to play a protective role[3,85,86]. Several proteins that function within this signaling pathway have been identified with direct and specific antiviral roles during flavivirus infection[82,83,87,88]. IFN-I has even been tested as a

treatment for clinical flavivirus disease, but has not been successful[89,90]. This may be explained by the universal ability of flaviviruses to inhibit the Janus kinase-signal transducer and activator of transcription (JAK-STAT) pathway. As discussed below, the NS proteins are the primary actors in this suppression, and understanding the molecular mechanisms mediating this suppression would contribute to the development of effective antiviral therapies.

The innate immune response is executed in two phases, initiation and amplification (Fig. 1). The initiation phase of innate immunity is triggered by sensing the pathogen-associated molecular patterns (PAMPs) via the cytosolic and endosomal pattern recognition receptors (PRRs) retinoic acid-inducible gene-1 (RIG-I), melanoma differentiation-associated protein 5 (MDA5), Toll-like receptor (TLR) 7/8 or TLR3[91-93]. PAMP sensing PRRs activate various kinases including inhibitor of nuclear factor kappa-B (NF-κB) kinase subunit epsilon (IKKε), tumor necrosis factor (TNF) receptor-associated factor (TRAF) family member-associated NF-κB (TANK)-binding kinase-1 (TBK-1), and TRAF3, which ultimately result in the phosphorylation of NF-κB and interferon regulatory factor 3 (IRF3)[92,94]. Activated NF-κB and IRF3 translocate to the nucleus to stimulate the production of type I IFNs (Fig. 1).

The type I IFNs consist primarily of two secreted cytokines, IFN-α and IFN-ß. In the amplification phase of the innate immune response, IFN-α/ß secreted from infected cells bind to their cognate receptor IFNAR on infected and neighboring cells (Fig. 1). IFNAR consists of two subunits (IFNAR1 and IFNAR2) whose intracellular domains are constitutively associated with the Janus kinases JAK1 and Tyk2. IFN binding to IFNAR

activates JAK1 and Tyk2 to phosphorylate the latent cytoplasmic signal transducers of activation 1 and 2 (STAT1 and STAT2). Tyrosine phosphorylated STAT1 and STAT2 dimerize and then associate with a third protein, interferon regulatory factor 9 (IRF9). This trimeric complex, known as interferon-stimulated gene factor 3 (ISGF3), translocates into the nucleus where it binds to interferon stimulated response elements (ISRE) to drive transcription of over 300 interferon stimulated genes (ISGs) that directly or indirectly counter viral infection (Fig. 1). IRF9 binds to the ISRE, STAT2 contributes a potent transactivation domain and STAT1 stabilizes the complex through additional DNA interactions[95,96].

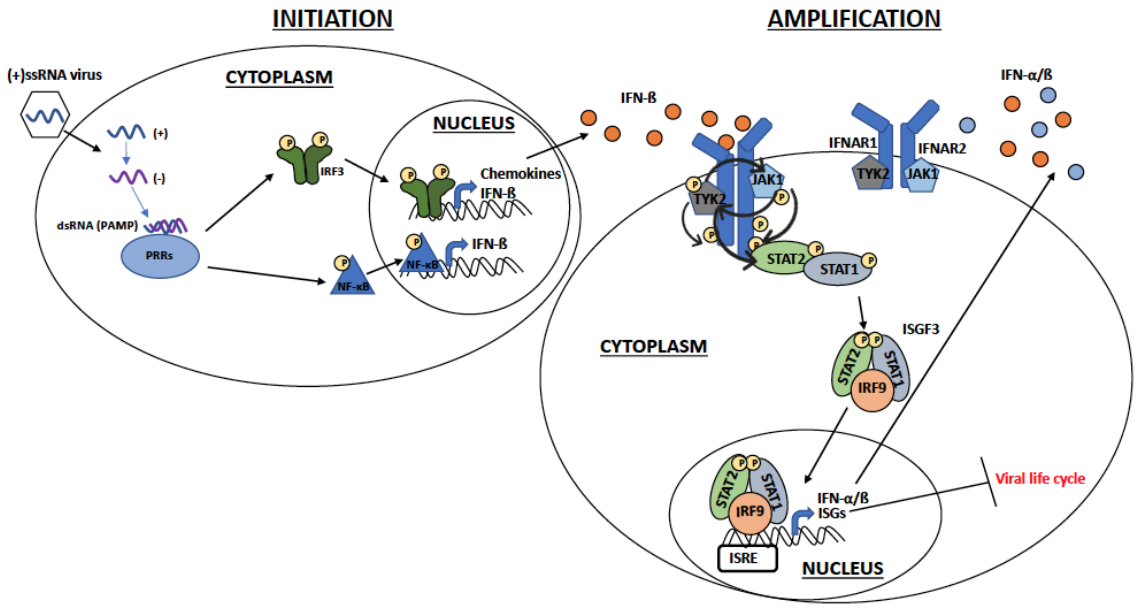

Figure 1. Biphasic induction of type I IFN response. The antiviral type I IFN response is executed in two phases: initiation and amplification. In the initiation phase, the viral genome is detected by cellular PRRs which leads to the phosphorylation of IRF3 and NF-κB. Activated IRF3 and NF-κB translocate into the nucleus where they stimulation the expression of IFN-ß. IFN-ß binds to the IFNAR receptor in an autocrine and paracrine manner. IFNAR stimulation triggers the phosphorylation of IFNAR, Tyk2, Jak1, STAT1 and STAT2. Upon phosphorylation, STAT1 and STAT2 interact with IRF9 to form the ISGF3 transcription factor. ISGF3 translocates to the nucleus where it upregulates IFN-I and ISGs which serve to inhibit the viral life cycle.

The components of ISGF3 are constitutively expressed at a low level and reside in the cytoplasm in their latent forms (Fig. 1). Upon IFN stimulation and tyrosine phosphorylation of STATs 1 and 2, ISGF3 rapidly assembles and directs a robust, transient antiviral response that includes the upregulation of ISGF3 components themselves. This response, however, additionally increases the expression of pro-apoptotic and anti-proliferative genes that can be damaging to the host cell, so downregulation of these genes occurs quickly after IFN stimulation. This response is

mediated by several negative feedback mechanisms, such as the suppressor of cytokine signaling (SOCS) proteins, which are also induced by type I IFN[97]. In contrast, a subset of the antiviral ISGs upregulated by the initial IFN stimulation, including STAT1, STAT2 and IRF9, are sustained for several days, resulting in increased levels of the unphosphorylated forms of these proteins[98]. These proteins interact to form the trimeric unphosphorylated ISGF3 (U-ISGF3), which is responsible for the sustained ISG transcription, allowing for extended resistance to viral infection[99].

Recently, evidence has emerged for the existence of STAT1-independent complexes that can drive IFN-I-stimulated ISG expression[100]. For example, STAT2 can interact with IRF9 to form an "ISGF3-like" complex that activates ISRE-promoted genes in response to type I IFN[101]. This complex can direct a similar but prolonged ISGF3-like transcriptome in the absence of STAT1. However, some STAT2/IRF9-specific ISGF3-independent ISGs have been identified, including *CCL8* and *CX3CL1*. The promoter regions of these genes do not contain the classical ISRE sequences, suggesting that a DNA sequence distinct from ISRE may be involved in STAT2/IRF9-specific gene regulation.

Although type I IFNs are produced by nearly all cells in the body and are essential for restricting viral replication, two additional IFN signaling pathways exist and have been shown to respond to viral infection. The type III IFNs (IFN-λ1-4) are the primary antiviral IFNs generated by epithelial cells and have similar functions and signaling pathways as IFN-I, but the cellular receptor is not ubiquitously expressed[102]. An antiviral effect for IFN-λ has been demonstrated for West Nile and Zika viruses. Mice deficient in

the IFN-λ receptor exhibited increased blood–brain barrier (BBB) permeability after WNV infection[103], suggesting type III IFN signaling is involved in WNV neurotropism. Primary human trophoblast cells from human placenta were found to release type III IFN constitutively, conferring resistance to ZIKV infection[104]. The ability of ZIKV to be vertically transmitted from mother to fetus suggests the existence of a viral factor that may be able to overcome the type III IFN response in placental cells. The NS5 protein from ZIKV is a likely candidate as it was shown to inhibit the type III response in HEK293T cells[105].

While ZIKV NS5 was shown to suppress both the type I and III IFN responses, it was also able to activate type II IFN signaling[105]. The type II IFNs (IFN-γ) are generated mainly by immune cells and have some antiviral functions. ZIKV infection, however, is enhanced by type II IFN signaling, which generates proinflammatory cytokines that can facilitate viral spread and exacerbate Zika disease[106]. The concurrent NS5-mediated suppression of type I and III pathways and activation of the type II pathway was suggested to occur through increased homodimerization of STAT1, which upregulates gene expression at γ-activated sites (GAS). Because ZIKV NS5 induces the degradation of STAT2 (discussed below), which is required for the formation of transcription complexes involved in type I and III IFN signaling, the intracellular balance of STAT-containing complexes shifts to STAT1-STAT1 dimers, resulting in increased IFN-γ-induced gene expression. To date, ZIKV NS5 is the only viral protein known to concurrently suppress type I and III IFN pathways while activating type II[105].

Flavivirus antagonism of host type I IFN response

Just as hosts have evolved multiple mechanisms for inhibiting viral infection, viral proteins have gained the ability to antagonize the host IFN response over time. One mechanism by which the type I IFN response is passively avoided by flaviviruses is evasion of the host PRRs, described above. Flaviviruses encode their own methyltransferase that caps the RNA genome to mimic the RNAs present in the host cell. The cap structure hides the viral genome from members of the interferon-induced tetratricopeptide repeats (IFIT) protein family, which binds to and sequesters viral RNA, and prevents recognition by the RIG-I[107]. Flaviviruses also shield their genome from host sensing by enclosing their replication complex (RC) in membranes on the ER surface, a mechanism that has been observed in the early stages of DENV, WNV and tick-borne encephalitis virus (TBEV) infections[20,59]. However, late in the infection, newly synthesized viral RNA is abundant, and the RC loses some integrity, which may lead to the release of RNA intermediates that could activate RIG-I or MDA5 signaling[108].

Flaviviruses have also been demonstrated to actively abrogate the activity of protein functioning within the type I IFN signaling pathway. One common mechanism is interference with post-translational modifications of these proteins. For example, the DENV, WNV and YFV NS4B inhibit STAT1 phosphorylation[109,110]. WNV NS4B is additionally implicated in preventing the phosphorylation of JAK1 and Tyk2[111,112], and NS2A, NS2B, NS3, NS4A and NS4B from Kunjin virus (KUN), a close relative to WNV, are all implicated in JAK-STAT inhibition[113]. This mechanism is not always mediated by NS proteins, however. Flaviviruses produce small RNAs called subgenomic

flavivirus RNAs (sfRNAs) that are generated by the incomplete degradation of the viral genome by the host endonuclease XrnI[114]. In DENV, this sfRNA binds to TRIM25, which normally interacts with RIG-I to promote its ubiquitination and interaction with mitochondrial antiviral signaling protein (MAVS)[115]. The DENV sfRNA prevents the deubiquitination of TRIM25, an essential upstream activator for RIG-I activation[116].

Another mechanism of active interference with the type I IFN system is competitive binding. DENV and WNV NS3 proteins compete with RIG-I for 14-3-3ε binding, a chaperone responsible for trafficking RNA-bound RIG-I to the mitochondrial membrane[117]. Additionally, the DENV NS4A protein sequesters MAVS, preventing RIG-I-MAVS interaction, IRF3 activation, and IFN-I production[118].

Finally, many flavivirus NS proteins have evolved mechanisms to degrade host immune proteins, or to induce the degradation of these proteins by hijacking the host proteasome system. For example, the DENV NS2B/NS3 viral protease suppresses the DNA sensing pathway and RIG-I sensing by cleaving STING, resulting in reduced type I IFN production[119]. Additionally, NS2B by itself promotes the autophagy-lysosome-dependent degradation of cGAS[119].

IFN suppressor function of flavivirus NS5

While multiple proteins capable of IFN antagonism have been described for the major disease-causing flaviviruses, NS5 is the most potent and direct antagonist[58]. This is significant because NS5-mediated IFN antagonism is required for counteraction of IFN in cell culture[120] and for virulence in mouse models[121]. Remarkably, even though this

protein utilizes similar MTase and RdRp mechanisms no matter the flavivirus species to replicate and cap their RNA genomes, the mechanism of NS5-mediated IFN suppression diverges within the genus. The evolution and divergence of this role for NS5 may have been facilitated by the strategy of expression of flaviviral proteins from a single open reading frame. This results in excess expression of NS5, while only small amounts are needed for RdRp and MTase functions. Due to the lack of high-resolution structures for the complexes of various NS5s and their interacting host partners, how NS5 is able to retain its roles as MTase and RdRp while evolving divergent IFN suppression mechanisms remains elusive.

NS5 frequently employs multiple strategies to suppress the JAK-STAT signaling pathway not only among different species of *Flavivirus,* but also within the same species. For example, the ZIKV NS5 protein has been shown to both inhibit the phosphorylation of STAT1 and induce the degradation of STAT2[8,71,105,122]. The JEV, DENV and WNV NS5 proteins have similarly been shown to antagonize this pathway at multiple steps. STAT2 is a common target for NS5-mediated IFN suppression, and at least two flavivirus NS5 proteins have been demonstrated to target this protein for degradation (Fig. 2). The mechanisms by which the DENV and ZIKV NS5s degrade STAT2 diverge, however, and the molecular details of these mechanisms are still being elucidated (Fig. 2).

DENV NS5 binds to human STAT2 and inhibits its phosphorylation, resulting in reduced ISG transcription. The mechanism of this inhibition has not been elucidated, but the IFN suppression activity was mapped to the RdRp domain[123]. Expression of NS5 also

reduces IFN-α-, but not IFN-γ-, mediated STAT1 phosphorylation, although NS5 does not directly interact with STAT1[123].

Ashour *et al.* demonstrated STAT2 degradation as an additional mechanism of DENV NS5-mediated IFN antagonism[124,125] (Fig. 2). However, while this study also found that binding of NS5 to STAT2 is sufficient to prevent IFN signaling, STAT2 degradation is detected only when the N-terminus of NS5 is proteolytically processed, as it would be in the context of viral infection. NS5 is separated from NS4B during polyprotein processing by the viral NS2B/NS3 protease, and co-expression of NS5 with NS2B/NS3 induces STAT2 degradation. Replacement of the viral cleavage site at the N-terminus of NS5 with a host protease cleavage site, however, also allows for the efficient degradation of STAT2, suggesting the cleavage does not need to be mediated by the viral protease. Additionally, the identity of the N-terminal residue of NS5 does not appear to be important to this processing event, as replacing the glycine residue at position 1 of NS5 with methionine resulted in efficient STAT2 degradation[125]. This study also demonstrated that NS5-mediated STAT2 degradation is dependent on the ubiquitin-proteasome pathway, implying the involvement of a host E3 ligase. In a follow-up study, the García-Sastre group identified this protein as UBR box N-recognin-4 (UBR4), which is part of the N-recognin family[57] (Fig. 2). Members of this family target proteins that undergo conformational changes to expose a destabilizing N-terminal residue for degradation, a mechanism for the N-end rule pathway[126]. UBR4 binds to the first five amino acids of NS5; deleting the first ten amino acids of NS5 eliminates its ability to induce STAT2 degradation[57,125]. The binding domain for STAT2, however, was mapped

to residues 202–306[125], suggesting that the DENV NS5 central and N terminal regions together serve as a bridge between STAT2 and UBR4. In this scenario, it is possible that NS5 and STAT2 are both targeted by UBR4 and similarly degraded[58]. Experimental evidence, however, is still needed for verification of the role of the N-end rule pathway in DENV NS5-mediated STAT2 degradation.

Similar to DENV NS5, ZIKV NS5 binds to human, but not mouse, STAT2, triggering its degradation (Fig. 2). However, unlike what was observed for DENV NS5, ZIKV NS5 does not need to undergo proteolytic processing for depletion of STAT2[8]. Additionally, it was demonstrated that the first ten amino acids of NS5 are dispensable for depletion of STAT2, suggesting that the N-end rule does not apply to ZIKV NS5[122]. STAT2 is ubiquitinated prior to degradation, and proteasome inhibitors rescue STAT2 protein levels in the presence of NS5[105]. However, unlike that occurs for DENV NS5, UBR4 is not involved in mediating STAT2 degradation[8]. This suggests that ZIKV NS5-mediated STAT2 degradation utilizes the host ubiquitin proteasome system and the participating host E3 ligase has yet to be identified (Fig. 2).

Chaudhary *et al*. demonstrated an additional consequence of ZIVK NS5-mediated STAT2 degradation, aside from decreased ISG induction. In an uninfected cell, unphosphorylated STAT2 can bind to both unphosphorylated and phosphorylated STAT1 to prevent translocation of STAT1 and activation of the type II IFN response[127]. In ZIKV-infected and NS5-transfected cells, however, an increase in STAT1 homodimerization is observed, concurrent with an increase in type II IFN and a decrease in type I IFN signaling. In this model, the degradation of STAT2 frees up STAT1

proteins to homodimerize and translocate to the nucleus to selectively activate ISGs controlled by gamma activated sites (GAS)[105].

As mentioned previously, ZIKV NS5 nuclear accumulation has recently been implicated in type I IFN suppression mechanisms[71,74,75]. NS5 NLS mutants are attenuated in their ability to suppress IRF3-mediated IFN-I suppression[74], but retain the ability to downregulate ISRE responses[71,74]. Specifically, NS5-mediated STAT2 degradation is unaffected by NLS mutations[71,74]. This suggests that the NS5-STAT2 association, which precedes STAT2 degradation, occurs in the cytoplasm. Whether STAT2 is activated by phosphorylation prior to NS5 interaction, however, is not known. Interestingly, one group found that in human brain microvascular endothelial cells (hBMECs), ZIKV NS5 displaces promyelocytic leukemia protein (PML) from nuclear bodies consisting of STAT2 and PML[75]. These nuclear bodies are constitutively present and are important for innate immunity. In the presence of NS5, NS5/STAT2 nuclear bodies are formed instead of PML/STAT2, resulting in PML degradation and reduced ISG transcription[75]. This data suggests the ZIKV NS5 may be able to interact with both activated (nuclear) and latent (cytoplasmic) forms of STAT2 to suppress type I IFN production.

The YFV NS5 also targets STAT2 as part of its IFN-I suppression mechanism (Fig. 2). YFV NS5 binds to human, but not mouse, STAT2 (Fig. 2). However, in contrast to DENV and ZIKV NS5, this interaction is dependent on host cell stimulation with type I or III IFNs[55] (Fig. 2). This stimulation induces several intracellular events required for NS5 association with STAT2. First, as in an uninfected cell, stimulation with IFN induces the phosphorylation and heterodimerization of STAT1 and STAT2. STAT2 does not need

to be phosphorylated for NS5 interaction. Instead, the association of STAT1 and STAT2 induces a conformational change within STAT2 that allows for NS5 binding[128]. Second, IFN stimulation promotes the ubiquitination of YFV NS5 by TRIM23 (Fig. 2); non-ubiquitinated NS5 cannot interact with STAT2[55]. Unlike the DENV and ZIKV NS5s, YFV NS5 does not induce the degradation of STAT2. YFV NS5 blocks IFN production either by interfering with ISGF3 formation or translocation into the nucleus (Fig. 2); the exact mechanism is unknown. A domain mapping study identified the first ten amino acids of the YFV NS5 as essential for both STAT2 interaction and IFN-I inhibition, consistent with the requirement of TRIM23 ubiquitinating K6 of NS5[128].

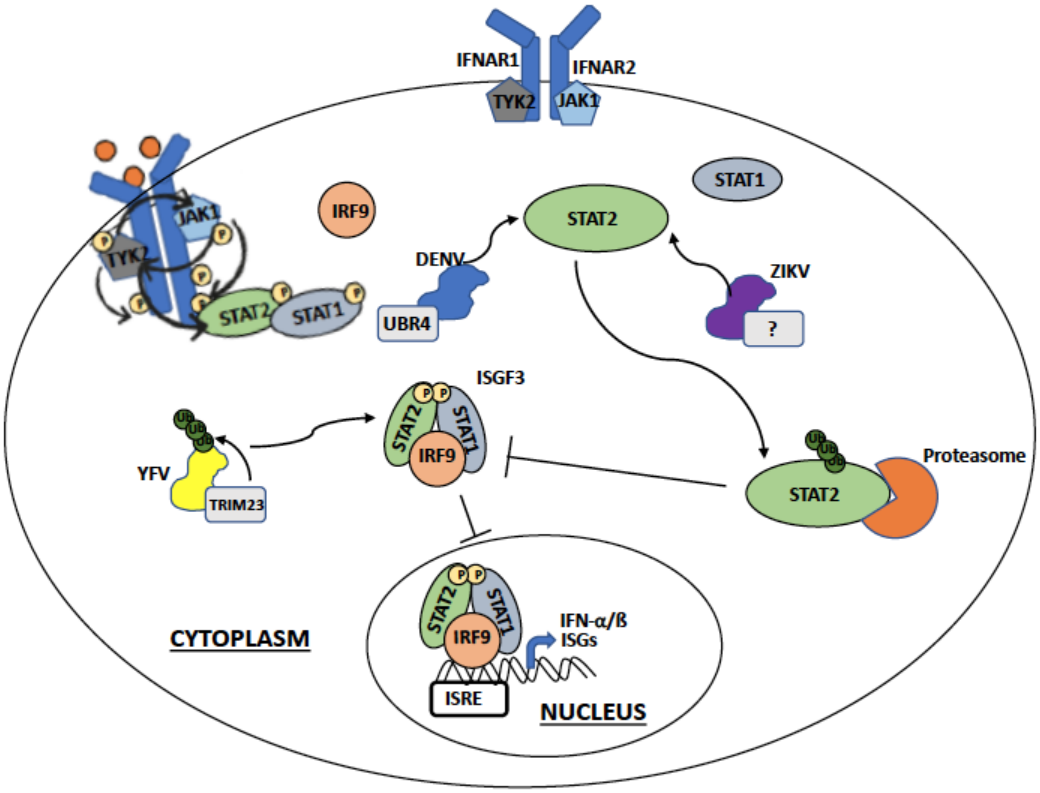

Figure 2. *Flavivirus* NS5-mediated suppression of human STAT2. Varied mechanisms of NS5-mediated antagonism of human STAT2. The NS5 proteins of DENV, ZIKV and YFV all bind to STAT2. Binding of STAT2 by DENV or ZIKV NS5 results in STAT2 degradation by the host proteasome. YFV NS5 requires IFN-I stimulation to interact with hSTAT2. Each of these three NS5 proteins utilizes a different E3 ubiquitin ligase in order to antagonize IFN-I signaling (TRIM23 (YFV), UBR4 (DENV) or an unidentified ligase in the case of ZIKV).

The ZIKV and DENV NS5s share ~60% amino acid identity and employ similar mechanisms of type I IFN suppression. Both proteins interact with hSTAT2 in order to induce its degradation. It is possible that the DENV and ZIKV NS5 proteins evolved similar mechanisms of hSTAT2 interaction. To this end, the focus of this dissertation is the elucidation of the hSTAT2 complex structures and binding mechanisms of these two

proteins, and the functional consequences of disrupting the NS5-hSTAT2 association. Chapter 2 describes the overall structure of the ZIKV NS5 protein, which lead to the re-purposing of a small molecule inhibitor of DENV3 NS5 for the inhibition of ZIKV NS5 RdRp activity. Chapter 3 reports on the ZIKV and DENV NS5-hSTAT2 structures and culminates in the creation of NS5 and hSTAT2 mutants that are deficient in NS5-hSTAT2 interaction. Finally, Chapter 4 uses these mutants as tools to interrogate the function of this interaction in the cell and during infection. The discoveries outlined in this thesis may contribute to the development of a pan-species *Flavivirus* NS5 drug and a live-attenuated ZIKV vaccine candidate.

References

1. Daep, C. A. *et al*. Flaviviruses, an expanding threat in public health: focus on dengue, West Nile, and Japanese encephalitis virus. *J. Neurovirol.* **20,** 539–560 (2014).

2. Wang, A. *et al*. Zika virus genome biology and molecular pathogenesis. *Emerg. Microbes Infect.* **6**, 1-6 (2017).

3. Krauer, F. *et al.* Zika virus infection as a cause of congenital crain abnormalities and Guillain-Barré syndrome: systematic review. *PLoS Med.* **14,** e1002203 (2017).

4. Gaunt, M. W. *et al.* Phylogenetic relationships of flaviviruses correlate with their epidemiology, disease association and biogeography. *J. Gen. Virol.* **82,** 1867–1876 (2001).

5. Screaton, G. *et al*. New insights into the immunopathology and control of dengue virus infection. *Nat. Rev. Immunol.* **15,** 745–759 (2015).

6. Issur, M. *et al.* The flavivirus NS5 protein is a true RNA guanylyltransferase that catalyzes a two-step reaction to form the RNA cap structure. *RNA* **15,** 2340–2350 (2009).

7. Chambers, T. J. *et al*. Flavivirus genome organization, expression, and replication. *Annu. Rev. Microbiol.* **44,** 649–688 (1990).

8. Grant, A. *et al.* Zika virus targets human STAT2 to inhibit type I interferon signaling. *Cell Host Microbe* **19,** 882–890 (2016).

9. Wang, B. *et al.* The structure of Zika virus NS5 reveals a conserved domain conformation. *Nat. Commun.* **8,** 14763 (2017).

10. Ackermann, M. & Padmanabhan, R. De novo synthesis of RNA by the dengue virus RNA-dependent RNA polymerase exhibits temperature dependence at the initiation but not elongation phase. *J. Biol. Chem.* **276,** 39926–39937 (2001).

11. Kao, C. C. *et al*. De novo initiation of viral RNA-dependent RNA synthesis. *Virology* **287,** 251–260 (2001).

12. Malet, H. *et al.* The flavivirus polymerase as a target for drug discovery. *Antivir. Res.* **80,** 23–35 (2008).

13. Selisko, B. *et al.* Molecular basis for nucleotide conservation at the ends of the dengue virus genome. *PLoS Pathog.* **8,** e1002912 (2012).

14. Ranjith-Kumar, C. T. *et al*. Requirements for de novo initiation of RNA synthesis by recombinant flaviviral RNA-dependent RNA polymerases. *J. Virol.* **76,** 12526–12536 (2002).

15. Li, H. *et al.* The serine protease and RNA-stimulated nucleoside triphosphatase and RNA helicase functional domains of dengue virus type 2 NS3 converge within a region of 20 amino acids. *J. Virol.* **73,** 3108–3116 (1999).

16. Matusan, A. E. *et al*. Mutagenesis of the dengue virus type 2 NS3 protein within and outside helicase motifs: effects on enzyme activity and virus replication. *J. Virol.* **75,** 9633–9643 (2001).

17. Bartelma, G. & Padmanabhan, R. Expression, purification, and characterization of the RNA 5'-triphosphatase activity of dengue virus type 2 nonstructural protein 3. *Virology* **299,** 122–132 (2002).

18. Benarroch, D. *et al.* The RNA helicase, nucleotide 5‘-triphosphatase, and RNA 5’-triphosphatase activities of dengue virus protein NS3 are Mg2+-dependent and require a functional Walker B motif in the helicase catalytic core. *Virology* **328,** 208–218 (2004).

19. Yon, C. *et al.* Modulation of the nucleoside triphosphatase/RNA helicase and 5'-RNA triphosphatase activities of Dengue virus type 2 nonstructural protein 3 (NS3) by interaction with NS5, the RNA-dependent RNA polymerase. *J. Biol. Chem.* **280,** 27412–27419 (2005).

20. Welsch, S. *et al.* Composition and three-dimensional architecture of the dengue virus replication and assembly sites. *Cell Host Microbe* **5,** 365–375 (2009).

21. Lu, G. & Gong, P. Crystal structure of the full-length Japanese encephalitis virus NS5 reveals a conserved methyltransferase-polymerase interface. *PLoS Pathog.* **9,** e1003549 (2013).

22. Zhao, Y. *et al.* A crystal structure of the dengue virus NS5 protein reveals a novel inter-domain interface essential for protein flexibility and virus replication. *PLoS Pathog.* **11,** e1004682 (2015).

23. Upadhyay, A. K. *et al.* Crystal structure of full-length Zika virus NS5 protein reveals a conformation similar to Japanese encephalitis virus NS5. *Acta Crystallogr. F Struct. Biol. Commun.* **73(Pt 3),** 116-122 (2017).

24. Zhao, B. *et al.* Structure and function of the Zika virus full-length NS5 protein. *Nat. Commun.* **8,** 1–9 (2017).

25. Bussetta, C. & Choi, K. H. Dengue virus nonstructural protein 5 adopts multiple conformations in solution. *Biochemistry* **51,** 5921–5931 (2012).

26. Potisopon, S. *et al.* The methyltransferase domain of dengue virus protein NS5 ensures efficient RNA synthesis initiation and elongation by the polymerase domain. *Nucleic Acids Res.* **42,** 11642–11656 (2014).

27. Tsai, C.-H. *et al.* Antiviral therapy targeting viral polymerase. *Curr. Pharm. Des.* **12,** 1339–1355 (2006).

28. Bullard-Feibelman, K. M. *et al.* The FDA-approved drug sofosbuvir inhibits Zika virus infection. *Antivir. Res.* **137,** 134–140 (2017).

29. Cai, L. *et al.* Viral polymerase inhibitors T-705 and T-1105 are potential inhibitors of Zika virus replication. *Arch. Virol.* **162,** 2847–2853 (2017).

30. Chen, L. *et al.* Antiviral activity of peptide inhibitors derived from the protein E stem against Japanese encephalitis and Zika viruses. *Antivir. Res.* **141,** 140–149 (2017).

31. Delvecchio, R. *et al.* Chloroquine, an endocytosis blocking agent, inhibits Zika virus infection in different cell models. *Viruses* **8,** (2016).

32. Eyer, L. *et al.* Nucleoside inhibitors of Zika virus. *J. Infect. Dis.* **214,** 707–711 (2016).

33. Ferreira, A. C. *et al.* Sofosbuvir protects Zika virus-infected mice from mortality, preventing short- and long-term sequelae. *Sci. Rep.* **7,** 9409 (2017).

34. Kamiyama, N. *et al.* Ribavirin inhibits Zika virus (ZIKV) replication in vitro and suppresses viremia in ZIKV-infected STAT1-deficient mice. *Antivir. Res.* **146,** 1–11 (2017).

35. Lu, G. *et al.* Analysis of ribonucleotide 5'-triphosphate analogs as potential inhibitors of Zika virus RNA-dependent RNA polymerase by using nonradioactive polymerase assays. *Antimicrob. Agents Chemother.* **61,** (2017).

36. Mumtaz, N. *et al.* Cell-line dependent antiviral activity of sofosbuvir against Zika virus. *Antivir. Res.* **146,** 161–163 (2017).

37. Savidis, G. *et al.* The IFITMs inhibit Zika virus replication. *Cell Rep.* **15,** 2323–2330 (2016).

38. Wang, C. *et al*. Nuclear import inhibitor N-(4-hydroxyphenyl) retinamide targets Zika virus (ZIKV) nonstructural protein 5 to inhibit ZIKV infection. *Biochem. Biophys. Res. Commun.* **493,** 1555–1559 (2017).

39. Taylor, R. T. & Best, S. M. Assessing ubiquitination of viral proteins: lessons from flavivirus NS5. *Methods* **55,** 166–171 (2011).

40. Morozova, O. V. *et al.* Phosphorylation of tick-borne encephalitis virus NS5 protein. *Virus Res.* **49,** 9–15 (1997).

41. Reed, K. E. *et al*. The NS5A/NS5 proteins of viruses from three genera of the family flaviviridae are phosphorylated by associated serine/threonine kinases. *J. Virol.* **72,** 6199–6206 (1998).

42. Bhattacharya, D. *et al.* Protein kinase G phosphorylates mosquito-borne flavivirus NS5. *J. Virol.* **83,** 9195–9205 (2009).

43. Keating, J. A. *et al.* Mosquito protein kinase G phosphorylates flavivirus NS5 and alters flight behavior in Aedes aegypti and Anopheles gambiae. *Vector Borne Zoonotic Dis.* **13,** 590–600 (2013).

44. Kapoor, M. *et al.* Association between NS3 and NS5 proteins of dengue virus type 2 in the putative RNA replicase is linked to differential phosphorylation of NS5. *J. Biol. Chem.* **270,** 19100–19106 (1995).

45. Keating, J. A. *et al.* West Nile virus methyltransferase domain interacts with protein kinase G. *Virol. J.* **10,** 242 (2013).

46. Saisawang, C. *et al.* Glutathionylation of dengue and Zika NS5 proteins affects guanylyltransferase and RNA dependent RNA polymerase activities. *PLoS ONE* **13,** e0193133–15 (2018).

47. Zhu, Z. *et al.* Targeting SUMO modification of the non-structural protein 5 of Zika virus as a host-targeting antiviral strategy. *Int. J. Mol. Sci.* **20,** (2019).

48. Su, C.-I. *et al*. SUMO modification stabilizes dengue virus nonstructural protein 5 to support virus replication. *J. Virol.* **90,** 4308–4319 (2016).

49. Liao, T.-L. *et al*. Ubiquitination and deubiquitination of NP protein regulates influenza A virus RNA replication. *EMBO J.* **29,** 3879–3890 (2010).

50. Farris, K. D. *et al.* Adeno-associated virus small rep proteins are modified with at least two types of polyubiquitination. *J. Virol.* **84,** 1206–1211 (2010).

51. Peloponese, J.-M. *et al.* Ubiquitination of human T-cell leukemia virus type 1 tax modulates its activity. *J. Virol.* **78,** 11686–11695 (2004).

52. Si, X. *et al.* Ubiquitination is required for effective replication of coxsackievirus B3. *PLoS ONE* **3,** e2585 (2008).

53. Wang, Y. E. *et al.* Ubiquitin-regulated nuclear-cytoplasmic trafficking of the Nipah virus matrix protein is important for viral budding. *PLoS Pathog.* **6,** e1001186 (2010).

54. Patnaik, A. *et al*. Ubiquitin is part of the retrovirus budding machinery. *Proc. Natl. Acad. Sci. USA* **97,** 13069–13074 (2000).

55. Miorin, L. *et al.* Host-specific NS5 ubiquitination determines yellow fever virus tropism. *J. Virol.* **93,** (2019).

56. Best, S. M. *et al.* Inhibition of interferon-stimulated JAK-STAT signaling by a tick-borne flavivirus and identification of NS5 as an interferon antagonist. *J. Virol.* **79,** 12828–12839 (2005).

57. Morrison, J. *et al.* Dengue virus co-opts UBR4 to degrade STAT2 and antagonize type I interferon signaling. *PLoS Pathog.* **9,** e1003265 (2013).

58. Best, S. M. The many faces of the flavivirus NS5 protein in antagonism of type I interferon signaling. *J. Virol.* **91,** (2017).

59. Gillespie, L. K. *et al.* The endoplasmic reticulum provides the membrane platform for biogenesis of the flavivirus replication complex. *J. Virol.* **84,** 10438–10447 (2010).

60. Westaway, E. G. *et al.* Flaviviridae. *Intervirology* **24,** 183–192 (1985).

61. Buckley, A. *et al*. Monoclonal antibodies identify the NS5 yellow fever virus non-structural protein in the nuclei of infected cells. *J. Gen. Virol.* **73 (Pt 5),** 1125–1130 (1992).

62. Uchil, P. D. *et al*. Nuclear localization of flavivirus RNA synthesis in infected cells. *J. Virol.* **80,** 5451–5464 (2006).

63. Lopez-Denman, A. J. *et al.* Nucleocytoplasmic shuttling of the West Nile virus RNA-dependent RNA polymerase NS5 is critical to infection. *Cell. Microbiol.* **20,** e12848 (2018).

64. Pryor, M. J. *et al.* Nuclear localization of dengue virus nonstructural protein 5 through its importin alpha/beta-recognized nuclear localization sequences is integral to viral infection. *Traffic* **8,** 795–807 (2007).

65. Wagstaff, K. M. *et al*. Ivermectin is a specific inhibitor of importin α/β-mediated nuclear import able to inhibit replication of HIV-1 and dengue virus. *Biochem. J.* **443,** 851–856 (2012).

66. Petering, H. *et al.* The biologic role of interleukin-8: functional analysis and expression of CXCR1 and CXCR2 on human eosinophils. *Blood* **93,** 694–702 (1999).

67. Rawlinson, S. M. *et al*. CRM1-mediated nuclear export of dengue virus RNA polymerase NS5 modulates interleukin-8 induction and virus production. *J. Biol. Chem.* **284,** 15589–15597 (2009).

68. De Maio, F. A. *et al.* The dengue virus NS5 protein intrudes in the cellular spliceosome and modulates splicing. *PLoS Pathog.* **12,** e1005841 (2016).

69. Kovanich, D. *et al.* Analysis of the Zika and Japanese encephalitis virus NS5 interactomes. *J. Proteome Res.* **18,** 3203–3218 (2019).

70. Hannemann, H. *et al.* Serotype-specific differences in dengue virus non-structural protein 5 nuclear localization. *J. Biol. Chem.* **288,** 22621–22635 (2013).

71. Hertzog, J. *et al.* Infection with a Brazilian isolate of Zika virus generates RIG-I stimulatory RNA and the viral NS5 protein blocks type I IFN induction and signaling. *Eur. J. Immunol.* **48,** 1120–1136 (2018).

72. Ng, I. H. W. *et al.* Zika virus NS5 forms supramolecular nuclear bodies that sequester importin-α and modulate the host immune and pro-inflammatory response in neuronal cells. *ACS Infect. Dis.* **5,** 932–948 (2019).

73. Ji, W. & Luo, G. Zika virus NS5 nuclear accumulation is protective of protein degradation and is required for viral RNA replication. *Virology* **541,** 124–135 (2020).

74. Zhao, Z. *et al.* Nuclear localization of Zika virus NS5 contributes to suppression of type I interferon production and response. *J. Gen. Virol.* DOI: 10.1099/jgv.0.001376 (2019).

75. Conde, J. N. *et al.* NS5 sumoylation directs nuclear responses that permit Zika virus to persistently infect human brain microvascular endothelial cells. *J. Virol.* JVI.01086-20; DOI: 10.1128/JVI.01086-20 (2020).

76. Fensterl, V. *et al.* No love lost between viruses and interferons. *Annu. Rev. Virol.* **2,** 549–572 (2015).

77. Kurane, I. *et al.* High levels of interferon alpha in the sera of children with dengue virus infection. *Am. J. Trop. Med. Hyg.* **48,** 222–229 (1993).

78. Simmons, C. P. *et al.* Patterns of host genome-wide gene transcript abundance in the peripheral blood of patients with acute dengue hemorrhagic fever. *J. Infect. Dis.* **195,** 1097–1107 (2007).

79. Becquart, P. *et al.* Acute dengue virus 2 infection in Gabonese patients is associated with an early innate immune response, including strong interferon alpha production. *BMC Infect. Dis.* **10,** 356 (2010).

80. Tolfvenstam, T. *et al.* Characterization of early host responses in adults with dengue disease. *BMC Infect. Dis.* **11,** 209 (2011).

81. Sun, P. *et al.* Sequential waves of gene expression in patients with clinically defined dengue illnesses reveal subtle disease phases and predict disease severity. *PLoS Negl. Trop. Dis.* **7,** e2298 (2013).

82. Jiang, D. *et al.* Identification of five interferon-induced cellular proteins that inhibit west nile virus and dengue virus infections. *J. Virol.* **84,** 8332–8341 (2010).

83. Helbig, K. J. *et al.* Viperin is induced following dengue virus type-2 (DENV-2) infection and has anti-viral actions requiring the C-terminal end of viperin. *PLoS Negl. Trop. Dis.* **7,** e2178 (2013).

84. Chang, T.-H. *et al.* Flavivirus induces interferon-beta gene expression through a pathway involving RIG-I-dependent IRF-3 and PI3K-dependent NF-kappaB activation. *Microbes Infect.* **8,** 157–171 (2006).

85. Nash, D. *et al.* The outbreak of West Nile virus infection in the New York City area in 1999. *N. Engl. J. Med.* **344,** 1807–1814 (2001).

86. Petersen, L. R. *et al*. West Nile virus: review of the literature. *JAMA* **310,** 308–315 (2013).

87. Lin, R.-J. *et al.* Distinct antiviral roles for human 2‘,5’-oligoadenylate synthetase family members against dengue virus infection. *J. Immunol.* **183,** 8035–8043 (2009).

88. Brass, A. L. *et al.* The IFITM proteins mediate cellular resistance to influenza A H1N1 virus, West Nile virus, and dengue virus. *Cell* **139,** 1243–1254 (2009).

89. Manns, M. P. *et al.* Peginterferon alfa-2b plus ribavirin compared with interferon alfa-2b plus ribavirin for initial treatment of chronic hepatitis C: a randomised trial. *Lancet* **358,** 958–965 (2001).

90. Solomon, T. *et al.* Interferon alfa-2a in Japanese encephalitis: a randomised double-blind placebo-controlled trial. *Lancet* **361,** 821–826 (2003).

91. Nasirudeen, A. M. A. *et al.* RIG-I, MDA5 and TLR3 synergistically play an important role in restriction of dengue virus infection. *PLoS Negl. Trop. Dis.* **5,** e926 (2011).

92. Wang, J. P. *et al.* Flavivirus activation of plasmacytoid dendritic cells delineates key elements of TLR7 signaling beyond endosomal recognition. *J. Immunol.* **177,** 7114–7121 (2006).

93. Suthar, M. S. *et al*. Innate immune sensing of flaviviruses. *PLoS Pathog.* **9,** e1003541 (2013).

94. Seth, R. B. *et al*. Identification and characterization of MAVS, a mitochondrial antiviral signaling protein that activates NF-kappaB and IRF 3. *Cell* **122,** 669–682 (2005).

95. Bhattacharya, S. *et al.* Cooperation of Stat2 and p300/CBP in signaling induced by interferon-alpha. *Nature* **383,** 344–347 (1996).

96. Martinez-Moczygemba, M. *et al*. Distinct STAT structure promotes interaction of STAT2 with the p48 subunit of the interferon-alpha-stimulated transcription factor ISGF3. *J. Biol. Chem.* **272,** 20070–20076 (1997).

97. Yoshimura, A. *et al.* SOCS proteins, cytokine signaling and immune regulation. *Nat. Rev. Immunol.* **7,** 454–465 (2007).

98. Cheon, H. & Stark, G. R. Unphosphorylated STAT1 prolongs the expression of interferon-induced immune regulatory genes. *Proc. Natl. Acad. Sci. U.S.A.* **106,** 9373–9378 (2009).

99. Cheon, H. *et al.* IFNβ-dependent increases in STAT1, STAT2, and IRF9 mediate resistance to viruses and DNA damage. *EMBO J* **32,** 2751–2763 (2013).

100. Blaszczyk, K. *et al.* The unique role of STAT2 in constitutive and IFN-induced transcription and antiviral responses. *Cytokine Growth Factor Rev.* **29,** 71–81 (2016).

101. Bluyssen, H. A. & Levy, D. E. Stat2 is a transcriptional activator that requires sequence-specific contacts provided by stat1 and p48 for stable interaction with DNA. *J. Biol. Chem.* **272,** 4600–4605 (1997).

102. Lazear, H. M. *et al*. Interferon-λ: immune functions at barrier surfaces and beyond. *Immunity* **43,** 15–28 (2015).

103. Lazear, H. M. *et al.* Interferon-λ restricts West Nile virus neuroinvasion by tightening the blood-brain barrier. *Sci. Transl. Med.* **7,** 284ra59 (2015).

104. Bayer, A. *et al.* Type III interferons produced by human placental trophoblasts confer protection against Zika virus infection. *Cell Host Microbe* **19,** 705–712 (2016).

105. Chaudhary, V. *et al.* Selective activation of type II interferon signaling by Zika virus NS5 protein. *J. Virol.* **91,** (2017).

106. Pingen, M. *et al.* Host inflammatory response to mosquito bites enhances the severity of arbovirus infection. *Immunity* **44,** 1455–1469 (2016).

107. Diamond, M. S. & Farzan, M. The broad-spectrum antiviral functions of IFIT and IFITM proteins. *Nat. Rev. Immunol.* **13,** 46–57 (2013).

108. Fredericksen, B. L. & Gale, M. West Nile virus evades activation of interferon regulatory factor 3 through RIG-I-dependent and -independent pathways without antagonizing host defense signaling. *J. Virol.* **80,** 2913–2923 (2006).

109. Muñoz-Jordán, J. L. *et al*. Inhibition of interferon signaling by dengue virus. *Proc. Natl. Acad. Sci. USA* **100,** 14333–14338 (2003).

110. Muñoz-Jordán, J. L. *et al.* Inhibition of alpha/beta interferon signaling by the NS4B protein of flaviviruses. *J. Virol.* **79,** 8004–8013 (2005).

111. Ziv, O. *et al.* COMRADES determines in vivo RNA structures and interactions. *Nat. Methods* **15,** 785–788 (2018).

112. Dethoff, E. A. *et al.* Pervasive tertiary structure in the dengue virus RNA genome. *Proc. Natl. Acad. Sci. U.S.A.* **115,** 11513–11518 (2018).

113. Liu, W. J. *et al.* Inhibition of interferon signaling by the New York 99 strain and Kunjin subtype of West Nile virus involves blockage of STAT1 and STAT2 activation by nonstructural proteins. *J. Virol.* **79,** 1934–1942 (2005).

114. Slonchak, A. & Khromykh, A. A. Subgenomic flaviviral RNAs: what do we know after the first decade of research. *Antivir. Res.* **159,** 13–25 (2018).

115. Gack, M. U. *et al.* TRIM25 RING-finger E3 ubiquitin ligase is essential for RIG-I-mediated antiviral activity. *Nature* **446,** 916–920 (2007).

116. Manokaran, G. *et al.* Dengue subgenomic RNA binds TRIM25 to inhibit interferon expression for epidemiological fitness. *Science* **350,** 217–221 (2015).

117. Chan, Y. K. & Gack, M. U. A phosphomimetic-based mechanism of dengue virus to antagonize innate immunity. *Nat. Immunol.* **17,** 523–530 (2016).

118. He, Z. *et al.* Dengue virus subverts host innate immunity by targeting adaptor protein MAVS. *J. Virol.* **90,** 7219–7230 (2016).

119. Aguirre, S. *et al.* Dengue virus NS2B protein targets cGAS for degradation and prevents mitochondrial DNA sensing during infection. *Nat. Microbiol.* **2,** 17037 (2017).

120. Laurent-Rolle, M. *et al.* The NS5 protein of the virulent West Nile virus NY99 strain is a potent antagonist of type I interferon-mediated JAK-STAT signaling. *J. Virol.* **84,** 3503–3515 (2010).

121. Lubick, K. J. *et al.* Flavivirus antagonism of type I interferon signaling reveals prolidase as a regulator of IFNAR1 surface expression. *Cell Host Microbe* **18,** 61–74 (2015).

122. Kumar, A. *et al.* Zika virus inhibits type-I interferon production and downstream signaling. *EMBO Rep.* **17,** 1766–1775 (2016).

123. Mazzon, M. *et al*. Dengue virus NS5 inhibits interferon-alpha signaling by blocking signal transducer and activator of transcription 2 phosphorylation. *J. Infect. Dis.* **200,** 1261–1270 (2009).

124. Jones, M. *et al.* Dengue virus inhibits alpha interferon signaling by reducing STAT2 expression. *J. Virol.* **79,** 5414–5420 (2005).

125. Ashour, J. *et al*. NS5 of dengue virus mediates STAT2 binding and degradation. *J. Virol.* **83,** 5408–5418 (2009).

126. Gibbs, D. J. *et al*. The eukaryotic N-end rule pathway: conserved mechanisms and diverse functions. *Trends Cell Biol.* **24,** 603–611 (2014).

127. Ho, J. *et al.* STAT2 is a pervasive cytokine regulator due to its inhibition of STAT1 in multiple signaling pathways. *PLoS Biol.* **14,** e2000117 (2016).

128. Laurent-Rolle, M. *et al.* The interferon signaling antagonist function of yellow fever virus NS5 protein is activated by type I interferon. *Cell Host Microbe* **16,** 314–327 (2014).

Chapter 2: The structure of Zika virus NS5 reveals a conserved domain conformation

Abstract

Zika virus (ZIKV) has been the cause of multiple epidemics since 2005, imposing a serious threat to public health. There are currently no approved therapeutic or prophylactic measures to restrain ZIKV infection. NS5 is a highly conserved flavivirus protein and re-purposing antiviral drugs used successfully against other flaviviruses is a practical approach to discovering antiviral drugs for ZIKV. Here we report the crystal structure of the ZIKV NS5 protein in complex with S-adenosyl-L-homocysteine, in which the tandem methyltransferase (MTase) and RNA-dependent RNA polymerase (RdRp) domains stack into one of the two alternative conformations reported for flavivirus NS5 proteins. The activity of the NS5 protein used for structural study was verified through a *de novo* RdRp assay on a subgenomic ZIKV RNA template. Importantly, our structural analysis lead to the identification of a conserved flavivirus drug-binding site, which might facilitate the development of novel antivirals for ZIKV.

Introduction

The outbreak of Zika virus (ZIKV) in the Americas and West Pacific islands in 2015 was a worldwide health concern, affecting more than 60 countries[1,2]. Increasing evidence has linked ZIKV infection to microcephaly in newborn infants[3], and to Guillain–Barre´ syndrome in adults[4]. The fact that no vaccines or therapeutics for prevention or treatment of ZIKV infection are currently available further deepens the concern. To develop effective antivirals against ZIKV infection, it is urgent to gain a comprehensive structural and mechanistic understanding of the molecular machineries underpinning the life cycle of ZIKV.

ZIKV belongs to the *Flavivirus* genus that includes a variety of mosquito-borne human pathogens, such as dengue virus (DENV1–4), yellow fever virus, West Nile virus, Spondweni virus and Japanese encephalitis virus (JEV)[5]. The genome of ZIKV is a single positive-sense RNA molecule that encodes three structural proteins (capsid, C; pre-membrane/membrane, prM/M; and envelope, E) and seven non-structural (NS) proteins (NS1, NS2A, NS2B, NS3, NS4A, NS4B and NS5)[6]. Among these, NS5 is the largest protein, containing an N-terminal methyltransferase (MTase) domain responsible for viral RNA capping and a C-terminal RNA-dependent RNA polymerase (RdRp) domain for viral RNA synthesis, with evidence indicating that the MTase and RdRp domains cooperate in RNA synthesis initiation and elongation[7]. In addition, NS5 proteins have been shown to inhibit type I interferon (IFN) signaling to evade antiviral defense in the host[8-16]. The essential role of NS5 in viral replication and immunosuppression makes it an ideal target for antivirals[17]. However, the molecular mechanism underlying the enzymatic

action of NS5 remains poorly understood. Prior to this report, crystal structures of full-length NS5 proteins had only been reported for JEV and DENV3[18,19]. Intriguingly, despite ~65% sequence identity (Appendix A, Supplementary Fig. 1), JEV NS5 and DENV3 NS5 adopt different orientations between the MTase and RdRp domains[18,19], raising the question of how the MTase and RdRp domains of NS5 cooperate during RNA replication and capping.

To illuminate the structure and mechanism of NS5 proteins, and, more importantly, to explore potential druggable sites for ZIKV, we determined the crystal structure of full-length ZIKV NS5 in complex with S-adenosyl-L-homocysteine (SAH), by-product of cofactor S-adenosyl-L-methionine, at 3.3Å resolution. Our structural analysis reveals that ZIKV NS5 folds into one of the two alternative conformations reported for flavivirus NS5 proteins, providing functional implication for the conformational dynamics of flavivirus NS5 proteins. We further verify the enzymatic activity of ZIKV NS5 through a *de novo* RdRp assay using a subgenomic ZIKV RNA as template. Finally, we show that the structure of ZIKV NS5 provides a framework for future development of novel antivirals against ZIKV infection.

Results

Overall structure of ZIKV NS5.

We were able to trace nearly the entire sequence of ZIKV NS5 (Fig. 3a), except for the first five N-terminal residues, residues 747–748 in the RdRp domain, and sixteen residues at the C terminus. The structure reveals an N-terminal classic S-adenosyl-L-methionine-dependent MTase domain situated on top of a C-terminal RdRp domain. The MTase domain is dominated by a Rossmann fold, with a seven-stranded ß-sheet sandwiched by two α-helices from one side and another α-helix from the other side. Near to the catalytic site, the SAH molecule is surrounded by a set of conserved residues (Appendix A, Supplementary Fig. 2). In addition, the N-terminal extension sequence (α1– α4, Appendix A, Supplementary Fig. 1) of the MTase domain pairs with its C-terminal extension sequence (α8– ß9, Appendix A, Supplementary Fig. 1) to form a helix bundle and an antiparallel two-stranded ß-sheet, adding another structural layer onto the Rossmann fold (Fig. 3b). As with other viral RdRps[20], the ZIKV NS5 RdRp adopts a capped right-hand structure with the palm, fingers and thumb subdomains and a priming sequence poised to receive RNA substrates (Fig. 3b). The RdRp domain also harbors two zinc ions, as observed for the NS5 proteins of JEV and DENV3[18,19]. The associations of the MTase domain with the RdRp domain do not involve extensive interdomain contacts, leading to a modest buried surface area of ~1,400 Å^2. In fact, structural superposition of the MTase domain in full-length NS5 and the recently reported domain alone[21] gives a root-mean-square deviation (RMSD) of 0.42Å over 242 Cα atoms, indicating that the

MTase–RdRp association does not lead to considerable conformational change of the MTase domain.

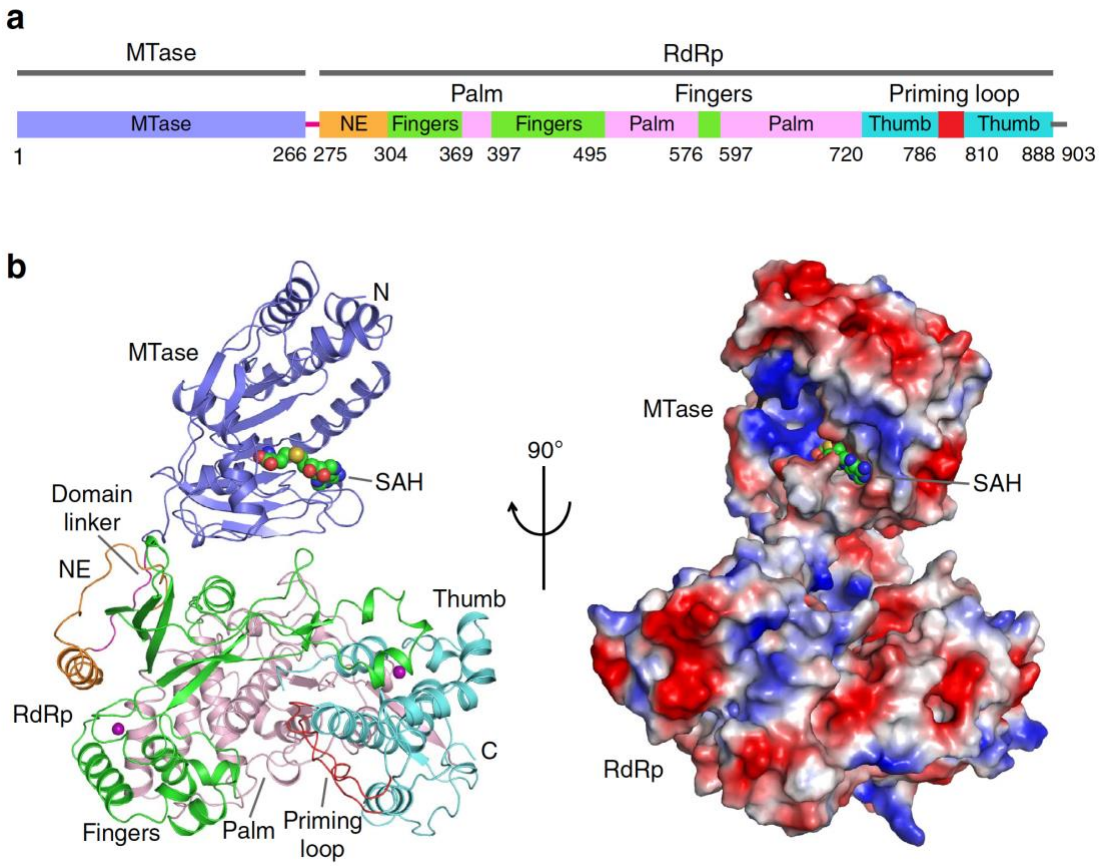

Figure 3. Structural overview of ZIKV NS5. a) Color-coded domain architecture of ZIKV NS5. b) Orthogonal views of ribbon (left) and electrostatic surface (right) representations of ZIKV NS5. The MTase domain, the N-terminal extension, palm, fingers, priming loop and thumb of the RdRp domain, and the interdomain linker are colored in slate, orange, pink, green, red, light blue and magenta, respectively. Zinc ions (purple) and SAH are shown in sphere representation.

Structural comparison with other flavivirus NS5 proteins.

ZIKV NS5 shares ~68% and ~66% sequence identity, respectively, with its JEV and DENV3 counterparts (Appendix A, Supplementary Fig. 1). However, these NS5 homologues appear to antagonize the IFN signaling through different mechanisms: JEV NS5 suppresses IFN signaling likely through blocking phosphorylation of the IFN signaling components[13], whereas DENV3 NS5 and ZIKV NS5 inhibit the IFN signaling through promoting protein degradation of signal transducer and activator of transcription 2 in an E3 ubiquitin ligase UBR4-dependent or -independent manner[10,16]. We compared the structure of ZIKV NS5 with those of JEV NS5 and DENV3 NS5 (Fig. 4a,b). Remarkably, ZIKV NS5 superimposes well with JEV NS5, with an RMSD of 0.63Å over 872 Cα atoms (Fig. 4a). In particular, the MTase–RdRp associations of ZIKV NS5 and JEV NS5 are both mediated by the same set of van de Waals contacts, involving the C-terminal extension of the MTase domain (P113, L115, Q117 and W121), and the index, ring and middle fingers of the RdRp domain (Y350, R354, F466 and P584 in ZIKV NS5) (Fig. 4c,d). Subtle structural divergences between ZIKV NS5 and JEV NS5 were mainly observed in the N- and C-terminal extension of the MTase domain, the MTase-RdRp domain linker, and a segment in the palm subdomain (residues E632-G653 in ZIKV NS5) (Appendix A, Supplementary Fig. 3a). Note that these regions have previously been linked to flavivirus NS5-mediated immunosuppression[13,14]. Therefore, such structural divergence may underlie the distinct mechanisms of ZIKV NS5 and JEV NS5 in IFN antagonism. By contrast, structural superposition of ZIKV NS5 and DENV3 NS5 gives a RMSD of 6.06Å over 844 Cα atoms, attributed in large part to the difference in the

relative orientation between the MTase and RdRp domains (Fig. 4b). Unlike the structure of ZIKV NS5 in which the MTase domain sits on the back of the RdRp domain, the MTase domain of DENV3 NS5 approaches towards the front of the RdRp domain, resulting in a more compact conformation (Fig. 4b). Distinct from those of ZIKV and JEV NS5 (Fig. 4c,d), the MTase–RdRp association of DENV3 is mediated by a set of hydrogen bonding, cation-π and electrostatic interactions between the N- (Q63, E67 and R68) and C-terminal extensions (E252 and D254) of the MTase domain and the index finger (F348, R352, E356 and K357) of the RdRp domain (Fig. 4e). These interactions of DENV3 NS5 appear to draw the MTase domain towards the NTP entrance of the RdRp domain, resulting in a ~100° rotation of the MTase domain in relation to the RdRp domain (Fig. 4b). Another prominent structural difference between ZIKV/JEV NS5 and DENV3 NS5 arises from the substrate binding motifs of RdRp, including motif F in the ring finger and motif G in the pinky finger[22,23] (Fig. 4b). The conformations of these two motifs appear to be stabilized by the MTase–ring finger association of ZIKV/JEV NS5 but are disordered in DENV3 NS5 due to the loss of the corresponding interactions (Appendix A, Supplementary Fig. 3b).

The fact that the structure of ZIKV NS5 exhibits an extended domain conformation similar to that of JEV NS5, but different from that of DENV3 NS5, implies a possible functional divergence between these two conformational states of NS5 proteins. On one hand, it is likely that the structures of ZIKV/JEV NS5 diverge from that of DENV3 NS5 through adaptive mutations of specific regions (for example, the domain linker) during evolution, as proposed previously[24]. On the other hand, the high sequence

conservation of both domain interfaces (Appendix A, Supplementary Fig. 1) strongly argues that the structures of ZIKV/JEV NS5 and DENV3 NS5 represent two alternative conformations of NS5 that may coexist in solution. Consistently, previous small-angle X-ray scattering analysis suggested the presence of a heterogeneous conformational ensemble of DENV3 NS5 in solution[24], and mutations at the two alternative domain interfaces lead to compromised methyltransferase activity or viral replication[19]. Additional biochemical and cellular analyses are required to reveal the functional implication of these two alternative conformations of flavivirus NS5 proteins.

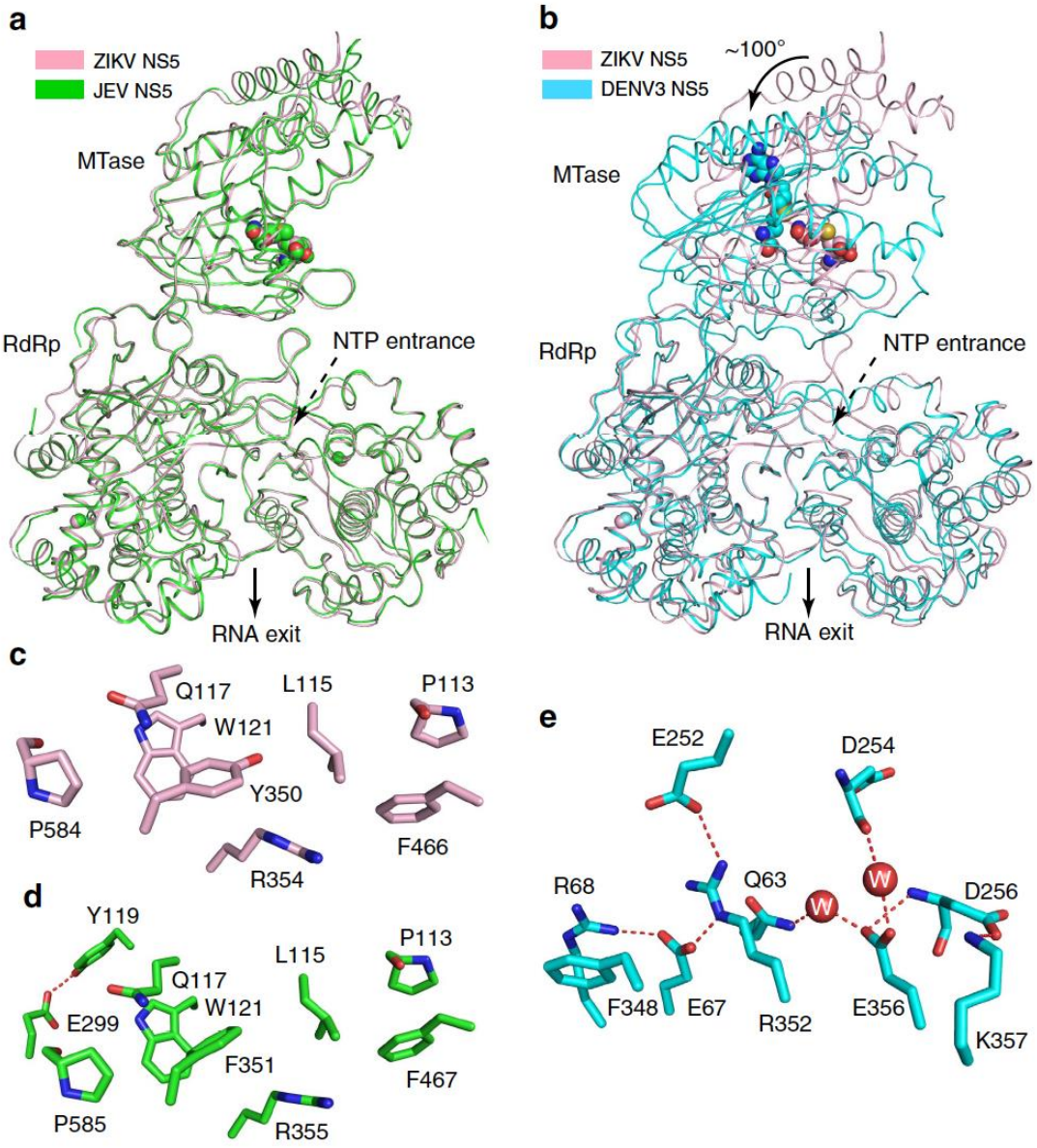

Figure 4. Structural comparison of NS5 proteins from ZIKV and two other flaviviruses. Structural superposition of ZIKV NS5 with a) JEV NS5 (PDB 4K6M) and b) DENV3 NS5 (PDB 4V0Q). Alignment of the RdRp domains of ZIKV NS5 and DENV3 NS5 leads to a ~100° change in orientation between the MTase and RdRp domains. The NTP entrance and RNA exit sites are labeled. c–e) The MTase–RdRp domain interactions of c) ZIKV NS5, d) JEV NS5 and e) DENV3 NS5.

De novo *RdRp assay of ZIKV NS5.*

To confirm that the ZIKV NS5 protein used for our structural study represents an active enzyme, we performed a *de novo* RdRp assay for ZIKV NS5 on a subgenomic ZIKV RNA template (Fig. 5a), using the recombinant ZIKV NS3 helicase domain (NS3-Hel) (Fig. 5b) as a negative control. We observed that the presence of ZIKV NS5 led to a time-dependent increase in the replication of the subgenomic ZIKV RNA at 33°C (Fig. 5c). However, the reaction product became dominated by a shorter RNA at 23°C, possibly due to early termination of the replication (Fig. 5c). On the other hand, the presence of ZIKV NS3-Hel failed to yield any RNA product (Fig. 5c). Together, these data not only confirm that the ZIKV NS5 protein used for the structural study is enzymatically active but also provide a basis for further functional characterization of ZIKV NS5.

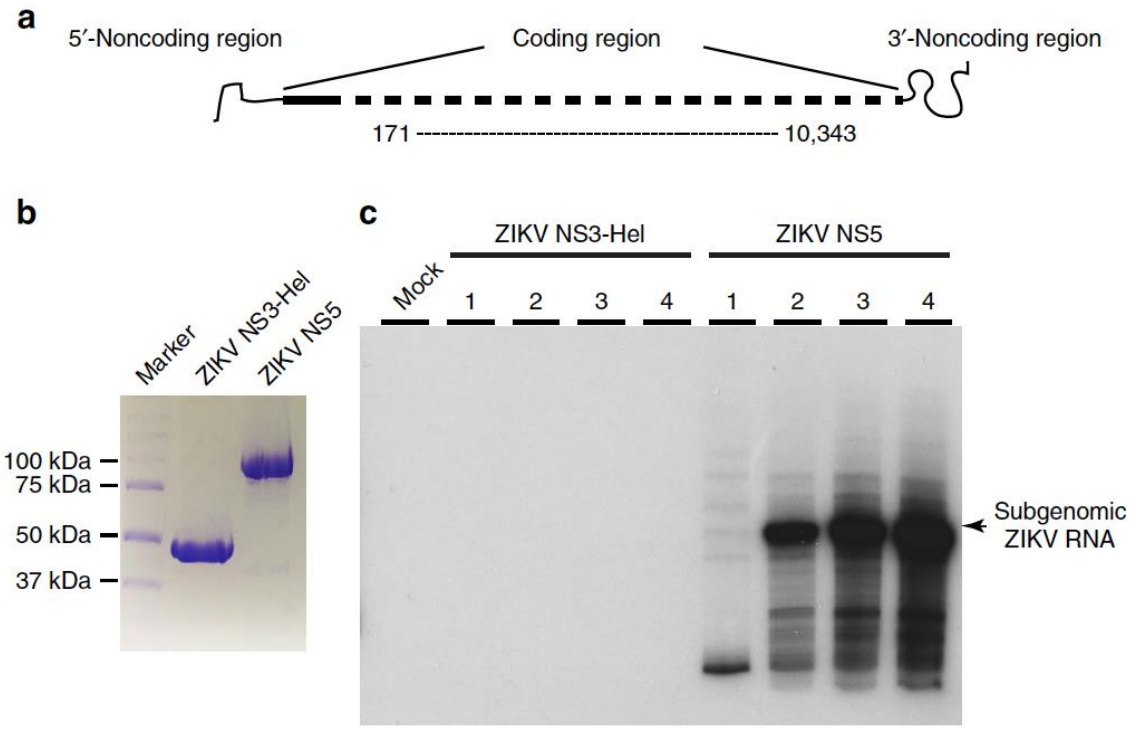

Figure 5. *De novo* RNA synthesis by ZIKV NS5 protein. a) The subgenomic ZIKV RNA contains an internal deletion from nucleotides 171 to 10,343 (GenBank accession no. KU963573.2). b) SDS–polyacrylamide gel electrophoresis analysis of purified ZIKV NS5 and ZIKV NS3-Hel. c) ZIKV *de novo* RNA replication assay. The subgenomic ZIKV RNA was incubated with recombinant ZIKV NS5 protein, ZIKV NS3-Hel or alone (mock). The relative amount of ^{32}P-labelled RNA product is displayed in the autoradiograph of the PAGE gel. The reactions containing recombinant proteins were divided into four groups. Group 1 was incubated at 23°C for 30 min. Groups 2, 3 and 4 were incubated at 33°C for 30, 60 or 120 min, respectively.

Re-purposing a DENV RdRp inhibitor for ZIKV NS5.

Finally, we asked whether the structure of ZIKV NS5 permits us to identify potential inhibitor-binding sites for its enzymatic inhibition. A previous study, through fragment-based crystallography method, identified a pocket near the active site of the DENV3 RdRp domain, termed 'N pocket', which binds to a small molecule that inhibits DENV3 NS5-mediated RNA initiation and elongation (Fig. 6a)[25]. Detailed analysis of this inhibitor-binding site revealed that the critical residues for the inhibitor binding are also conserved in ZIKV NS5, arranged in a similar structural environment (Fig. 6b), suggesting that the same compound may also be inhibitory to the enzymatic activity of ZIKV NS5. To that end, the ZIKV *de novo* RdRp assay was used to assess the ability of the 'N pocket' compound to inhibit ZIKV NS5-mediated RNA replication (Fig. 6c). We observed that RNA replication was inhibited at drug concentrations as low as 12.5 μM with complete loss of RdRp activity observed at 100 μM (Fig. 6c). This result demonstrates that DENV RdRp inhibitors may be re-purposed for anti-ZIKV therapy.

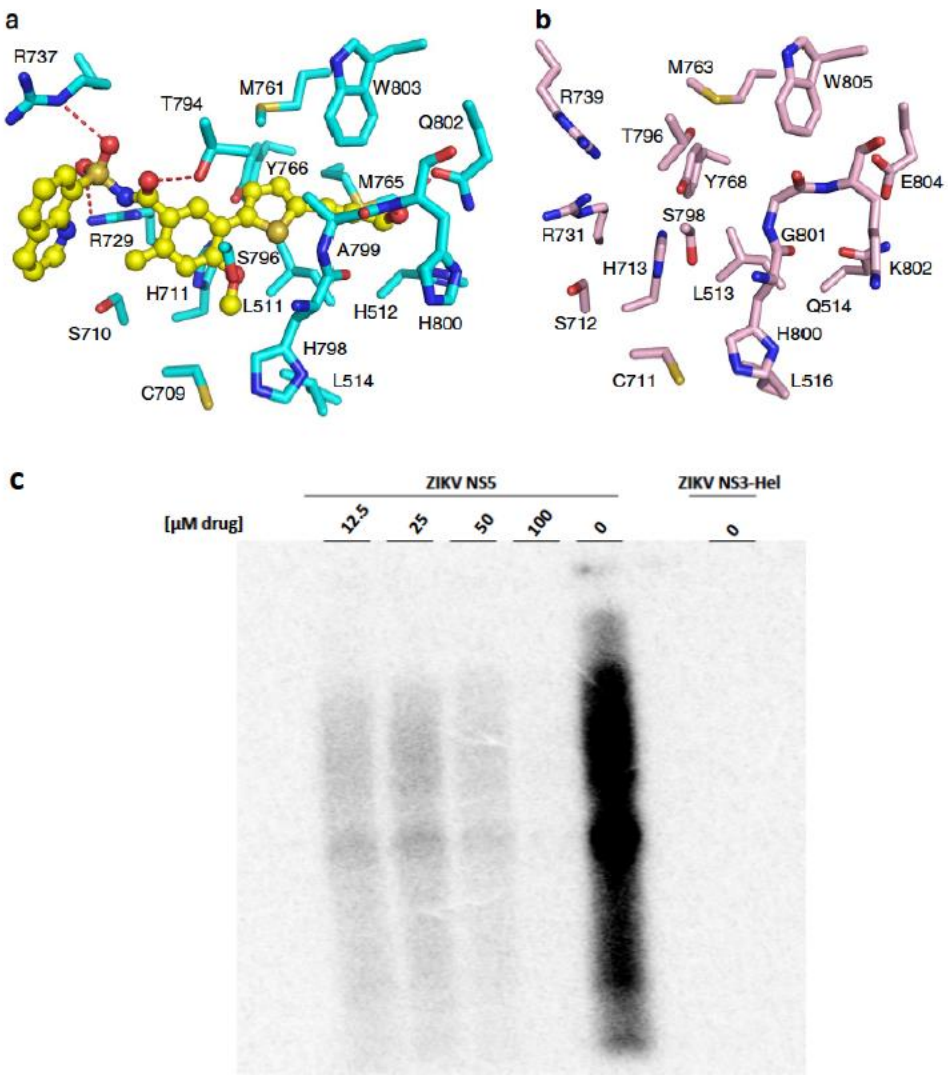

Figure 6. A DENV RdRp inhibitor is re-purposed for ZIKV NS5. a) Binding of a small-molecule inhibitor of DENV3 NS5 at its 'N pocket'. The residues of DENV3 NS5 and small-molecule inhibitor are shown in blue and yellow sticks, respectively. The hydrogen bonding interactions are depicted as dashed lines. b) The residues of ZIKV NS5 corresponding to the inhibitor binding site of DENV3 NS5 are shown in pink sticks. c) ZIKV *de novo* RNA replication assay. The subgenomic ZIKV RNA was incubated with recombinant ZIKV NS5 protein or ZIKV NS3-Hel with 12.5, 25, 50 or 100 μM of the 'N pocket' drug or DMSO (0 μM) for 90 minutes. The relative amount of ^{32}P-labelled RNA product is displayed in the autoradiograph of the PAGE gel.

Table 1. ZIKV NS5 X-ray crystallography data collection and refinement statistics

	ZIKV NS5
Data Collection	
Space group	*P*2 2_1 2_1
Cell dimensions	
a, *b*, *c* (Å)	95.1, 136.5, 197.0
α, β, γ (°)	90, 90, 90
Wavelength	0.9764
Resolution (Å)	50.00–3.30 (3.42–3.30)[a]
R_{sym} or R_{merge}	31.3 (83.5)
$I/\sigma(I)$	5.3 (1.7)
$CC_{1/2}$	0.979 (0.748)
Completeness (%)	99.4 (97.1)
Redundancy	6.2 (5.7)
Refinement	
Resolution (Å)	48.3–3.28 (3.36–3.28)
No. Reflections	39,405 (3,511)
R_{work} / R_{free}	0.262/0.293 (0.344/0.405)
No. atoms	
Protein	13,391
Ligand	38
B factors	
Protein	69.82
Ligand	68.85
RMSD	
Bond lengths (Å)	0.002
Bond angles (°)	0.55

[a]Values in parentheses are for highest-resolution shell.

Discussion

Our structural study of ZIKV NS5 sheds light onto the conformational dynamics and functional regulation of ZIKV NS5. The observation that ZIKV NS5 adopts one of the two defined conformations of flavivirus NS5 proteins provides first evidence on the conservation of domain conformation within NS5 proteins, which may be required for their functional regulation. To confirm the enzymatic activity of the recombinant ZIKV NS5 protein, we developed a *de novo* RdRp assay of ZIKV NS5 on a subgenomic ZIKV RNA template, which provides a basis for future mechanistic characterization of ZIKV NS5. Furthermore, we identified that the small molecular inhibitor binding site of DENV3 NS5 is structurally conserved in ZIKV NS5, and that the DENV NS5 inhibitor is able to inhibit ZIKV NS5 RdRp activity similarly. This study provides a foundation for future dissection of the functional coupling between the MTase and RdRp domains and a framework for the design of novel inhibitors against ZIKV infection.

Methods

Expression and purification of ZIKV NS5 and NS3 helicase.

The DNA sequence encoding full-length ZIKV NS5 or ZIKV NS3-Hel (residues 171–617) was amplified from the cDNA of ZIKV/Macaca mulatta/UGA/MR-766/1947 and inserted into a modified pRSFDuet-1 vector (Novagen) (see Appendix A, Supplementary Table 1 for primer sequences), in which the NS5 or NS3-Hel gene was preceded by an N-terminal His_6-SUMO tag and ULP1 (ubiquitin-like protease 1) cleavage site. The obtained plasmids were then transformed into BL21 (DE3) RIL cell strain (Agilent Technologies) for expression. The cells were first grown at 37°C and then shifted to room temperature when A_{600} reached 1.0, followed by the addition of 0.4 mM isopropyl b-D-galactoside for induction. After another 18h of cell growth, the cells were collected and the His_6- SUMO-tagged ZIKV NS5 or ZIKV NS3-Hel was purified using a Ni-NTA affinity column. ZIKV NS5 was further purified on a Phenyl Sepharose column (GE Healthcare) for separation from degraded protein products, followed by removal of the His_6-SUMO tag through ULP1 cleavage and size-exclusion chromatography on a Superdex 200 16/600 column (GE Healthcare) pre-equilibrated in buffer containing 25 mM Tris, pH 7.5, 500 mM NaCl, 5 mM DTT (dithiothreitol) and 5% glycerol. The ZIKV NS3-Hel fusion protein was first subject to ULP1 cleavage, and subsequently purified on a Phenyl Sepherase column and a Superdex 200 16/600 column preequilibrated in buffer containing 25 mM Tris, pH 7.5, 250 mM NaCl, 5 mM DTT and 5% glycerol. SDS–polyacrylamide gel electrophoresis analysis indicated that the purities of NS5 and NS3-Hel proteins were >95% and >90%, respectively. Protein solution of purified NS5 and

NS3-Hel, with concentrations of ~20 and ~70 mg ml^{-1}, respectively, were stored at -80°C.

Crystallization and X-ray data collection.

Full-length ZIKV NS5 was mixed with SAH and GTP in a 1:3:3 molar ratio for complex formation. Initial crystallization conditions were identified through sparse-matrix screens (Hampton Research Inc.). The crystals were subsequently reproduced by hanging-drop vapor diffusion method at 4°C, from drops mixed from 1 ml of ZIKV NS5 and 1 ml of precipitant solution (0.7–0.9 M lithium sulfate, 0.1 M MES, pH 6–7). Crystals were soaked for 1 min in a cryoprotectant solution, comprising of crystallization buffer and 20% glycerol, before flash frozen in liquid nitrogen. The X-ray diffraction data for ZIKV NS5 were collected on the BL 5.0.3 beamline at the Advanced Light Source, Lawrence Berkeley National Laboratory. The diffraction data were indexed, integrated and scaled using the HKL2000 program[26]. The structure was solved using the molecular replacement method in PHASER[27], with the structure of Japanese encephalitis virus NS5 (PDB ID: 4K6M) as search model. The resulting electron density revealed that there are two molecules of ZIKV NS5 in each asymmetric unit. Despite being present in the crystallization mixture, GTP molecules were not modelled, presumably due to low occupancy under the crystallization condition. The structure of ZIKV NS5 was improved by iterative model building and refinement with Coot[28] and PHENIX[29] software packages. The same R-free test set was used throughout the refinement. The statistics for data collection and structural refinement of ZIKV NS5 is summarized in Table 1.

De novo RdRp assay.

The *de novo* RdRp reaction (20 µl) contained 50 mM Tris (pH 8.0), 10 mM NaCl, 5 mM $MgCl_2$, 2 mM $MnCl_2$, 10 mM DTT, 0.5 mM ATP, 0.5 mM UTP, 0.5 mM GTP, 5 mM CTP, 15 µCi of [α-^{32}P] (10 µCi µl^{-1}, 3,000 Ci mmol^{-1}; Perkin-Elmer), 1 µg of RNA template and 2 µg of ZIKV NS5 protein or ZIKV NS3-Hel. The RNA template was *in vitro* transcribed from a PCR product using T7 polymerase (New England BioLabs). The PCR product contained a T7 promoter, followed by a cDNA fragment representing a ZIKV subgenome with deletion of nucleotides 171–10,343 (GenBank accession no. KU963573.2). The *de novo* RdRp reaction mixtures were incubated at 23°C for 30 min, or 33°C for 30, 60 and 120 min. The final reactions were further extracted with phenol–chloroform and precipitated with isopropanol. The RNA pellet was dissolved in 20 µl of 1X denaturing gel loading dye and loaded onto a 10% denaturing polyacrylamide gel with 7 M urea. ^{32}P-labelled RNA results were detected via the autoradiograph of the PAGE gel.

Data availability.

Coordinates and structure factors for ZIKV NS5–SAH complexes have been deposited in the Protein Data Bank under accession code 5TMH. The PDB accession codes 5TMH, 5JJR, 4K6M and 4V0Q and GenBank entry KU963573.2 were used in this study.

References

1. Duffy, M. R. *et al.* Zika virus outbreak on Yap Island, Federated States of Micronesia. *N. Engl. J. Med.* **360,** 2536–2543 (2009).

2. Faria, N. R. *et al.* Zika virus in the Americas: early epidemiological and genetic findings. *Science* **352,** 345–349 (2016).

3. Rasmussen, S. A. *et al.* Zika virus and birth defects – reviewing the evidence for causality. *N. Engl. J. Med.* **374,** 1981–1987 (2016).

4. Cao-Lormeau, V.-M. *et al.* Guillain-Barré syndrome outbreak associated with Zika virus infection in French Polynesia: a case-control study. *Lancet* **387,** 1531–1539 (2016).

5. Petersen, L. R. *et al.* Zika virus. *N. Engl. J. Med.* **374,** 1552–1563 (2016).

6. Shan, C. *et al.* An infectious cDNA clone of Zika virus to study viral virulence, mosquito transmission and antiviral inhibitors. *Cell Host Microbe* **19,** 891–900 (2016).

7. Potisopon, S. *et al.* The methyltransferase domain of dengue virus protein NS5 ensures efficient RNA synthesis initiation and elongation by the polymerase domain. *Nucleic Acids Res.* **42,** 11642–11656 (2014).

8. Ashour, J. *et al.* Mouse STAT2 restricts early dengue virus replication. *Cell Host Microbe* **8,** 410–421 (2010).

9. Best, S. M. *et al.* Inhibition of interferon-stimulated JAK-STAT signaling by a tick-borne flavivirus and identification of NS5 as an interferon antagonist. *J. Virol.* **79,** 12828–12839 (2005).

10. Grant, A. *et al.* Zika virus targets human STAT2 to inhibit type I interferon signaling. *Cell Host Microbe* **19,** 882–890 (2016).

11. Laurent-Rolle, M. *et al.* The NS5 protein of the virulent West Nile virus NY99 strain is a potent antagonist of type I interferon-mediated JAK-STAT signaling. *J. Virol.* **84,** 3503–3515 (2010).

12. Laurent-Rolle, M. *et al.* The interferon signaling antagonist function of yellow fever virus NS5 protein is activated by type I interferon. *Cell Host Microbe* **16,** 314–327 (2014).

13. Lin, R.-J. *et al*. Blocking of interferon-induced JAK-STAT signaling by Japanese encephalitis virus NS5 through a protein tyrosine phosphatase-mediated mechanism. *J. Virol.* **80,** 5908–5918 (2006).

14. Lubick, K. J. *et al.* Flavivirus antagonism of type I interferon signaling reveals prolidase as a regulator of IFNAR1 surface expression. *Cell Host Microbe* **18,** 61–74 (2015).

15. Mazzon, M. *et al*. Dengue virus NS5 inhibits interferon-alpha signaling by blocking signal transducer and activator of transcription 2 phosphorylation. *J. Infect. Dis.* **200,** 1261–1270 (2009).

16. Morrison, J. *et al.* Dengue virus co-opts UBR4 to degrade STAT2 and antagonize type I interferon signaling. *PLoS Pathog.* **9,** e1003265 (2013).

17. Lim, S. P. *et al*. The dengue virus NS5 protein as a target for drug discovery. *Antivir. Res.* **119,** 57–67 (2015).

18. Lu, G. & Gong, P. Crystal Structure of the full-length Japanese encephalitis virus NS5 reveals a conserved methyltransferase-polymerase interface. *PLoS Pathog.* **9,** e1003549 (2013).

19. Zhao, Y. *et al.* A crystal structure of the Dengue virus NS5 protein reveals a novel inter-domain interface essential for protein flexibility and virus replication. *PLoS Pathog.* **11,** e1004682 (2015).

20. Ferrer-Orta, C. *et al*. A comparison of viral RNA-dependent RNA polymerases. *Curr. Opin. Struct. Biol.* **16,** 27–34 (2006).

21. Coloma, J. *et al*. Structures of NS5 methyltransferase from Zika virus. *Cell Reports* **16,** 3097–3102 (2016).

22. Iglesias, N. G. *et al*. The F1 motif of dengue virus polymerase NS5 is involved in promoter-dependent RNA synthesis. *J. Virol.* **85,** 5745–5756 (2011).

23. Yap, T. L. *et al.* Crystal structure of the dengue virus RNA-dependent RNA polymerase catalytic domain at 1.85-angstrom resolution. *J. Virol.* **81,** 4753–4765 (2007).

24. Bussetta, C. & Choi, K. H. Dengue virus nonstructural protein 5 adopts multiple conformations in solution. *Biochemistry* **51,** 5921–5931 (2012).

25. Lim, S. P. *et al.* Potent allosteric dengue virus NS5 polymerase inhibitors: mechanism of action and resistance profiling. *PLoS Pathog.* **12,** e1005737 (2016).

26. Otwinowski, Z. & Minor, W. Processing of X-ray diffraction data collected in oscillation mode. *Meth. Enzymol.* **276,** 307–326 (1997).

27. McCoy, A. J. *et al.* Phaser crystallographic software. *J. Appl. Crystallogr.* **40,** 658–674 (2007).

28. Emsley, P. & Cowtan, K. Coot: model-building tools for molecular graphics. *Acta Crystallogr. D Biol. Crystallogr.* **60,** 2126–2132 (2004).

29. Adams, P. D. *et al.* PHENIX: building new software for automated crystallographic structure determination. *Acta Crystallogr. D Biol. Crystallogr.* **58,** 1948–1954 (2002).

Chapter 3: Structural basis for STAT2 suppression by flavivirus NS5

Abstract

Signal transducer and activator of transcription 2 (STAT2) mediates the host interferon (IFN) response against infections and is frequently targeted by viruses for suppression. For example, non-structural protein 5 (NS5) of both Zika virus (ZIKV) and dengue virus (DENV) antagonizes innate immunity through binding to, and promoting the proteasome-mediated degradation of, human STAT2 (hSTAT2), thus suppressing the IFN response and supporting virus spread. However, the mechanism and functional consequences of this interaction are poorly understood due to the lack of structural information. Here, we report the cryoEM and crystal structures of hSTAT2 in complex with NS5 of ZIKV or DENV, revealing a multivalent interaction mechanism between NS5 and hSTAT2. hSTAT2 assumes an elongated conformation, with its SH2 domain blocked by the phosphotyrosine (pY)-containing tail segment. Our atomic models of the NS5 – hSTAT2 complexes reveal that one end of the coiled-coil domain of hSTAT2 occupies a pre-configured cleft between the methyltransferase and RNA-dependent RNA polymerase (RdRp) domains of NS5 in a manner that would occlude the association of hSTAT2 with interferon regulatory factor 9 (IRF9), while the N-terminal domain of hSTAT2 binds at a separate surface of the NS5 RdRp domain. Structure-guided mutagenesis, pull-down and immunofluorescence assays confirmed these interactions in cells. These mechanistic insights into viral suppression of hSTAT2 should inform rational design of therapeutic strategies against flaviviruses.

Introduction

The interferon (IFN)-mediated innate immune response constitutes a first line of host defense against viral infection[1]. The three types of IFN pathways—IFN-α/β (type I), IFN-γ (type II), and IFN-λ (type III)—share the same regulator, signal transducer and activator of transcription 2 (STAT2), whose activation by Janus kinases (JAKs) triggers the expression of over 300 genes for antiviral response[2]. To establish infection, viruses have evolved a variety of STAT2-specific suppression schemes[3]. In particular, recent studies have revealed that dengue virus (DENV) and Zika virus (ZIKV), members of the *Flavivirus* genus of the *Flaviviridae* family, employ their non-structural protein 5 (NS5) to promote human STAT2 (hSTAT2) degradation and suppression of the IFN response[4-6]. These NS5 proteins directly bind to hSTAT2 and promote its degradation through the ubiquitin-mediated pathway[4,5]. However, how NS5 interacts with hSTAT2 and whether these interactions directly contribute to hSTAT2 degradation and other suppression mechanisms are not known due to the lack of atomic structures of the NS5 – hSTAT2 complexes (or of any complexes of viral proteins bound to STATs) and structure-based functional analyses. Both ZIKV and DENV have imposed serious threats to global health, with ZIKV linked to neurological disorders, such as congenital microcephaly[7] and Guillain–Barré syndrome (GBS)[8] during the recent epidemic, and DENV associated with dengue hemorrhagic fever (DHF)[9]. However, currently there are no antivirals available for either of them.

STAT2 belongs to a seven-member STAT family of transcriptional regulators[10], composed of an N-terminal domain (ND), followed by a coiled-coil domain (CCD), a

DNA binding domain (DBD), a linker domain (LD), a SRC homology 2 (SH2) domain, a tyrosine-phosphorylation site (pY)-containing tail segment and a transcriptional activation domain (TAD). STAT2-mediated transcriptional activation involves tyrosine phosphorylation of STAT2 by JAKs, followed by formation of a STAT1-STAT2 dimer via a mutual SH2-pY interaction[11]. The STAT1-STAT2 dimer further associates with IFN regulatory factor 9 (IRF9) to form the IFN-stimulated gene factor-3 (ISGF3) complex[12], whose translocation to the nucleus stimulates expression of antiviral genes[13]. It has been demonstrated that the NS5 proteins from DENV and ZIKV directly bind to and promote the ubiquitin-mediated degradation of hSTAT2[4,5]. However, the underlying mechanism is unclear. NS5 is the largest flaviviral non-structural protein, containing an N-terminal methyltransferase (MTase) domain that mediates viral RNA capping in tandem with an RNA-dependent RNA polymerase (RdRp) domain responsible for replication of the viral genome[14]. In addition to their critical role in viral replication, the NS5 proteins from all currently identified flaviviruses serve as potent antagonists of IFN signaling[15]. Due to the lack of structural knowledge, the molecular basis underlying NS5-mediated antagonism has not been elucidated for any of these viruses.

Results

Domain Mapping the ZIKV NS5 hSTAT2-interacting regions

To provide the structural basis for NS5-mediated hSTAT2 suppression, we characterized the interaction between ZIKV NS5 and hSTAT2 through both *in vivo* and *in vitro* binding assays. Co-immunoprecipitation (co-IP) using HA-tagged ZIKV NS5 and FLAG-tagged hSTAT2 or human STAT1 (hSTAT1) revealed a strong interaction between ZIKV NS5 and hSTAT2, but not hSTAT1, consistent with previous reports (Fig. 7a)[5,16]. The co-IP assay, together with *in vitro* GST pull-down assay (Fig. 7b), further detected an interaction of hSTAT2 individually with the NS5 RdRp and MTase domains, suggesting that the interaction between ZIKV NS5 and hSTAT2 is mediated by both the MTase and RdRp domains of ZIKV NS5. Furthermore, size-exclusion chromatography analysis revealed that an N-terminal fragment of hSTAT2 (residues 1-713, hSTAT2$_{1-713}$) is sufficient for interaction with ZIKV NS5 (Fig. 7c). Together, these data defined the interacting domains for the ZIKV NS5 – hSTAT2 complex.

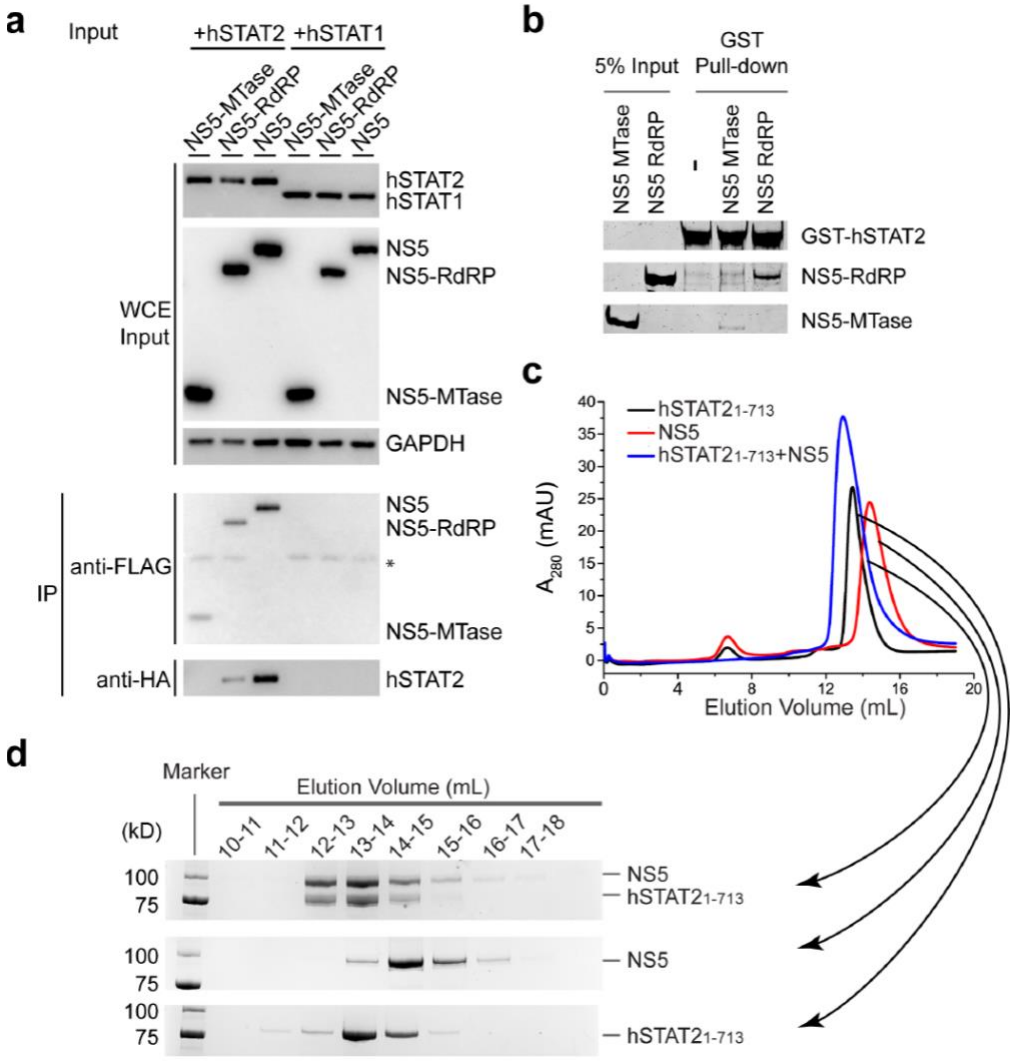

Figure 7. Biochemical analysis of the interaction between ZIKV NS5 and hSTAT2. a) Co-IP assay of 293T cells transfected with plasmids encoding C-terminally HA-tagged NS5 (NS5-HA) and FLAG-tagged hSTAT2 (hSTAT2-FLAG) or hSTAT1 (hSTAT1-FLAG). Immunoblot analysis of the whole cell extract (WCE) was used as input. IP was performed using antibodies against HA, FLAG and GAPDH. *antibody heavy chain. b) GST pull-down assay of the MTase and RdRp domains of ZIKV NS5 using GST-tagged full-length hSTAT2. c) Size-exclusion chromatography analysis of the interaction between hSTAT2$_{1-713}$ and ZIKV NS5. d) SDS-PAGE analysis of the elution fractions in (c).

Crystal Structure of the ZIKV RdRp-hSTAT2 complex

To define the atomic details of the ZIKV NS5–hSTAT2 interaction, we co-crystalized the ZIKV RdRp domain with a fragment of hSTAT2 (residues 1-713, hSTAT2$_{1-713}$) and solved the structure at 3.0 Å resolution (Fig. 8b,c, Table 2). We were able to trace NS5 RdRp, the core fragment (CF, residues 137-680) and the pY-tail segment (residues 690–705) of hSTAT2, along with partial hSTAT2 ND (residues 24–68 and residues 76–112) (Fig. 8b,c). The CF of hSTAT2 assumes an elongated fold, similar to that of STAT1[17,18] and other STAT proteins[19-21], with the CCD, DBD, LD and SH2 domains sequentially packed against each other to form an integrated core. Structural alignment of the hSTAT2 CF with the corresponding region of hSTAT1 gives a root-mean-square deviation (RMSD) of 0.57 Å over 404 Cα atoms, in line with the ~40% sequence identity between the CFs of these two proteins (Appendix B, Supplementary Fig. 4). The RdRp domain adopts a right-hand cup fold composed of palm, fingers and thumb subdomains with two zinc finger clusters, as previously observed (Fig. 8b and Appendix B, Supplementary Fig. 5a)[22-25]. Association of hSTAT2 with NS5 RdRp is mediated by the CCD of hSTAT2, which fills in a surface groove next to the RNA entrance tunnel of ZIKV RdRp (Appendix B, Supplementary Fig. 4b,c). In addition, the ND of hSTAT2 joins the rest of hSTAT2 only through an unresolved flexible linker and docks at the outer wall of the RNA exit tunnel of ZIKV RdRp (Appendix B, Supplementary Fig. 4b,d), yielding an average B-factor (~123 Å$_2$) significantly higher than the rest of the complex (~67 Å$_2$).

The pY-tail segment of hSTAT2 forms a β-strand that augments in antiparallel the β-sheet of the SH2 domain, with the side chain of its R694 forming a salt bridge with a sulfate ion embedded in the pY-engaging pocket of SH2. The same sulfate ion also engages a salt bridge with the potential pY-binding residue R601, mimicking the interaction between SH2 and the phosphate group of pY[26] (Appendix B, Supplementary Fig. 6a,b). Therefore, this intramolecular association of hSTAT2 potentially occludes the hSTAT2 SH2 domain from accessing other pY-containing fragments. At the N-terminus of the tail segment, the phosphorylation target Y690 is free of phosphorylation and in contact with SH2 residues H647 and Q649 through side-chain hydrogen bonding interactions (Appendix B, Supplementary Fig. 6a). These observations rationalize why dimerization of STAT2 with STAT1 entails the phosphorylation of STAT2 Y690[26], which presumably facilitates the displacement of the hSTAT2 pY-tail segment from the SH2 domain *in cis*.

It has been demonstrated that the pY-tail segment mediates homodimerization of STAT1, STAT3 and STAT6 proteins through both the reciprocal SH2–pY interaction and antiparallel tail pairing[17,19,20]. Given that the pY-tail segment of hSTAT2 bears high sequence homology with the corresponding fragments of STAT1 and other STAT family members (Appendix B, Supplementary Fig. 6c), it is conceivable that STAT2 heterodimerizes with STAT1 in a similar fashion as homodimerization of STAT1. We built a model of the ZIKV NS5–hSTAT2–hSTAT1-DNA complex based on the structure of the hSTAT1 homodimer and the ZIKV NS5–hSTAT2 complexes (Appendix B, Supplementary Fig. 6d). The structural model of the ZIKV NS5–hSTAT2–hSTAT1–

DNA complex suggests that hSTAT2 interacts with NS5 and DNA via distinct regions (Appendix B, Supplementary Fig. 6d). The hSTAT2 DBD, like the corresponding region of hSTAT1, participates in DNA binding through a positively charged surface (Appendix B, Supplementary Fig. 6d).

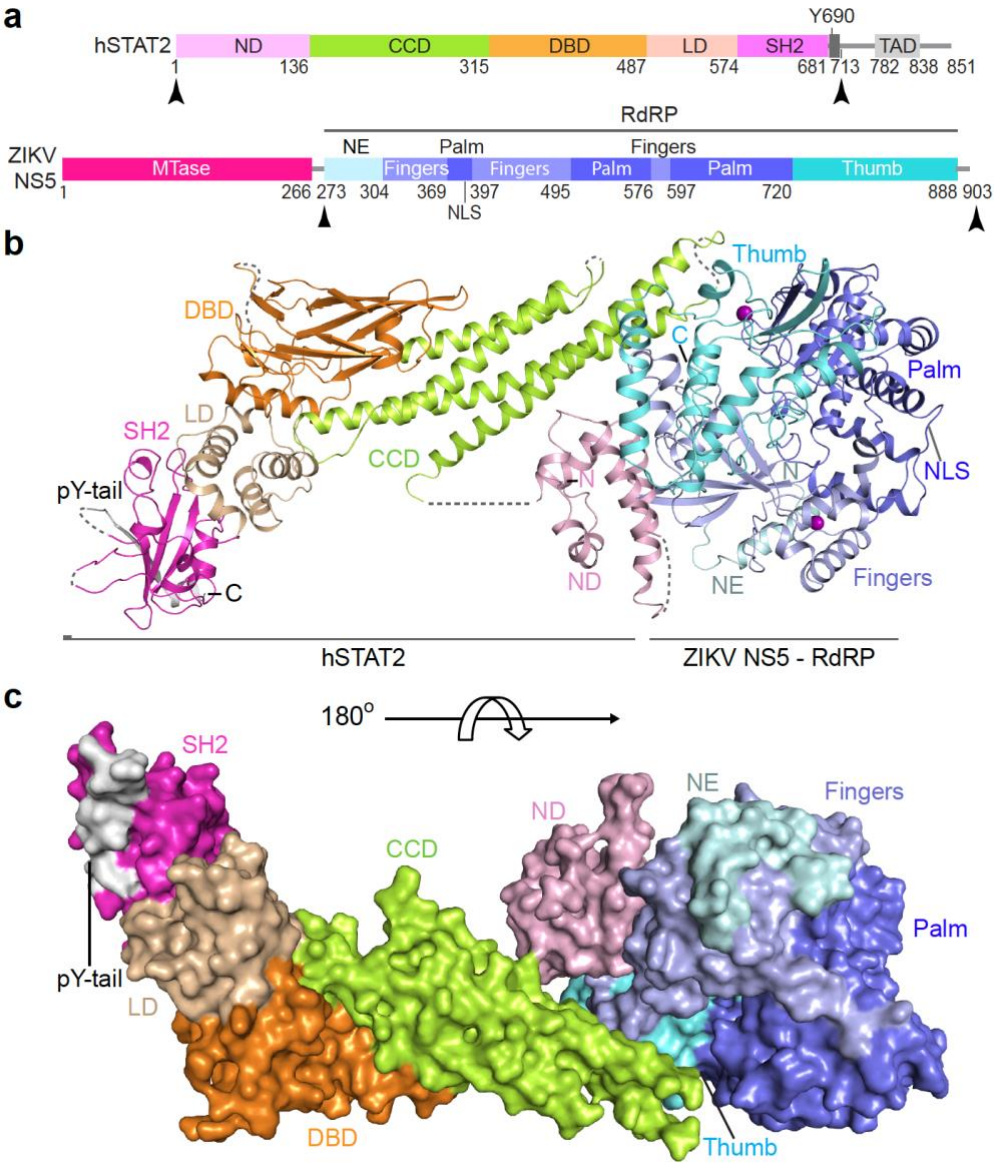

Figure 8. Crystal structure of the RdRp domain of ZIKV NS5 complexed with hSTAT2$_{1-713}$. a) ZIKV NS5 and hSTAT2 primary sequences with domains used for crystallization marked with arrowheads. NLS, nuclear localization signal. b) Ribbon representation of the ZIKV RdRp–hSTAT2$_{1-713}$ complex. The disordered linkers are shown as dashed lines. c) Surface representation of the ZIKV RdRp–hSTAT2$_{1-713}$ complex. The color scheme in (a-c) is applied to subsequent figures unless otherwise indicated.

Table 2. ZIKV RdRp - hSTAT2$_{1-713}$ X-ray crystallography data collection and refinement statistics

	ZIKV RdRp - hSTAT2$_{1-}$ (PDB 6UX2)
Data Collection	
Space group	*P*1 2$_1$ 1
Cell dimensions	
a, *b*, *c* (Å)	85.11, 124.7, 84.78
α, β, γ (°)	90, 109.39, 90
Resolution (Å)	50.00-3.00 (3.11-3.00)[a]
R_{merge}	0.126 (0.696)
$I/\sigma(I)$	10.26 (1.67)
$CC_{1/2}$	0.996 (0.813)
Completeness (%)	97.86 (83.07)
Redundancy	6.0 (5.0)
Refinement	
Resolution (Å)	49.24-3.01 (3.12-3.01)
No. Reflections	32543 (2733)
R_{work} / R_{free}	24.2/26.4 (35.6/37.8)
No. atoms	
Protein	9260
Ion (zinc, sulfate)	22
Water	83
B factors	
Protein	69.82
Ligand/ion	89.00
Water	56.40
RMSD	
Bond lengths (Å)	0.006
Bond angles (°)	1.00

[a]Values in parentheses are for highest-resolution shell.

Cryo-EM structure of full-length ZIKV NS5–hSTAT2 complex

To investigate how full-length ZIKV NS5 interacts with hSTAT2, we also determined the structure of full-length NS5 in complex with hSTAT2$_{1-713}$ using cryo-EM at 4.0 Å resolution (Fig. 9a,b, Table 3 and Appendix B, Supplementary Fig. 7-9). Due to structural flexibility and the existence of multiple conformations, the cryo-EM structure has resolutions varying from 3.5–4.0 Å for CCD, MTase and RdRp, to 4.0–5.0 Å for DBD, and 5.0–7.5 Å for LD and SH2 (Appendix B, Supplementary Fig. 7c). The cryo-EM map is of sufficient quality to allow atomic modeling of CCD, DBD and partial LD of hSTAT2, and both the MTase and RdRp domains of NS5 (Fig. 9a,b and Appendix B, Supplementary Fig. 8). Except for the MTase domain, these individual domains have been modeled in our crystal structure of NS5-RdRp – hSTAT2$_{1-713}$, which matches well with the cryo-EM density map (Appendix B, Supplementary Fig. 8). This fitting also reveals the densities corresponding to the MTase domain[24]. The atomic model of NS5–hSTAT2$_{1–713}$ shows that the tip of hSTAT2 CCD is anchored at the interdomain cleft formed between the MTase and RdRp domains of NS5 (Fig. 9a,b). This observation, consistent with our domain mapping analyses *ex vivo* and *in vitro* (Fig. 7), suggests that both the MTase and RdRp domains of NS5 interact with hSTAT2. Structural comparison of hSTAT2-bound NS5 with the previously reported free state[23-25] reveals a similar domain orientation between the MTase and RdRp domains (Appendix B, Supplementary Fig. 10a,b), with an RMSD of 2.3 Å over 778 aligned Cα atoms. The major difference between the two states concerns a slight movement of the MTase domain toward the hSTAT2 CCD in the hSTAT2-bound state (Appendix B, Supplementary Fig. 10b). The

lack of major changes in the NS5 structure between the two states implies that ZIKV NS5 has evolved with a conformation well poised for interaction with hSTAT2.

Table 3. ZIKV NS5 - hSTAT2 cryo-EM data collection, refinement and validation statistics

	ZIKV NS5 - hSTAT2 (EMD-21618, PDB 6WCZ)
Data collection and processing	
Magnification	x130,000
Voltage (kV)	300
Electron exposure (e^{-}/Å^2)	48
Defocus range (μm)	1.0-3.0
Pixel size (Å)	1.07
Symmetry imposed	*C1*
Initial particle images (no.)	868,048
Final particle images (no.)	118,760
Map resolution (Å)	4.0
FSC threshold	0.143
Map resolution range (Å)	50 – 4.0
Refinement	
Initial model used	6UX2
Model resolution (Å)	4.0
FSC threshold	0.143
Model resolution range (Å)	50 – 4.0
Map sharpening *B* factor (Å^2)	-167
Model composition	
Non-hydrogen atoms	9,893
Protein residues	1,231
Ion (zinc)	2
B factors (Å^2)	
Protein	-167
Ion (zinc)	-167
RMSD	
Bond lengths (Å)	0.01
Bond angles (°)	1.01
Validation	
MolProbity score	2.55
Clashscore	13.3
Poor rotamers (%)	2.08
Ramachandran plot	
Favored (%)	86.98
Allowed (%)	13.02
Disallowed (%)	0

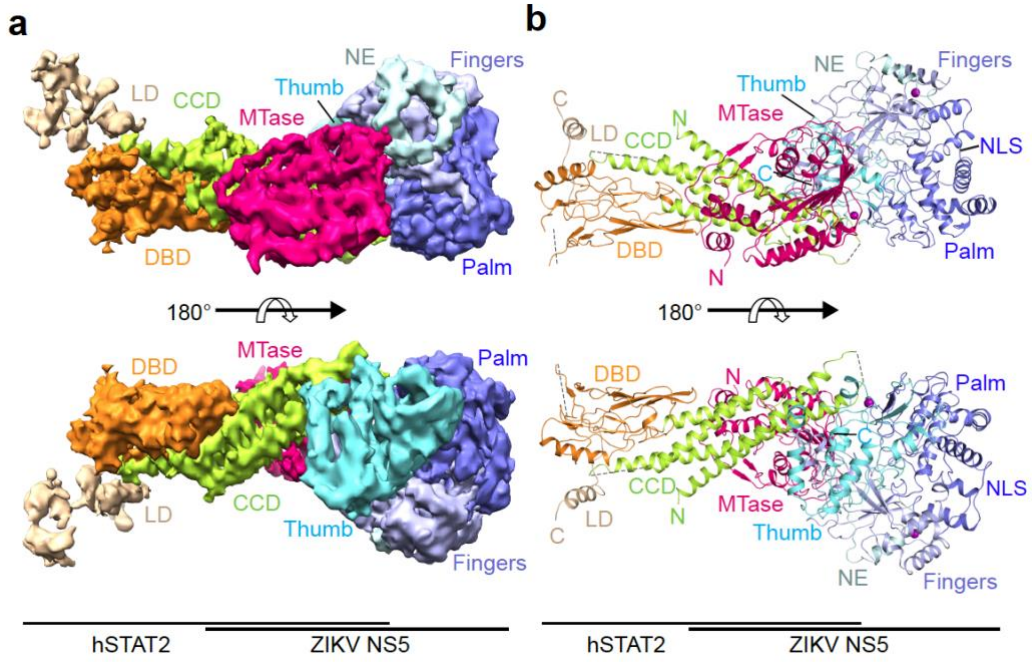

Figure 9. Cryo-EM structure of the full-length ZIKV NS5–hSTAT2$_{1-713}$ complex. a,b) Shaded surface views of the cryo-EM density map (a) and ribbon representation of the atomic model (b) of the ZIKV NS5–hSTAT2$_{1-713}$ complex from opposite sides.

The ZIKV RdRp–hSTAT2 association is mediated by complementarity between the convex surfaces formed by the helical ND and CCD of hSTAT2 and two separate surface grooves of RdRp (Fig. 10a–c). Of particular note are the aromatic ring stacking between hSTAT2 F175 and RdRp H855, and the hydrogen bonds between R176 from hSTAT2 CCD and RdRp residues, including the one with the backbone of G850 and the bidentate one with the side chain of D734 (Fig. 10b and Appendix B, Supplementary Fig. 5c). These interactions are reinforced by van der Waals contacts involving Q165, D168, Q169, D171, V172, I179, E195 and T202 of hSTAT2 CCD and V335-T337, L847, W848 and L852 of RdRp (Fig. 10b). At the second interface, hSTAT2 ND approaches the RdRp through van der Waals and hydrogen bonding interactions involving D53, F61, R92, Q95,

S98 and Q99 of hSTAT2 ND and T314, S317, V322, R327, A343 and I750 of RdRp (Fig. 10c and Appendix B, Supplementary Fig. 5d).

The NS5 MTase domain is anchored to the middle segment of hSTAT2 CCD, with the potential RNA binding surface of the MTase domain arching over the second and fourth helix of hSTAT2 CCD (Fig. 10d–f, and Appendix B, Supplementary Fig. 10c,d). Indeed, electrophoretic mobility shift assay (EMSA) confirms that hSTAT2 competes against a capped RNA molecule for ZIKV NS5 binding *in vitro* (Appendix B, Supplementary Fig. 10e). Notably, an α-helix from the MTase domain, comprised of residues S20-K28, is positioned in close proximity to residues K218, T225, L299, R300, Q303, E306 and R310 of hSTAT2 (Fig 8e), while the loop segment projected from the central β sheet of MTase, containing residues G107–H110, is docked onto a concave surface walled by hSTAT2 Q200, L203, N204, D207, Q289, D291 and P292 (Fig. 10f). These MTase–hSTAT2 interactions and the RdRp–hSTAT2 binding described above together constitute the molecular basis of ZIKV NS5–hSTAT2 association.

ZIKV NS5–hSTAT2 interaction and cellular localization of ZIKV NS5

To test our structural observations, we mutated key interaction-defining residues, including Y25 from NS5 MTase, R327, D734 and H855 from NS5 RdRp, and F175 and R176 from hSTAT2. The effects of these mutations on the protein-protein interaction were analyzed by co-IP assays using 293T cells transfected with HA-tagged ZIKV NS5 and FLAG-tagged hSTAT2. Mutation to alanine of hSTAT2 F175 or R176 substantially reduced the binding of hSTAT2 with NS5 (Fig. 10g). Likewise, introduction of the

D734A/H855A (NS5 Mut$_{DH}$), Y25A/D734A/H855A (NS5 Mut$_{YDH}$), R327A/D734A/H855A (NS5 Mut$_{RDH}$) or Y25A/R327A/D734A/H855A (NS5 Mut$_{YRDH}$) mutations into ZIKV NS5 also largely reduced the NS5–hSTAT2 interaction (Fig. 10h). Consistently, co-IP assays with endogenous hSTAT2 indicate that hSTAT2 binds strongly to wildtype ZIKV NS5, but not to NS5 Mut$_{YRDH}$ (Fig. 10i). Additional *in vitro* GST pull-down assays with these NS5 mutants confirmed the co-IP results (Fig. 10j). These data lend strong support to the interaction mechanism identified in our NS5–hSTAT2$_{1-713}$ structures.

A previous study demonstrated that, as with other flaviviruses[27], ZIKV NS5 localizes predominantly within the nucleus in the absence of hSTAT2 overexpression; yet co-expression of ZIKV NS5 with hSTAT2 leads to their co-localization in the cytoplasm[5]. To evaluate the effect of the ZIKV NS5–hSTAT2 interaction on cellular localization of ZIKV NS5, we performed immunofluorescence (IF) assays on ZIKV NS5 and hSTAT2 using 293T cells. Consistent with the previous study[5], co-expression of wildtype ZIKV NS5 with hSTAT2 led to complete retention of ZIKV NS5 in the cytoplasm (Fig. 11). By contrast, ~60-90% of NS5 Mut$_{DH}$, Mut$_{YDH}$, Mut$_{RDH}$ or Mut$_{YRDH}$ proteins were localized to the nucleus, with hSTAT2 remaining in the cytoplasm (Fig. 11). Cytoplasmic co-localization of ZIKV NS5 and hSTAT2 was most severely disrupted with the expression of NS5 Mut$_{RDH}$ or Mut$_{YRDH}$ (Fig. 11). These results suggest that the interaction of ZIKV NS5–hSTAT2 underlies the cytoplasmic co-localization of ZIKV NS5 and hSTAT2.

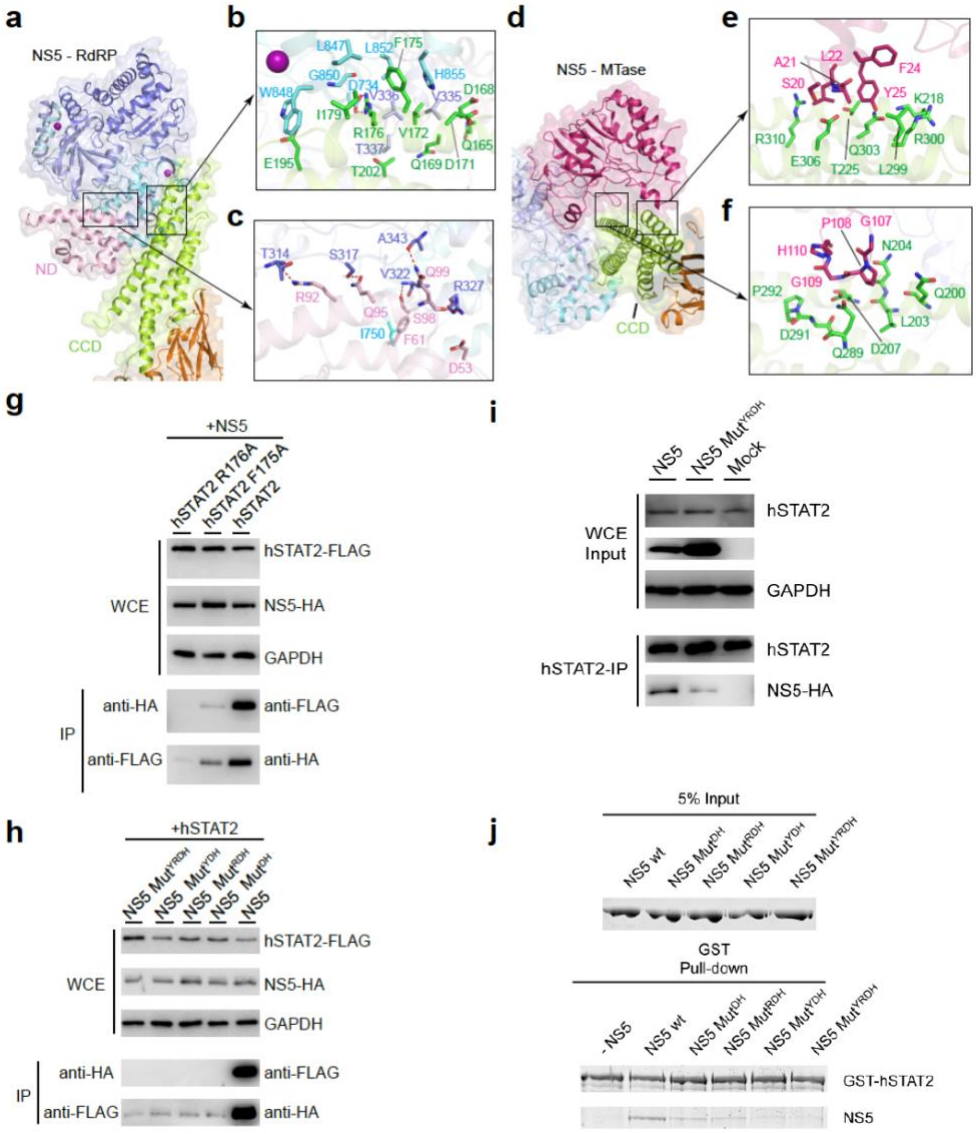

Figure 10. Mutational analysis of the ZIKV NS5–hSTAT2 interaction. a–c) Ribbon and surface view showing NS5 RdRp–hSTAT2 interaction (a), with the details for the CCD- and ND mediated interactions highlighted in expanded views (b) and (c), respectively. d–f) Ribbon and surface view of the NS5 MTase–hSTAT2 interaction (d), with details highlighted in expanded views (e) and (f). Hydrogen bonds in are shown as dashed lines. g,h) Co-IP analysis showing the effects of hSTAT2 mutations (g) and NS5 mutations (h) on the NS5–hSTAT2 interaction. i) IP analysis of endogenous hSTAT2 in 293T cells transfected with WT or NS5 MutYRDH. Immunoblot analysis of the IPs and whole cell extracts (WCE) were performed using antibodies against HA, FLAG, hSTAT2 and GAPDH. j) *In vitro* pull-down assay of ZIKV NS5 mutations using GST-hSTAT2 as bait. wt: wildtype.

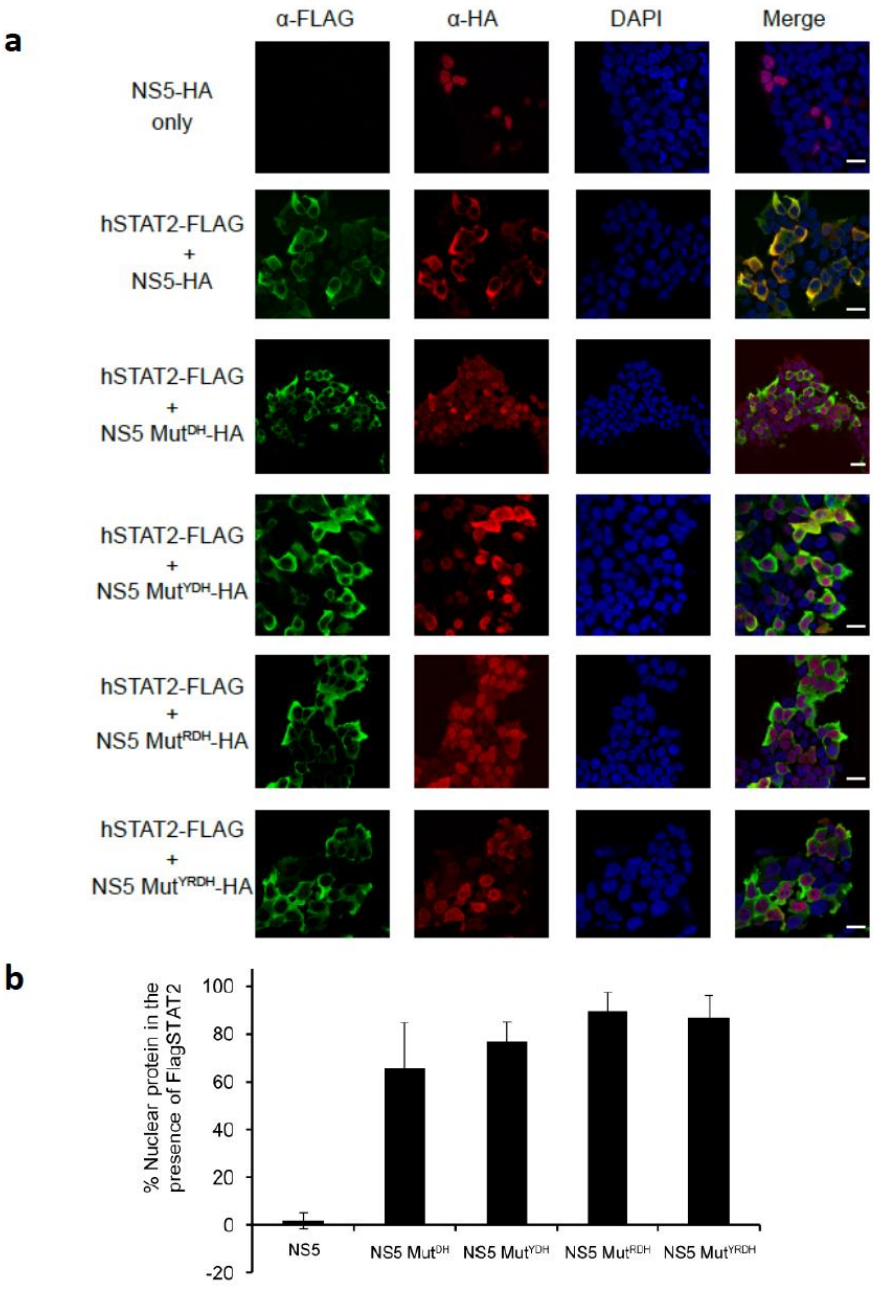

Figure 11. Cellular analysis of the interaction between ZIKV NS5 and hSTAT2. a) Representative IF images of 293T cells transfected with plasmids encoding NS5-HA and/or hSTAT2-FLAG. The transfected cells were fixed for immune staining using antibodies against HA (red) and FLAG (green). Nuclei were visualized by DAPI (blue) counter staining. Scale bars, 20 μm. b) Quantification of nuclear localization of NS5 (wildtype) or mutants as shown in (a). Data are mean ± s.d. (n=3 biologically independent samples).

ZIKV NS5 competes against IRF9 for hSTAT2 binding

STAT2 and IRF9 form a cognate complex in cells, which plays a critical role in regulating the nuclear shuffling of STAT2 and IFN response[28,29]. Previous studies revealed that the interaction between STAT2 and IRF9 is also mediated by the STAT2 CCD[30,31]. Structural comparison of ZIKV NS5- and IRF9-bound STAT2 proteins reveals a remarkably similar surface for ZIKV NS5 and IRF9 binding[31] (Fig. 12a,b), and our ITC binding assays confirm that both ZIKV NS5 and IRF9 bind to hSTAT2 strongly, with the dissociation constants (Kd) falling into the ranges of μM and sub-μM, respectively (Fig. 12c,d). To determine whether the presence of ZIKV NS5 affects the association of STAT2 with IRF9, we carried out co-IP assays using 293T cells transfected with FLAG-tagged hSTAT2, HA-tagged ZIKV NS5 or myc-tagged IRF9 and found that increasing expression of NS5 led to a gradual decrease of IRF9 – hSTAT2 association and vice versa (Fig. 12e). Consistently, *in vitro* GST pull-down assay indicated that the association of ZIKV NS5 with hSTAT2 decreases with increasing amounts of IRF9 (Fig. 12f). Furthermore, our FLAG-IP assay indicates that ZIKV NS5 interaction-defective F175A or R176A mutation of hSTAT2 also disrupted the hSTAT2-IRF9 interaction (Fig. 12g). These data therefore suggest that ZIKV NS5 competes against IRF9 for STAT2 binding, which may consequently disrupt the formation of ISGF3 complex required for antiviral gene expression. Inhibition of the ISGF3 complex formation might further contribute to the cytoplasmic retention of hSTAT2 and facilitate NS5-mediated IFN suppression. Together, our structural and functional studies define the atomic details of the NS5–hSTAT2 interaction underlying not only the infection-triggered hSTAT2 degradation but

also possible degradation-independent ISGF3 suppression, leading to multimodal inhibition of IFN responses, and to establishment of successful viral infection.

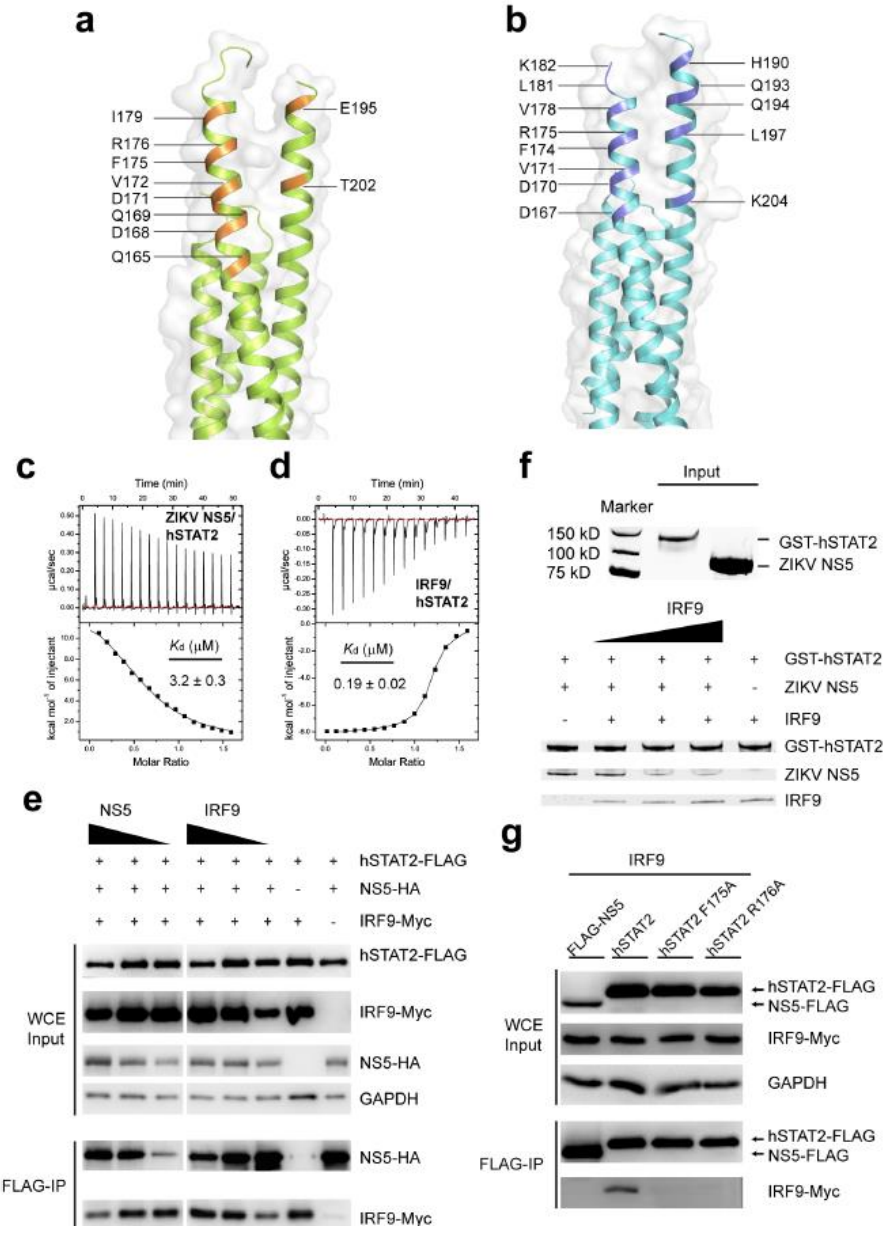

Figure 12. ZIKV NS5 competes against IRF9 for hSTAT2 binding. a) Ribbon and surface view of the ZIKV NS5-binding sites (orange) of hSTAT2 CCD. b) Ribbon and surface view of the ZIKV NS5-binding sites (blue) of mouse STAT2 CCD. c,d) ITC binding curves of hSTAT2 over ZIKV NS5 (c) and IRF9 (d). The ITC binding assays were performed twice for the hSTAT2-NS5 interaction with similar result, and once for the hSTAT2-IRF9 interaction. e) Co-IP assay of HA-tagged ZIKV NS5 (NS5-HA), FLAG-tagged hSTAT2 (hSTAT2-FLAG) or hSTAT1 (hSTAT1-FLAG) and myc-tagged IRF9 (IRF9-Myc). f) In vitro pulldown assay of ZIKV NS5 using GSThSTAT2 in the presence of various amount of IRF9. g, IP assay of IRF9-Myc with hSTAT2-FLAG, wild type or mutant. The experiment in (g) was repeated once with similar results.

DENV-2 and ZIKV NS5s share a similar hSTAT2-binding mechanism

Sequence analysis of the ZIKV NS5 regions that interact with hSTAT2 shows relatively high conservation among the flaviviruses for the residues interacting with the CCD region but less conservation for the residues interacting with the ND region (Appendix B, Supplementary Fig. 11), which might contribute to the evolutionarily divergent mechanisms of NS5-mediated immunosuppression[5]. On the other hand, the hSTAT2-interacting residues of ZIKV NS5 are considerably well-conserved in DENV and other members of the *Flaviviridae* family (Appendix B, Supplementary Fig. 11c,d), raising the possibility that DENV NS5 might interact with hSTAT2 similarly. To test this, we determined the EM structure of the DENV serotype 2 (DENV-2) NS5–hSTAT2 complex (Fig. 13a and Appendix B, Supplementary Fig. 11e,f). Indeed, DENV-2 NS5 associates with hSTAT2 in a similar manner as ZIKV NS5, with one end of the hSTAT2 CCD embraced by both the MTase and RdRp domains of DENV-2 NS5. Note that two different conformations of DENV NS5 have been reported previously, with an extended conformation observed for DENV-2 NS5[32] and a compact conformation observed for DENV-3 NS5[33], which likely arises from conformational heterogeneity of DENV NS5 in solution[34]. The structure of hSTAT2-bound ZIKV NS5, mimic of hSTAT2-bound DENV-2 NS5, fits well with the extended conformation of DENV-2 NS5 (Fig. 13), but not with the compact fold of DENV-3 NS5 (Appendix B, Supplementary Fig. 11g). These observations suggest a conserved conformational selection mechanism in the interaction between flavivirus NS5 and hSTAT2.

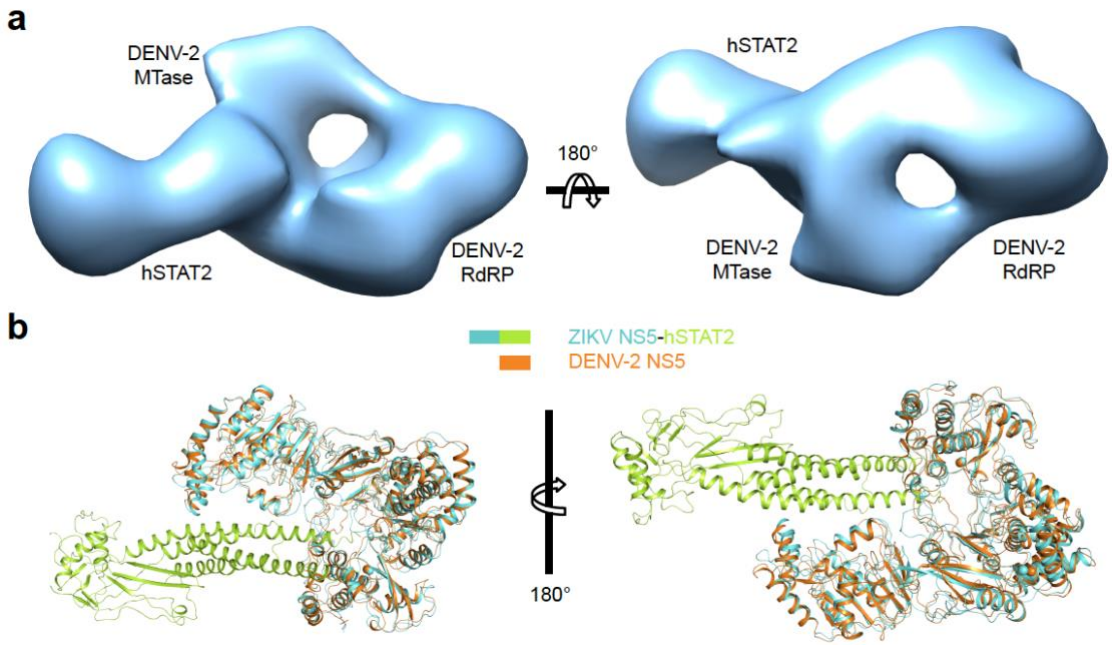

Figure 13. Cryo-EM structure of the full-length DENV-2 NS5–hSTAT2$_{1-713}$ complex and comparison with ZIKV NS5–hSTAT2$_{1-713}$. a) Two opposite views of the EM density map for the DENV-2 NS5–hSTAT2 complex. b) Superposition of the crystal structure of free DENV-2 NS5 (orange; PDB 5ZQK) and the cryo-EM structure of ZIKV NS5-hSTAT2 complex.

To confirm our structural observations, we mutated the residues D732 and L853 of DENV-2 NS5, equivalent to D734 and H855 of ZIKV NS5 (Fig. 14a), to alanine and performed co-IP assay using 293T cells co-transfected with FLAG-tagged hSTAT2 and HA-tagged DENV-2 NS5. Wildtype DENV-2 NS5 interacted strongly with hSTAT2, but variants carrying the single mutations D732A or L853A or double mutation D732A/L853A did not (Fig. 14a). Furthermore, our FLAG-IP assay indicates that hSTAT2 mutations F175A or R176A, which inhibit ZIKV NS5 interaction (Fig. 10g), also disrupt the hSTAT2-DENV-2 NS5 interaction (Fig. 14b). Finally, IF analysis reveals that ectopic expression of hSTAT2 led to retention of wildtype, but not D732A/L853A-

mutated DENV-2 NS5, to the cytoplasm (Fig. 14c). Together, these data suggest that DENV-2 NS5 and ZIKV NS5 engage hSTAT2 in a similar fashion.

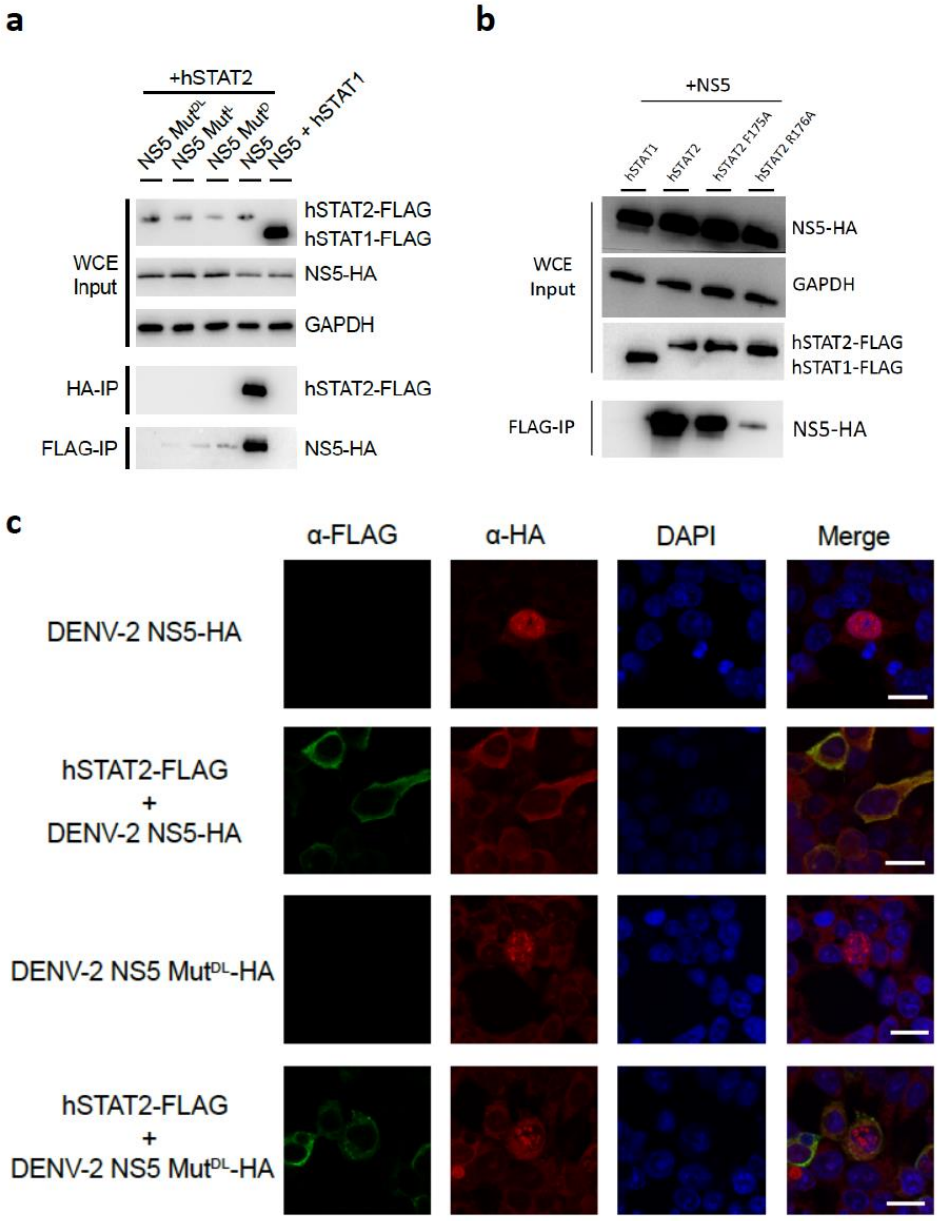

Figure 14. Mutational and cellular analysis of DENV-2 NS5 interaction with hSTAT2. a) Co-IP assay of HA-tagged DENV-2 NS5 (NS5-HA), FLAG-tagged hSTAT2 (STAT2-FLAG) or hSTAT1 (hSTAT1-FLAG). The D732A, L853A and D732A/L853A mutations are denoted as MutD, MutL and MutDL, respectively. b) Co-IP assay showing the effects of hSTAT2 mutations F175A and R176A on DENV-2 NS5 interaction. c) Representative IF images of 293T cells transfected with plasmids encoding DENV-2 NS5-HA and/or hSTAT2-FLAG. The transfected cells were fixed for immune staining using antibodies against HA (red) and FLAG (green). Nuclei were visualized by DAPI (blue) counter staining. Scale bars, 20 μm.

Discussion

The STAT family of proteins, in particular STAT1 and STAT2, plays critical roles in eliciting IFN responses against viral infection. Not surprisingly, these proteins are among the first targets of viral attacks. To date, the molecular basis for virus-mediated suppression of STAT function remains unclear, due to the lack of structural information on the complexes between STATs and any viral antagonist. The structural, biochemical and cellular analyses of the ZIKV NS5–hSTAT2 and DENV-2 NS5–hSTAT2 complexes presented here reveal for the first time the underlying principle for the interactions between STAT proteins and viral antagonists. This study not only provides important mechanistic insights into the IFN suppression by a viral antagonist, but also sheds light onto the rational design of vaccine or other therapeutic strategies against viral infections.

Flavivirus NS5 proteins have widely evolved into antagonists for IFN signaling[5,35-40]. For instance, the NS5 proteins from ZIKV, DENV and yellow fever virus (YFV) have been shown to interact with hSTAT2 to promote its degradation[4,5] or prevent its binding to promoter elements of target genes[37]. Interestingly, none of these NS5s are able to interact with mouse STAT2[5,41,42]. The amino acid sequence identity among most of the STAT family is highly conserved between mouse and human, ranging from 85% identity for STAT6 to 98% for STAT3. In contrast, the STAT2 sequence identity between mouse and human is only 68%[43,44], perhaps explaining the differential binding abilities between NS5 and mouse and human STAT2s.

How the sequence and conformation of flavivirus NS5s were shaped to underpin hSTAT2 antagonistic activity is an intriguing question considering the evolutionary

constraints imposed on this protein to retain its enzymatic activity. Interestingly, ZIKV NS5 is most similar to that of Spondweni virus (SPOV) with 77% amino acid identity[45]. However, the mechanism of ZIKV NS5 IFN-I antagonism most closely resembles that of DENV NS5 (discussed below), with which it shares only 65% identity. SPOV NS5 inhibits JAK-STAT signaling from within the nucleus at a point downstream of STAT2 and does not interact with STAT2[5]. Similarly, ZIKV NS5 is only 61% identical to the YFV NS5, which also interacts with hSTAT2. However, IFN stimulation is required for YFV NS5-hSTAT2 association, in contrast with ZIKV and DENV NS5[37,42]. It has been suggested that the STAT2 conformational change induced by STAT1-STAT2 heterodimerization may be required for YFV NS5 association[37]. In this case, the hSTAT2-interacting residues of YFV NS5 would likely be very different from those of ZIKV and DENV NS5s. Indeed, most of the hSTAT2-interacting residues of ZIKV and DENV NS5 identified here are not conserved in the YFV NS5 protein (Appendix B, Supplementary Fig. 11). The YFV NS5 residues required for hSTAT2 interaction have not been identified and the structure of this complex has not been solved. This information would help elucidate how the different flavivirus NS5s are able to associate with hSTAT2.

The structures of ZIKV NS5–hSTAT2 and DENV-2 NS5–hSTAT2 complexes reveal multivalent interactions. The interdomain cleft between the MTase and RdRp domains of the NS5 proteins provides a surface complementarity with the CCD of hSTAT2 for specific molecular recognition. This interaction mode is shared between ZIKV NS5 and DENV NS5, suggesting a conserved mechanism for the interactions

between hSTAT2 and flavivirus NS5 proteins (Fig. 15). As the largest and most highly conserved flavivirus protein, NS5 has been shown to exist in multiple conformations in solution, presumably due to the weak MTase–RdRp domain interaction[24,25,33,34,46,47]. So far, structural evidence has revealed two alternative conformations of flavivirus NS5, corresponding to two distinct domain interfaces: the structures of free ZIKV NS5, DENV-2 NS5 and JEV NS5 represent an extended fold, with a large interdomain cleft exposed to solvent[24,25,46,47]. By contrast, the crystal structure of DENV-3 NS5 exhibits a compact fold, with a less accessible MTase–RdRp domain interface, a conformation that is closely related to the conformation adopted for NS5-mediated RNA replication[33]. Given that these two alternative domain interfaces are both conserved in sequence[48], it is conceivable that the two conformations of NS5 coexist in solution. The structures of the hSTAT2-bound either to DENV-2 NS5 or ZIKV NS5 presented in this study indicated that both proteins adopt the extended conformation for hSTAT2 interaction, suggesting a conformational selection mechanism in their binding to hSTAT2 (Fig. 15).

Structural and biochemical analyses presented in this study demonstrate that the interaction between ZIKV NS5 and hSTAT2 may lead to multiple functional consequences. Intriguingly, we observe that ZIKV NS5 competes against IRF9 for the same interaction interface on hSTAT2, potentially leading to suppression of the complex formation of ISGF3. In light of the critical role of the ISGF3 complex in STAT2-mediated IFN response, these data suggest that ZIKV NS5 suppresses hSTAT2 not only through promoting its proteasome-mediated degradation, but also through blocking the formation of ISGF3 complex. Inhibition of the ISGF3 complex formation not only

suppresses antiviral gene expression but might also affect the nuclear shuffling of hSTAT2 and its proteasome-mediated degradation, therefore constituting a multifaceted regulatory mechanism of hSTAT2 suppression (Fig. 15). It is worth noting that previous studies have identified multiple mechanisms for nuclear relocation of flavivirus NS5s[49,50]. For instance, a C-terminal 18-residue fragment of DENV-2 NS5 has been shown to mediate its nuclear localization; such a fragment is not conserved in DENV-1 NS5, leading to cytoplasmic localization of DENV-1[49]. Given the diversity between different serotypes of DENV, it is worth noting that the mechanism by which the hSTAT2 interaction affects DENVs other than serotype 2 remains to be determined. In addition, a recent study has identified residues K390-R393 of ZIKV NS5 as a nuclear localization sequence, which mediates the association of ZIKV NS5 with importin-α to form supramolecular nuclear bodies in cells[50]. In this regard, this study mapped the hSTAT2-interaction sites onto distinct regions of ZIKV NS5 (Fig. 8 and 9) or DENV-2 NS5 (Fig. 13a,b), suggesting that the interaction of NS5 with hSTAT2 would not prevent its binding to importin, thereby implying a novel mechanism for cytoplasmic retention of ZIKV NS5. On the other hand, our data also indicate that the interaction between hSTAT2 and ZIKV NS5 potentially impairs the activity of the NS5 protein through reducing its RNA binding affinity (Appendix B, Supplementary Fig. 10), suggesting multi-layered functional antagonism between hSTAT2 and ZIKV NS5.

A common theme among all members of the STAT family is pY-dependent dimerization. The crystal structures of homodimeric STAT1, STAT3 and STAT6 reveal that dimerization of STATs is mediated by the mutual SH2–pY association, reinforced by

the anti-parallel pairing of the tail segment immediately downstream of the pY site[17,19,20]. However, how the phosphorylation event triggers the monomer-dimer transition of STATs remains unclear. Surprisingly, the structure of hSTAT2 presented in this study reveals that the unphosphorylated pY-tail segment of hSTAT2 folds back to block the pY-binding site of the SH2 domain, with phosphorylation site Y690 interacting with SH2 through side-chain hydrogen bonding interactions (Appendix B, Supplementary Fig. 6a). Phosphorylation of hSTAT2 Y690 presumably would lead to impaired tail–SH2 association of hSTAT2, permitting the repositioning of the tail segment for an inter-molecular interaction, thereby providing a potential autoinhibitory mechanism in controlling the dimerization of STAT2 or other STATs. Furthermore, our modeling analysis suggests that the complex of STAT1–STAT2 dimer adopts the same architecture as the STAT1 homodimer and presents a potential DNA-binding surface of the hSTAT2 DBD. Together, these data provide a framework for understanding the regulation and structure of the ISGF3 complex.

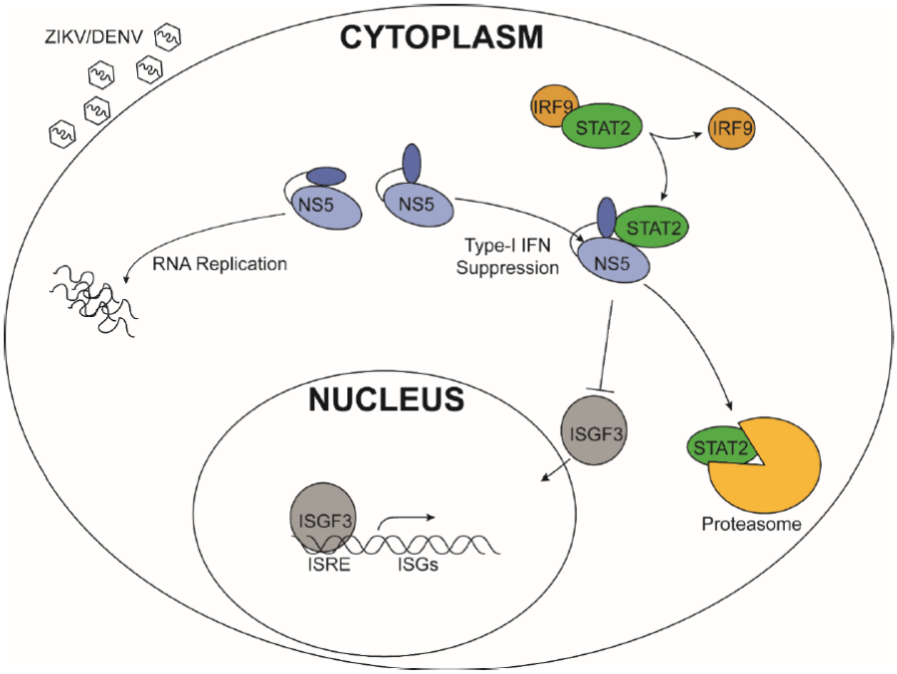

Figure 15. Model of ZIKV/DENV NS5-mediated hSTAT2 degradation and IFN response suppression. Inside an infected cell, ZIKV/DENV NS5 exhibits heterogeneous conformations, with the extended fold poised for hSTAT2 binding and the compact fold likely involved in RNA replication. The NS5 – hSTAT2 interaction suppresses the formation of ISGF3 through promoting hSTAT2 degradation and inhibiting the hSTAT2 – IRF9 interaction.

Materials and Methods

Protein expression and purification.

For structural studies, the cDNA sequences encoding full-length ZIKV NS5, its MTase (residues 1-273) and RdRp (residues 273-903) domains, full-length DENV-2 NS5, an N-terminal fragment of hSTAT2 (residues 1-713, $hSTAT2_{1-713}$) and full-length human IRF9 were each inserted into a modified pRSFDuet-1 vector (Novagen), preceded by a His_6-SUMO tag and ULP1 (Ubiquitin like protease 1) cleavage site. For *in vitro* pull-down assays, the cDNA sequence encoding full-length hSTAT2 was cloned into the pGEX6P-1 vector (GE Healthcare). Expression and purification of the His_6-SUMO-tagged ZIKV NS5, full-length or fragments, and $hSTAT2_{1-713}$, followed a previously described protocol with slight modifications[24]. In short, the NS5 or $hSTAT2_{1-713}$ fusion proteins were expressed in *E. coli* BL21 DE3 (RIL) cell strains (Agilent Technologies) and purified sequentially using a Ni^{2+}-NTA column and a butyl Sepharose column (GE Healthcare). The His_6-SUMO tag was subsequently removed through ULP1-mediated cleavage, followed by size exclusion chromatography on a Superdex 200 16/600 column (GE Healthcare) pre-equilibrated with buffer containing 25 mM Tris-HCl (pH 7.5), 500 mM NaCl, 5 mM DTT and 5% glycerol. His_6-SUMO-tagged IRF9 was expressed and purified similarly as ZIKV NS5 and hSTAT2, except that additional ion exchange chromatography on a heparin column was introduced between Ni-NTA chromatography and size-exclusion chromatography. Protein solutions of RdRp and $hSTAT2_{1-713}$ were respectively concentrated to 20 mg/mL and 30 mg/mL through ultrafiltration with Amicon filters (Millipore), and were frozen at -80°C for storage. For GST pull-down

assays, the GST-tagged full-length hSTAT2 protein was first purified using a glutathione Sepharose Fast Flow 4 column, followed by ion exchange chromatography on a Heparin column (GE Healthcare) and size-exclusion chromatography on a Superdex 200 16/600 column (GE Healthcare) using the buffer as described above.

Expression and purification of DENV-2 NS5, and ZIKV NS5 and hSTAT2 mutants followed the same approach as that for wildtype proteins, except that purification of DENV-2 NS5 did not require the butyl Sepharose step.

Crystallization and X-ray structure determination.

To assemble the NS5 RdRp–hSTAT2 complex, equimolar ZIKV RdRp and $hSTAT2_{1-713}$ were mixed to achieve a final protein concentration of ~6 mg/mL. The crystallization condition was initially identified via sparse matrix screening kits (Qiagen Inc.), and further optimized through hanging-drop vapor diffusion method by mixing 1 μL of the ZIKV RdRp–$hSTAT2_{1-713}$ complex with 1 μL of precipitant solution (0.2 M ammonium sulfate, 11% PEG 8000 and 0.1 M Tris-HCl, pH 8.5). Crystals were equilibrated in a cryoprotectant comprised of precipitant solution supplemented with additional 30% glycerol and were subsequently flash-frozen in liquid nitrogen.

The X-ray diffraction data for the ZIKV RdRp–hSTAT2 complex were collected on the BL 5.0.1 beamline at the Advanced Light Source, Lawrence Berkeley National Laboratory. The diffraction data were processed using the HKL2000 program[51]. The complex structure was solved by the molecular replacement method using PHASER[52] with the structures of free ZIKV NS5 (PDB ID: 5TMH) and human STAT1 (PDB ID:

1YVL) as search models. The structure was further refined by iterative model building and refinement with Coot[53] and Phenix[54], respectively. The statistics of data collection and structure determination are summarized in Table 2.

Cryo-EM data acquisition.

The protein samples of hSTAT2$_{1-713}$ and ZIKV NS5 were mixed in a 1:1 molar ratio, followed by size-exclusion chromatography on a Superdex 200 10/300 column (GE Healthcare) pre-equilibrated with buffer containing 25 mM Tris-HCl (pH 7.5), 175 mM NaCl and 5 mM DTT. The peak was collected and subjected to negative stain electron microscopy for sample optimization.

For cryo-EM sample preparation, an aliquot of 2.5 μL of the above optimized ZIKV NS5–hSTAT2$_{1-713}$ sample at a concentration of approximately 0.5 mg/ml was applied to a Quantifoil holey carbon grid (1.2/1.3, 300 mesh), that was glow discharged for 25 seconds with a PELCO Easy Glow system. The grid was blotted and plunge-frozen in liquid ethane with a Vitrobot IV (Thermo-Fisher) at 4°C under 100% humidity. The frozen grids were stored in liquid nitrogen before use. For cryo-EM image acquisition, the cryo-EM grids were loaded into an FEI Titan Krios electron microscope equipped with Gatan Quantum imaging filter (GIF) and a post-GIF K2 Summit direct electron detector. Movies were recorded as dose-fractionated frames in super-resolution mode with Legion3.1[55] at nominal magnification of 130,000X, corresponding to a calibrated pixel size 0.535 Å on the specimen. The slit width in the GIF system was set to 20eV to remove inelastically scattered electrons. A total of 1859 movies were recorded for the

data set, the dose rate on the camera was set to 1.7 electrons/pixel/s, corresponding to 6.0 electrons/Å^2/s. An exposure time of 8 sec was used at a rate of 0.2 s/frame, giving rise to 40 frames and a total dosage of 48 electrons/Å^2 for each movie. Details of the experimental conditions are summarized in Table 3.

Cryo-EM data processing.

All but the first and last frames in each movie were motion-corrected with a subframe 5x5 to generate two motion-corrected micrographs (with and without dose-weighting), which were both binned 2x2 to yield a pixel size of 1.07Å with MotionCor2[56]. The micrographs without dose-weighting were used for contrast transfer function (CTF) determination with ctffind version 4.1.18[57] and for particle picking with Gautomatch (https://www.mrc-lmb.cam.ac.uk/kzhang/). The micrographs with dose-weighing were used for particle extraction and 3D reconstruction, as detailed below.

We selected 1762 micrographs by discarding those either with under-focus values greater than 3.0 μm or containing crystalline ice. A total of 1,088,157 particles were extracted from these selected micrographs using RELION[58,59]. These particles were subjected to a reference-free 2D classification by requesting 200 classes. Based on the presence of structures in the 2D class averages, we selected 868,048 particles (Appendix B, Supplementary Fig. 9), which were subjected to a three-dimensional (3D) classification in RELION with C1 symmetry. The initial reference used for this 3D classification step was generated by cryoSPARC[60] from the same particles. The 3D classification was used to sort particles into 3 classes with 5 pixels and 3.8º as the

translation and rotation search parameters, respectively. 35% of the particles were classified into a class with clear secondary structures features (Appendix B, Supplementary Fig. 9). The particles in this "good" class were then subjected to another round of 3D classification by requesting 3 classes, which further yielded a new "good" class with improved structural features. The 118,760 particles in this new "good" class were subjected to 3D auto-refinement and post process, yielding a map at 4.0 Å resolution (Appendix B, Supplementary Fig. 7). Data processing workflow is detailed in Appendix B, Supplementary Fig. 9.

The global resolution reported above is based on the ''gold standard'' refinement procedures and the 0.143 Fourier shell correlation (FSC) criterion. Local resolution evaluation (Appendix B, Supplementary Fig. 7) was performed with Resmap[61].

Atomic model building based on the cryo-EM map.

Atomic model building was accomplished in an iterative process involving Coot, Chimera[62] and Phenix. Briefly, the above crystal structure of ZIKV RdRp–hSTAT2 was fitted into the cryo-EM map as initial models by using the 'fit in map' routine in Chimera. This fit revealed the extra density corresponding to the MTase domain and the absence of density for ND, suggesting high flexibility of ND in solution (indeed, even in the crystal, ND is partially disordered). The cryo-EM densities for SH2 and partial LD were of insufficient quality for model building. The crystal structure of the MTase domain (PDB 5TMH) fits perfectly into the cryo-EM density and was combined with our crystal structure of NS5 RdRp–hSTAT2$_{1\text{-}713}$ to create an initial atomic model for NS5–

hSTAT2$_{1-713}$, which was refined by 'real-space refinement' in Phenix. We then manually adjusted side chains and linker loops to match the cryo-EM density map with Coot. This process of real space refinement and manual adjustment steps was repeated iteratively until the peptide backbone and side chain conformations were optimized. Ramachandran and secondary structure restrains were used during the refinement. Our final atomic model consists of the full-length NS5 and residues 140-509 of hSTAT2 with good model geometry, as summarized in Table 3.

Negative-stain data acquisition and structure determination.

The protein samples of hSTAT2$_{1-713}$ and DENV-2 NS5 were mixed in a 1:1 molar ratio, and purified in the same manner as that for the hSTAT2$_{1-713}$–ZIKV NS5 complex. An aliquot of 3 μL of the complex sample was then applied to the carbon-coated grid and incubated for 1 min. After removal of the excess sample solution, the grid was stained with 1% (w/v) uranyl formate. Negative-stain EM micrographs were acquired manually and a TIETZ F415MP 16-megapixel CCD camera at 68,027X magnification in an FEI Tecnai F20 electron microscope operated at 200 kV. The micrographs were saved by 2X binning to yield a pixel size of 4.4 Å.

For negative-stain EM data processing, 138,246 particles were extracted from 300 micrographs using RELION. These particles were subjected to a reference-free 2D classification by requesting 100 classes. Based on the 2D class averages results, we selected 116,778 particles, which were subjected to a three-dimensional (3D) classification by requesting 3 classes. The initial reference used for this 3D classification

step was generated by cryoSPARC from the same particles. Based on the 3D classification results, 35,062 particles in one class were subjected to 3D auto-refinement, yielding a map at about 17.1 Å resolution (Fig. 11a, Appendix B, Supplementary Fig. 11e,f). The crystal structures of the MTase and RdRp domains of DENV-2 NS5 (PDB 5ZQK) and hSTAT2 (from this study) were respectively fitted into the EM map by using the 'fit in map' routine in Chimera.

GST pull-down assays.

60 μg of GST-hSTAT2 fusion protein was incubated with 150 μg of ZIKV NS5, in the form of either full-length or individual domains, wildtype or mutants, in a 1 mL pull-down buffer (10 mM Tris-Cl, pH 8.0, 100 mM NaCl, 5% glycerol, 5mM DTT and 0.1% Triton X-100) for 1 hour at 4°C. The mixtures were centrifuged at the speed of 15,000 rpm on an 5424R Eppendorf microcentrifuge for 15 min, followed by incubation of the supernatant with 20 μL glutathione sepharose 4 fast flow resins (GE Healthcare) for 15 min. Subsequently, the beads were separated from the supernatant through centrifugation at the speed of 500 rpm and subjected to two and four washes with the pull-down buffer for NS5 mutants and hSTAT2 mutants, respectively. The bound proteins were analyzed by SDS–PAGE followed by SYPRO Ruby protein gel stain (Bio-Rad). For IRF9 competition assay, the mixture of GST-hSTAT2 and ZIKV NS5 was further incubated with IRF9 in an IRF9:NS5 molar ratio of 1:40, 1:20 or 1:10, followed by washes and SDS-PAGE analyses as described above.

Electrophoretic mobility shift assay.

ZIKV NS5–RNA complex formation was assayed with an *in vitro* transcribed, cap-1 yeast mRNA (YLR164W, 749 nt), by agarose gel electrophoretic mobility shift. NS5 and STAT2 stocks were first diluted to 1 μM in THE-300 buffer (34 mM Tris, 57 mM HEPES, adjusted to pH 7.5 with glacial acetic acid; 0.1 mM EDTA, 300 mM NaCl, 0.05% (v/v) TWEEN 20, 25% (v/v) glycerol, 2 mM DTT, 0.2 mg/mL BSA). The mRNA was diluted to 522 ng/μL (~2 μM) in water, heated to 65°C for 5 minutes in a dry block, then snap-cooled in ice. Final samples (7.5 μL) contained RNA (52 ng/μL), NS5 (110 nM), and STAT2 (90 nM), in THE-150 buffer (composition is the same as THE-300 buffer, but with 150 mM NaCl). Samples were mixed, incubated for 15 minutes at room temperature (~25 °C), and then directly loaded onto a 35 mL, pre-chilled (6°C, > 30 minutes) 1% agarose gel cast with 34 mM Tris, 57 mM HEPES, pH 7.5, 0.1 mM EDTA, 10% (v/v) glycerol. The glycerol content of the samples was sufficient to allow loading in the absence of additional loading buffer. The gel was electrophoresed at 80 V in the casting buffer at 6°C for 35 minutes, then stained with ethidium bromide and imaged with a Bio-Rad Gel Doc EZ imager. Images were analyzed with ImageJ.

ITC measurements.

Full-length ZIKV NS5 (120 μM) or human IRF9 (165 μM) proteins were each titrated with hSTAT2 (~20 μM) on a MicroCal iTC200 system (GE Healthcare). All protein samples were dialyzed against the ITC buffer (25 mM Tris-HCl, pH 7.5, 500 mM NaCl, 5% glycerol, 2 mM β-mercaptoethanol) at 4°C overnight. A total of 15 injections

with a spacing of 180 seconds and a reference power of 5 μcal/s were performed at 5°C. The ITC curves were processed with software ORIGEN (MicroCal) using one-site fitting model.

Cell lines and viruses.

293T, Vero and A549 cells were purchased from ATCC and cultured in high glucose Dulbecco's modified Eagle's medium (DMEM) supplemented with 5 mM L-glutamine and 10% fetal bovine serum (FBS). All cells tested mycoplasma-negative using the PlasmoTest™ kit (InvivoGen) following the standard protocol. The sub-cultures were validated by morphological evaluation under light microscope regularly. Zika virus (ZIKV/Macaca mulatta/UGA/MR-766/1947: GenBank: KX601169.1) and VSV-GFP were grown in Vero cells. Virus titers were determined by plaque assay with Vero cells.

Plasmids and transfections.

ZIKV NS5 and NS5 mutants were amplified by RT-PCR from total viral RNA and cloned into the pCAGGS vector. C-terminal HA or FLAG tags for these constructs were encoded in the reverse primer sequences. Dengue virus type 2 strain TSV01 (GenBank: AY037116.1) NS5, and NS5 mutants were amplified from a viral cDNA clone provided by Dr. Shou-wei Ding (Department of Microbiology and Plant Pathology, University of California, Riverside) and cloned into pCAGGS with a C-terminal HA tag encoded in the reverse primer. STAT1 and STAT2 mutants were cloned into pCAGGS

by RT-PCR from RNA isolated from 293T cells, with C-terminal FLAG tags encoded in the reverse primer sequences. Transfections were done in 293T cells using polyethylenimine (PEI).

Co-immunoprecipitation.

Using PEI, $1x10_6$ 293T cells were co-transfected with 0.5 μg each of pCAGGS encoding STAT1- or STAT2-FLAG and DENV or ZIKV NS5-HA, or their mutants. Cells were harvested 30 hours post-transfection (hpt) in NP-40 buffer (0.25% NP-40, 50 mM Tris (pH 7.4), 150 mM NaCl, 5 mM EDTA, 10% glycerol, and 1 mM PMSF). Transfected cells were subsequently lysed by rotating end-over-end at 4°C for 15 minutes, followed by centrifugation at 15,000 rpm in 4°C for 15 minutes. To evaluate the interaction between ZIKV NS5 and the endogenous hSTAT2 proteins, $1x10_6$ 293T cells were transfected with 0.5 μg each of pCAGGS encoding ZIKV NS5-HA, WT or mutant. Cells were harvested 30 hpt and lysed. To minimize the variation of the level of endogenous hSTAT2 proteins in the immunoprecipitation procedure, we supplied the lysate of $2x10_6$ 293T cells to each lysate sample transfected with ZIKV NS5-HA, WT or mutant. Immunoprecipitation was performed on the whole cell extract (WCE) by rotating end-over-end at 4°C for 1 hour with 1 μg mAb anti-FLAG antibody (F1804, Sigma) or 1 μg mAb anti-HA antibody (Catalog #26183, Thermo-Fisher) followed by rotating end-over-end at 4°C for 1 hour with recombinant protein G Sepharose 4B beads (Catalog #101243, Thermo-Fisher) pre-blocked with 5% bovine serum albumin (BSA). The beads were pelleted and washed 2 times with PBS, and bound protein was eluted by boiling in

Laemmli buffer. Co-IPs and WCE were analyzed by SDS-PAGE followed by immunoblotting with mouse anti-GAPDH (Catalog #10087-384, VWR), anti-HA, and anti-FLAG primary antibodies followed by goat anti-mouse IgG (H+L) HRP-linked secondary antibody (Catalog #31160, Thermo-Fisher).

Confocal immunofluorescence microscopy.

To analyze the co-localization of over-expressed hSTAT2 and NS5 mutants, 293T cells grown on glass coverslips were co-transfected using PEI with 0.25 μg each of pCAGGS encoding hSTAT1- or hSTAT2-FLAG and ZIKV/DENV-2 NS5-HA, or their mutants. About 48 hpt, cells were fixed and permeabilized with methanol for 20 minutes at -20°C, and then blocked with 3% BSA/0.2% Tween-20/PBS at 30°C for 1 hour. The cells were incubated with mAb anti-HA and rabbit anti-FLAG primary antibodies (Catalog #14793S, Cell Signaling) for 1 hour at 30°C, followed by two 5-minute washes with PBS+0.2% Tween-20 (PBS-T). Alexa Fluor 555-conjugated anti-mouse and Alexa Fluor 488-conjugated anti-rabbit secondary antibodies were added to the cells for 1 hour at 30°C. After two additional washes with PBS, the coverslips were mounted onto slides with Vectashield (Vector Laboratories) containing DAPI. Images were captured using a Leica SP5 confocal microscope. Confocal laser scanning was performed using a Zeiss LSM 880 Meta (Carl Zeiss Microimaging, Thornwood, NY) fitted with a Plan Apochromatic X63/1.4 or X40/1.4 oil objective lens. Images were collected at 16 bits and at a resolution of 1024 by 1024 pixels. A total of 100 cells per condition were counted

and analyzed by microscopy. Image processing and analysis were carried out using Fiji/ImageJ software.

References

1. Hoffmann, H.-H. *et al*. Interferons and viruses: an evolutionary arms race of molecular interactions. *Trends Immunol.* **36,** 124–138 (2015).

2. Sadler, A. J. & Williams, B. R. G. Interferon-inducible antiviral effectors. *Nat. Rev. Immunol* **8,** 559–568 (2008).

3. Chowdhury, F. Z. & Farrar, J. D. STAT2: a shape-shifting anti-viral super STAT. *JAK-STAT* **2,** e23633 (2013).

4. Ashour, J. *et al*. NS5 of dengue virus mediates STAT2 binding and degradation. *J. Virol.* **83,** 5408–5418 (2009).

5. Grant, A. *et al.* Zika virus targets human STAT2 to inhibit type I interferon signaling. *Cell Host Microbe* **19,** 882–890 (2016).

6. Morrison, J. *et al.* Dengue virus co-opts UBR4 to degrade STAT2 and antagonize type I interferon signaling. *PLoS Pathog.* **9,** e1003265 (2013).

7. Rasmussen, S. A. *et al.* Zika virus and birth defects – reviewing the evidence for causality. *N. Engl. J. Med.* **374,** 1981–1987 (2016).

8. Cao-Lormeau, V.-M. *et al.* Guillain-Barré syndrome outbreak associated with Zika virus infection in French Polynesia: a case-control study. *Lancet* **387,** 1531–1539 (2016).

9. Gubler, D. J. Dengue and dengue hemorrhagic fever. *Clin. Microbiol. Rev.* **11,** 480–496 (1998).

10. Lim, C. P. & Cao, X. Structure, function, and regulation of STAT proteins. *Mol. Biosyst.* **2,** 536–550 (2006).

11. Shuai, K. *et al.* Interferon activation of the transcription factor Stat91 involves dimerization through SH2-phosphotyrosyl peptide interactions. *Cell* **76,** 821–828 (1994).

12. Fu, X. Y. *et al*. ISGF3, the transcriptional activator induced by interferon alpha, consists of multiple interacting polypeptide chains. *Proc. Natl. Acad. Sci. USA* **87,** 8555–8559 (1990).

13. Brierley, M. M. & Fish, E. N. Stats: multifaceted regulators of transcription. *J. Interferon Cytokine Res.* **25,** 733–744 (2005).

14. Davidson, A. D. Chapter 2. New insights into flavivirus nonstructural protein 5. *Adv. Virus Res.* **74,** 41–101 (2009).

15. Best, S. M. The many faces of the flavivirus NS5 protein in antagonism of type I interferon signaling. *J. Virol.* **91,** (2017).

16. Kumar, A. *et al.* Zika virus inhibits type-I interferon production and downstream signaling. *EMBO Rep.* **17,** 1766–1775 (2016).

17. Chen, X. *et al.* Crystal structure of a tyrosine phosphorylated STAT-1 dimer bound to DNA. *Cell* **93,** 827–839 (1998).

18. Mao, X. *et al.* Structural bases of unphosphorylated STAT1 association and receptor binding. *Molecular Cell* **17,** 761–771 (2005).

19. Becker, S. *et al*. Three-dimensional structure of the Stat3beta homodimer bound to DNA. *Nature* **394,** 145–151 (1998).

20. Li, J. *et al.* Structural basis for DNA recognition by STAT6. *Proc. Natl. Acad. Sci. U.S.A.* **113,** 13015–13020 (2016).

21. Neculai, D. *et al.* Structure of the unphosphorylated STAT5a dimer. *J. Biol. Chem.* **280,** 40782–40787 (2005).

22. Duan, W. *et al.* The crystal structure of Zika virus NS5 reveals conserved drug targets. *EMBO J* **36,** 919–933 (2017).

23. Godoy, A. S. *et al.* Crystal structure of Zika virus NS5 RNA-dependent RNA polymerase. *Nat. Commun.* **8,** 14764 (2017).

24. Wang, B. *et al.* The structure of Zika virus NS5 reveals a conserved domain conformation. *Nat. Commun.* **8,** 14763–6 (2017).

25. Zhao, B. *et al.* Structure and function of the Zika virus full-length NS5 protein. *Nat. Commun.* **8,** 1–9 (2017).

26. Improta, T. *et al.* Transcription factor ISGF-3 formation requires phosphorylated Stat91 protein, but Stat113 protein is phosphorylated independently of Stat91 protein. *Proc. Natl. Acad. Sci. USA* **91,** 4776–4780 (1994).

27. Uchil, P. D. *et al*. Nuclear localization of flavivirus RNA synthesis in infected cells. *J. Virol.* **80,** 5451–5464 (2006).

28. Blaszczyk, K. *et al.* The unique role of STAT2 in constitutive and IFN-induced transcription and antiviral responses. *Cytokine Growth Factor Rev.* **29,** 71–81 (2016).

29. Platanitis, E. *et al.* A molecular switch from STAT2-IRF9 to ISGF3 underlies interferon-induced gene transcription. *Nat. Commun.* **10,** 2921 (2019).

30. Martinez-Moczygemba, M. *et al*. Distinct STAT structure promotes interaction of STAT2 with the p48 subunit of the interferon-alpha-stimulated transcription factor ISGF3. *J. Biol. Chem.* **272,** 20070–20076 (1997).

31. Rengachari, S. *et al.* Structural basis of STAT2 recognition by IRF9 reveals molecular insights into ISGF3 function. *Proc. Natl. Acad. Sci. U.S.A.* **115,** E601–E609 (2018).

32. Sahili, El, A. *et al.* NS5 from dengue virus serotype 2 can adopt a conformation analogous to that of its Zika virus and Japanese encephalitis virus homologues. *J. Virol.* **94,** 935 (2019).

33. Zhao, Y. *et al.* A crystal structure of the dengue virus NS5 protein reveals a novel inter-domain interface essential for protein flexibility and virus replication. *PLoS Pathog.* **11,** e1004682 (2015).

34. Bussetta, C. & Choi, K. H. Dengue virus nonstructural protein 5 adopts multiple conformations in solution. *Biochemistry* **51,** 5921–5931 (2012).

35. Best, S. M. *et al.* Inhibition of interferon-stimulated JAK-STAT signaling by a tick-borne flavivirus and identification of NS5 as an interferon antagonist. *J. Virol.* **79,** 12828–12839 (2005).

36. Laurent-Rolle, M. *et al.* The NS5 protein of the virulent West Nile virus NY99 strain is a potent antagonist of type I interferon-mediated JAK-STAT signaling. *J. Virol.* **84,** 3503–3515 (2010).

37. Laurent-Rolle, M. *et al.* The interferon signaling antagonist function of yellow fever virus NS5 protein is activated by type I interferon. *Cell Host Microbe* **16,** 314–327 (2014).

38. Lin, R.-J. *et al*. Blocking of interferon-induced Jak-Stat signaling by Japanese encephalitis virus NS5 through a protein tyrosine phosphatase-mediated mechanism. *J. Virol.* **80,** 5908–5918 (2006).

39. Lubick, K. J. *et al.* Flavivirus antagonism of type I interferon signaling reveals prolidase as a regulator of IFNAR1 surface expression. *Cell Host Microbe* **18,** 61–74 (2015).

40. Mazzon, M. *et al*. Dengue virus NS5 inhibits interferon-alpha signaling by blocking signal transducer and activator of transcription 2 phosphorylation. *J. Infect. Dis.* **200,** 1261–1270 (2009).

41. Ashour, J. *et al.* Mouse STAT2 restricts early dengue virus replication. *Cell Host Microbe* **8,** 410–421 (2010).

42. Miorin, L. *et al.* Host-specific NS5 ubiquitination determines yellow fever virus tropism. *J. Virol.* **93,** (2019).

43. Park, C. *et al*. Murine Stat2 is uncharacteristically divergent. *Nucleic Acids Res.* **27,** 4191–4199 (1999).

44. Paulson, M. *et al.* Stat protein transactivation domains recruit p300/CBP through widely divergent sequences. *J. Biol. Chem.* **274,** 25343–25349 (1999).

45. Grard, G. *et al.* Genomics and evolution of Aedes-borne flaviviruses. *J. Gen. Virol.* **91,** 87–94 (2010).

46. Lu, G. & Gong, P. Crystal structure of the full-length Japanese encephalitis virus NS5 reveals a conserved methyltransferase-polymerase interface. *PLoS Pathog.* **9,** e1003549 (2013).

47. Upadhyay, A. K. *et al.* Crystal structure of full-length Zika virus NS5 protein reveals a conformation similar to Japanese encephalitis virus NS5. *Acta Crystallogr. F Struct. Biol. Commun.* **73(Pt 3),** 116-122 (2017).

48. Wang, B. *et al*. Structure and function of Zika virus NS5 protein: perspectives for drug design. *Cell. Mol. Life Sci.* **75,** 1723–1736 (2018).

49. Tay, M. Y. F. *et al.* The C-terminal 18 amino acid region of dengue virus NS5 regulates its subcellular localization and contains a conserved arginine residue essential for infectious virus production. *PLoS Pathog.* **12,** e1005886 (2016).

50. Ng, I. H. W. *et al.* Zika virus NS5 forms supramolecular nuclear bodies that sequester importin-α and modulate the host immune and pro-inflammatory response in neuronal cells. *ACS Infect. Dis.* **5,** 932–948 (2019).

51. Otwinowski, Z. & Minor, W. Processing of X-ray diffraction data collected in oscillation mode. *Meth. Enzymol.* **276,** 307–326 (1997).

52. McCoy, A. J. *et al.* Phaser crystallographic software. *J. Appl. Crystallogr.* **40,** 658–674 (2007).

53. Emsley, P. & Cowtan, K. Coot: model-building tools for molecular graphics. *Acta Crystallogr. D Biol. Crystallogr.* **60,** 2126–2132 (2004).

54. Adams, P. D. *et al.* PHENIX: building new software for automated crystallographic structure determination. *Acta Crystallogr. D Biol. Crystallogr.* **58,** 1948–1954 (2002).

55. Suloway, C. *et al.* Automated molecular microscopy: the new Leginon system. *J. Struct. Biol.* **151,** 41–60 (2005).

56. Zheng, S. Q. *et al.* MotionCor2: anisotropic correction of beam-induced motion for improved cryo-electron microscopy. *Nat. Methods* **14,** 331–332 (2017).

57. Zhang, K. Gctf: Real-time CTF determination and correction. *J. Struct. Biol.* **193,** 1–12 (2016).

58. Scheres, S. H. W. RELION: implementation of a Bayesian approach to cryo-EM structure determination. *J. Struct. Biol.* **180,** 519–530 (2012).

59. Scheres, S. H. W. A Bayesian view on cryo-EM structure determination. *J. Mol. Biol.* **415,** 406–418 (2012).

60. Punjani, A. *et al*. cryoSPARC: algorithms for rapid unsupervised cryo-EM structure determination. *Nat. Methods* **14,** 290–296 (2017).

61. Vilas, J. L. *et al.* MonoRes: Automatic and accurate estimation of local resolution for electron microscopy maps. *Structure* **26,** 337–344.e4 (2018).

62. Pettersen, E. F. *et al.* UCSF Chimera--a visualization system for exploratory research and analysis. *J. Comput. Chem.* **25,** 1605–1612 (2004).

Chapter 4: Functional characterization of ZIKV NS5-mediated suppression of human STAT2

Abstract

Zika virus (ZIKV), a *Flavivirus*, is a human pathogen which has caused major epidemics around the world. To establish infection, it is vital for viruses to overcome the antiviral state induced by type I interferon (IFN). A common host target for suppression among flaviviruses is the human signal transducer and activator of transcription 2 (hSTAT2) protein, a key signaling intermediary for IFN responses. The ZIKV non-structural protein 5 (NS5) interacts with hSTAT2, triggering the proteasome-dependent degradation of hSTAT2, which results in a weakened antiviral response from the host, allowing ZIKV to cause disease. However, the underlying molecular mechanism of ZIKV NS5-mediated hSTAT2 suppression remains elusive. Previously, we elucidated the cryoEM and crystal structures of hSTAT2 in complex with the ZIKV NS5. Here, we show that disruption of the ZIKV NS5 – hSTAT2 association compromises NS5-mediated hSTAT2 degradation and downstream IFN response suppression, but not RIG-I-mediated IFN production. Additionally, we demonstrate that the NS5-hSTAT2 interaction is essential for productive viral infection under IFN-competent conditions. This study provides a basis for using flaviviruses to understand the functional antagonism between viral proteins and the host innate immune system.

Introduction

Type I interferon (IFN)-mediated innate immune response constitutes the first line of host defense against viral infection[1]. Induction of type I IFN signaling requires activation of the signal transducer of transcription 2 (STAT2), which triggers the expression of hundreds of IFN stimulated genes (ISGs) to inhibit infection[2]. To achieve successful infection, viruses thus must suppress activation of STAT2-triggered IFN responses[3]. Mechanistic understanding of this "arms race" between hosts and viruses is essential for the development of novel therapeutic strategies against viral infections.

STAT2-mediated transcriptional activation initiates with tyrosine phosphorylation of STAT2 and STAT1 by the Janus kinases (JAKs), followed by formation of a trimer consisting of STAT1, STAT2 and interferon regulatory factor 9 (IRF9), termed IFN-stimulated gene factor-3 (ISGF3)[4-6]. ISGF3 translocates to the nucleus to where it interacts with interferon stimulated response elements (ISREs) to upregulate expression of interferon stimulated genes (ISGs) which function to suppress viral replication[7].
To establish viral infection, viruses have evolved a variety of ISGF3 suppression mechanisms[3]. Prominent examples include dengue virus (DENV) and Zika virus (ZIKV), members of the *Flavivirus* genus of the *Flaviviridae* family, both of which employ their respective non-structural protein 5 (NS5) to suppress human STAT2 (hSTAT2)-mediated IFN response[8-10]. NS5 contains an N-terminal methyltransferase (MTase) domain that catalyzes viral RNA capping, and an RNA-dependent RNA polymerase (RdRp) domain that is responsible for replicating the viral genome[11]. These NS5 proteins directly bind to hSTAT2 and promote its degradation through the proteasome-mediated pathway[8,9].

Previously, we elucidated the structural basis for ZIKV and DENV NS5-mediated hSTAT2 interaction. However, the role of NS5-mediated hSTAT2 degradation and IFN suppression in the cell remains elusive.

In this study, we show that the interaction between ZIKV NS5 and hSTAT2 is essential for degradation of hSTAT2, suppression of type I IFN responses, and efficient viral infection under IFN-competent conditions. Mutations that inhibit hSTAT2 interaction are specific to ISGF3-mediated IFN production and do not affect RIG-I-activated pathways. Together, these data provide key insights into the interactions between viral antagonists and STATs. This knowledge will make it possible to generate an attenuated ZIKV strain for use in a vaccine that is unable to inhibit the host antiviral response and may contribute to the development of antiviral therapeutics that target the NS5 protein.

Results

ZIKV NS5–hSTAT2 interaction leads to hSTAT2 degradation and IFN suppression

Previously, we had determined the crystal and cryo-EM structures of the ZIKV NS5-hSTAT2 complex (Ch. 3, Fig. 8,9). Guided by these structures, key residues involved in the NS5-hSTAT2 association were identified by mutagenesis and co-IP analysis (Ch. 3, Fig. 12). Here, we further evaluated the effect of the ZIKV NS5–hSTAT2 interaction on the stability of hSTAT2 and related type I IFN response in cells. Expression of wildtype ZIKV NS5 in 293T cells led to a dose-dependent decrease in the protein level of endogenous hSTAT2 (Fig. 16a), consistent with previous observations[9,12,13]. The NS5-dependent degradation of hSTAT2 was slightly attenuated in cells transfected with NS5 Mut^{DH} and became even less evident in cells transfected with NS5 Mut^{RDH} or Mut^{YRDH} (Fig. 16a). These results indicate that the hSTAT2-NS5 association is required for subsequent hSTAT2 degradation.

Next, we performed the vesicular stomatitis virus (VSV)-GFP based IFN bioassay[14] to evaluate the impact of the NS5–hSTAT2 interaction on IFN production. The replication efficiency of VSV, which is impaired in the presence of high levels of IFN, was increased in A549 cells treated with supernatants from cell cultures transfected with wildtype NS5 compared to those treated with NS5 Mut^{YRDH} (Fig. 16b), suggesting that the NS5 Mut^{YRDH} mutation impaired NS5-mediated suppression of IFN production. Consistent with these results, qRT-PCR analysis of two representative type I IFN-stimulated genes, ISG54 and OAS-1, in IFN-treated 293T cells revealed that the

expression of wildtype ZIKV NS5, but not NS5 Mut$_{YRDH}$, led to a dose-dependent reduction of ISG54 and OAS-1 expression (Fig. 16c).

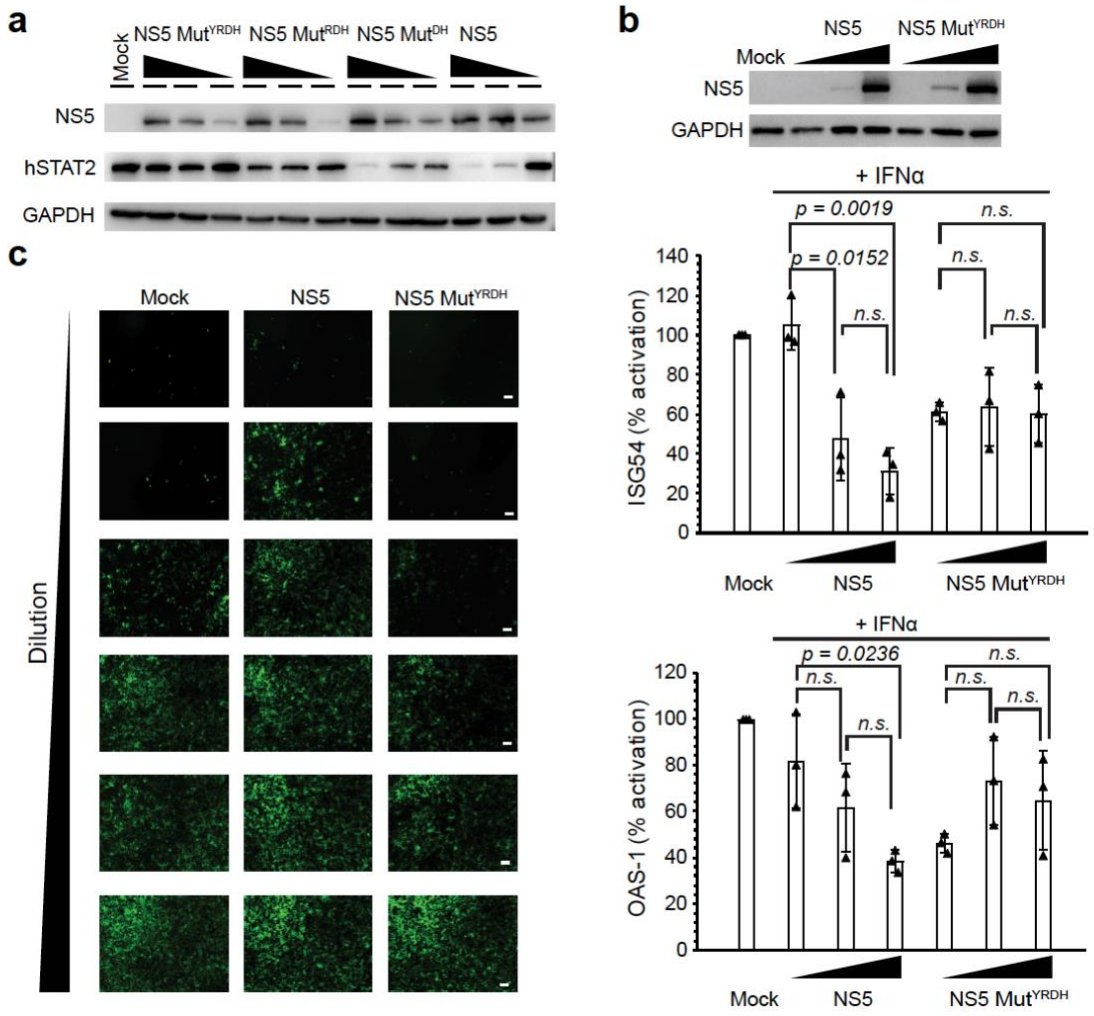

Figure 16. Role of the ZIKV NS5–hSTAT2 interaction in ZIKV NS5-mediated degradation of hSTAT2 and type I IFN signaling suppression. a) Immunoblot analysis of 293T cells transfected with indicated plasmids encoding wildtype or mutant NS5-HAs at three different amounts using antibodies against HA, hSTAT2, and GAPDH. b) Immunoblot of NS5 and GAPDH (top) and qRT-PCR analysis of ISG54 and OAS-1 mRNAs (bottom) of non-transfected 293T cells (mock), or cells transfected with plasmids encoding wildtype or mutant NS5-HAs, followed by treatment with IFN for 18 hr. Data in graphs are mean ± s.d. (n=3 independent transfections). Statistical analysis used two-tailed Student's t-test; ns, $p > 0.05$. c, VSV-GFP infection of A549 cells treated with 1:2 serial dilutions of the supernatants derived from poly(I:C)-stimulated 293T cells, non-transfected (mock), or transfected with NS5 or NS5 Mut^{YRDH}. Representative images of three independent experiments.

Previous studies had shown that ZIKV NS5, in addition to suppression of hSTAT2, inhibits IFN-β production through targeting the retinoic acid-inducible gene I (RIG-I) pathway[13,15-20]. We thus further interrogated the effects of ZIKV NS5 mutations on type I IFN suppression along the RIG-I signaling pathway. Toward this, we performed an IFN-β promoter-driven luciferase assay to determine whether the NS5 mutation also affects the RIG-I-(2CARD)-, TBK1-, and IRF3-activated IFN-β production. Consistent with previous observations[13,15-20], cells transfected with wildtype NS5, in comparison with controls, showed substantial suppression of the luciferase activity activated by RIG-I-(2CARD), TBK1, or IRF3 (Fig. 17a). Transfection with NS5 Mut^{YRDH} led to a similar suppression of the luciferase activity (Fig. 17a), suggesting that mutations affecting hSTAT2 association did not compromise the inhibitory role of ZIKV NS5 in the RIG-I pathway.

The mechanism by which ZIKV NS5 interferes with the RIG-I pathway diverges among the Asian and African lineages. Asian lineage NS5 proteins reportedly interact with RIG-I[20], IKKε[19], TBK1[19] and IRF3[15,18] resulting in reduced IRF3 phosphorylation[19] and reduced RIG-I ubiquitination[20]. The NS5 protein from the African ZIKV lineage, in contrast, has been shown to associate with TBK1, but not IRF3, leading to reduced IRF3 phosphorylation[17]. To determine if our African lineage NS5 can interact with IRF3, we performed a co-immunoprecipitation (co-IP) assay in 293T cells co-transfected with African or Asian (Panamanian isolate) NS5 and IRF3 with and without RIG-I-(2CARD) stimulation. While strong associations were observed between hSTAT2 and both NS5 proteins, IRF3 interacted very weakly, if at all, with NS5s from both African and Asian

lineages regardless of 2CARD stimulation (Fig. 17b). The Asian lineage (a Cambodian isolate[15]) NS5 reported to interact with IRF3 differs from the Asian lineage protein used here (a Panamanian isolate) by ~4%, amounting to 35 amino acid differences, which could be responsible for the discrepant results. Further investigation is needed to determine how African and Asian NS5 proteins interact with the RIG-I pathway.

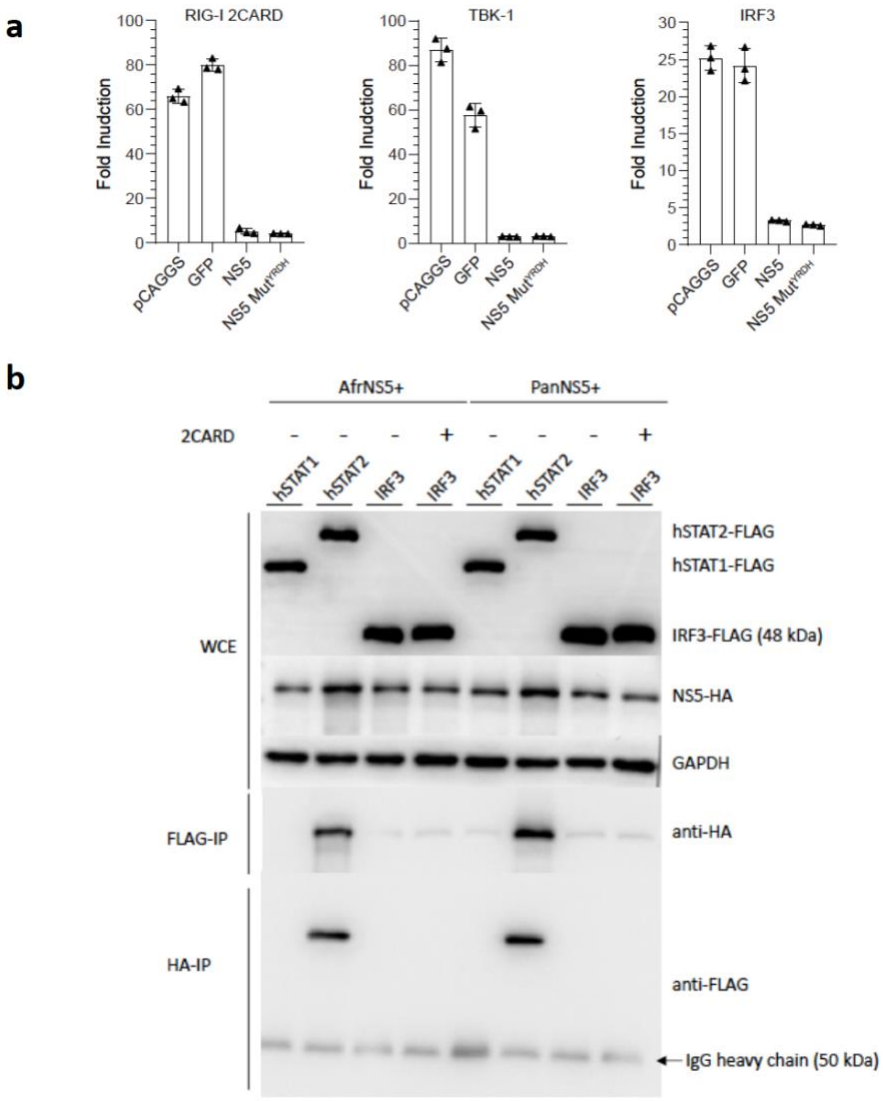

Figure 17. Role of ZIKV NS5 in RIG-I pathway. a) IFN-β promoter-driven luciferase activity assay. Fold increase of interferon β production activated by (left to right) RIG-2CARD, TBK-1 and IRF3 in 293T cells transfected with empty pCAGGS vector, GFP, WT or Mut^{YRDH} ZIKV NS5. Data are mean ± s.d. (n=3 independent transfections). b) Co-IP analysis of HA-tagged NS5 proteins from African lineage ("AfrNS5") or Asian lineage ("PanNS5") association with FLAG-tagged hSTAT1, hSTAT2 or IRF3. Immunoblot analysis of the IPs and whole cell extracts (WCE) were performed using antibodies against HA, FLAG and GAPDH.

ZIKV NS5–hSTAT2 interaction is required for efficient viral infection of IFN-competent cells.

Next, we sought to determine the effect of the ZIKV NS5–hSTAT2 interaction on ZIKV infection. Toward this end, we first introduced different NS5 mutations to the cDNA-ZIKV-MR766 construct, a rescue plasmid that has previously been used for generating recombinant MR766 ZIKV[21]. We generated both the recombinant wild-type (rWT) virus and the mutant viruses through transfecting 293T cells with the cDNA-ZIKV-MR766 construct, as described previously[21]. Interestingly, the rescue plasmids carrying the Y25A (Mut^{Y}), H855A (Mut^{H}), Mut^{RDH}, or Mut^{YRDH} failed to yield recombinant viruses, likely due to a severe attenuation effect caused by these mutations. Nevertheless, we were able to rescue viruses with wildtype or R327A NS5. Additionally, we rescued a D734A-containing virus, in which an additional G338E mutation recurrently emerged during two independent rescue processes and remained stable after several passages in Vero cells.

Both of the two mutant ZIKV exhibited similar replication kinetics as rWT ZIKV in IFN-deficient Vero cells[22] (Fig. 18a), suggesting the mutations introduced did not significantly impact the essential RdRp and MTase enzymatic activities of NS5. We similarly performed multi-cycle growth curve experiments using IFN-competent A549 cells. Compared to rWT ZIKV, both mutant viruses yielded significantly reduced virus titers at 48 hours post infection (Fig. 18b), suggesting an IFN-dependent attenuation effect for the R327A and G338E/D734A NS5 mutations. Consistent with this notion,

both mutant viruses exhibited less efficient NS5-mediated hSTAT2 degradation during the A549 growth curve experiment compared to rWT (Fig. 18c).

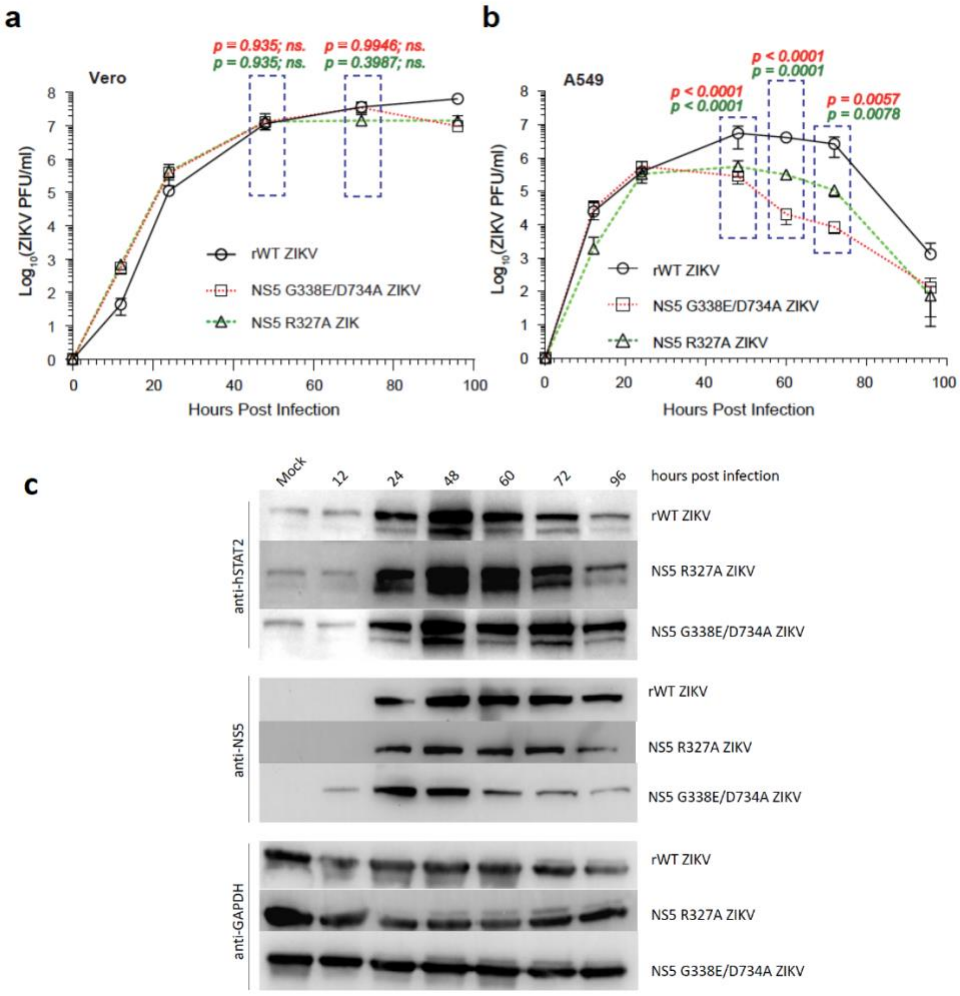

Figure 18. Role of the ZIKV NS5-hSTAT2 interaction during infection. a,b) Growth curves of Vero (a) and A549 (b) cells infected with the rWT and mutant MR766 viruses. Values of titers are expressed in PFU per milliliter. Data are mean ± s.d. (n=3 independent infections). Statistical analysis was performed using the two-way ANOVA test; ns, $p > 0.05$. c) Western blot analysis of virus-infected A549 cells using antibodies against hSTAT2, NS5 and GAPDH.

To determine if the R327A and G338E/D734A mutations affected hSTAT2 association, we performed co-IP and immunofluorescence (IF) analysis in 293T cells co-transfected with NS5 mutants and hSTAT2 (Fig. 19a,c). Co-IP and IF analyses indicated that the G338E/D734A mutation affects the NS5-hSTAT2 interaction and cellular localization of ZIKV NS5 in a manner similar to that of D734A or Mut^{YRDH} mutations (Ch. 3 Fig. 11, Fig. 19a,c). Likewise, the R327A mutation also impairs the interaction and cytoplasmic co-localization of ZIKV NS5 and hSTAT2, albeit to a lesser extent (Fig. 19a,c). Additionally, consistent with the hSTAT2 degradation results from the A549 growth curve (Fig. 18c), transfected NS5 Mut^{R} or Mut^{GD} exhibited reduced ability to degrade hSTAT2 compared to wildtype NS5 (Fig. 19b). Together, these data establish that the hSTAT2-NS5 interaction is critical for productive ZIKV infection under IFN-competent condition.

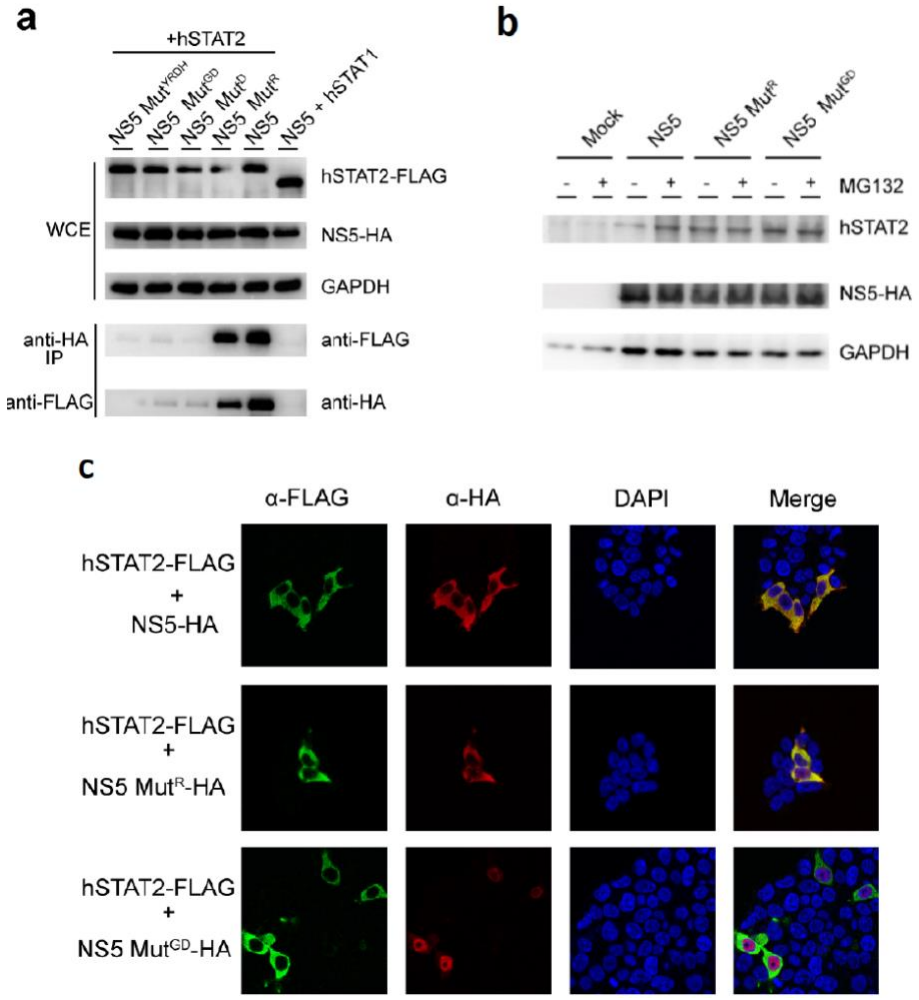

Figure 19. Cellular analysis of the ZIKV NS5 R327A and G338E/D734A mutations on hSTAT2 interaction and degradation. a) Co-IP analysis showing the effects of MutR and MutGD in comparison with D734A (MutD) and MutYRDH on the NS5–hSTAT2 interaction. Immunoblot analysis of the IP and whole cell extract (WCE) was performed using antibodies against HA, FLAG and GAPDH. b) Immunoblot analysis of 293T cells transfected with indicated plasmids encoding wildtype or mutant NS5-HAs using antibodies against HA, hSTAT2 and GAPDH, incubated with or without proteasome inhibitor MG132. c) IF analysis of 293T cells transfected with plasmids encoding NS5-HA, wildtype or mutant, and hSTAT2-FLAG. The transfected cells were fixed for immune staining using antibodies against HA (red) and FLAG (green). Nuclei were visualized by DAPI (blue) counter staining.

RdRp activity of ZIKV NS5 mutants

As described above, several attempts were made at recovering ZIKV with Y25A, H855A, RDH or YRDH NS5 mutations. Additionally, ZIKV with a single D734A mutation could not be rescued without a second-site mutation, G338E. To investigate whether these amino acid changes impact the enzymatic activity of NS5, we purified NS5 mutants and performed an *in vitro* RdRp assay using a subgenomic ZIKV RNA as template (Ch. 2 Fig. 5a, Fig. 20). We observed no significant difference in RdRp activity between wildtype NS5 and NS5 Mut$_{Y}$ or Mut$_{H}$ proteins at the 15- or 90-minute time points (Fig. 20a). NS5 Mut$_{R}$ and Mut$_{D}$ proteins, on the other hand, generated slightly less RNA product after 90 minutes compared to wildtype NS5 (Fig. 20a,c). NS5 proteins incorporating three (Mut$_{RDH}$) or four amino acid changes (Mut$_{YRDH}$) exhibited even less activity in both 15- and 90-minute incubation groups (Fig. 20b). Finally, a comparison between the NS5 D734A (Mut$_{D}$) protein and NS5 D734A/G338E (Mut$_{GD}$) showed no significant difference in RdRp activity, although both were deficient compared to wildtype NS5 (Fig. 20c). Together, these results suggest that deficiency in RdRp activity likely does not contribute to our inability to recover ZIKV with NS5 Y25A or H855A mutations, as these proteins perform similarly to wildtype NS5 (Fig. 20a). Additionally, the recurring G338E mutation in the ZIKV NS5 D734A recovery does not appear to restore RdRp activity to the NS5 D734A protein to wildtype levels (Fig. 20c).

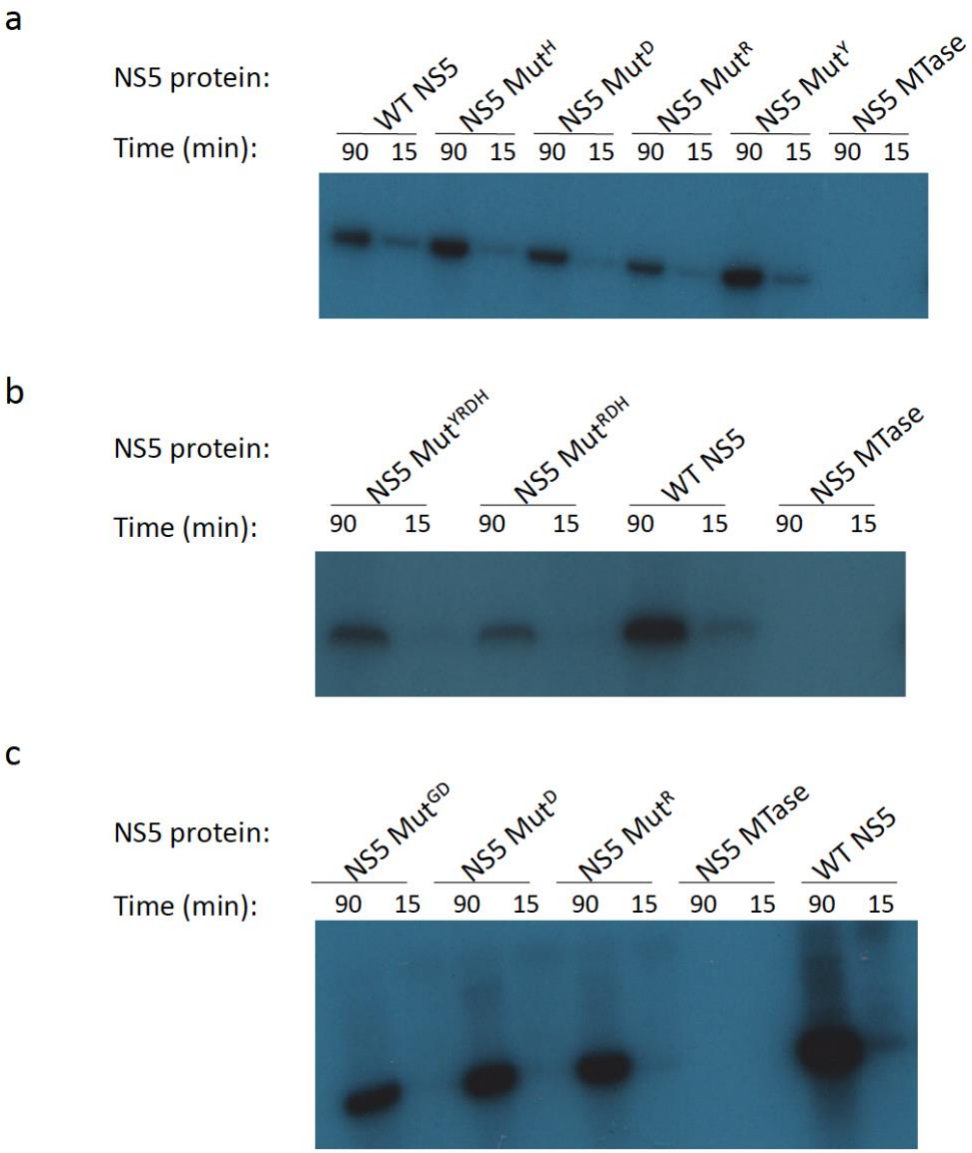

Figure 20. *In vitro* RdRp activity of NS5 mutants. a-c) The subgenomic ZIKV RNA (Ch. 2 Fig. 3a) was incubated with recombinant ZIKV NS5 protein (WT NS5), ZIKV NS5 MTase or NS5 mutants for 15 or 90 min. The relative amount of ^{32}P-labelled RNA product is displayed in the autoradiograph of the PAGE gel.

Discussion

Effective inhibition of type I IFN production is necessary for flaviviruses to establish infection in mammalian hosts. The viral non-structural proteins have evolved to be multi-functional, encoding diverse IFN suppression mechanisms in addition to their essential roles in the viral life cycle. NS5 is one of the most potent IFN-I antagonists. Two of the most pervasive disease-causing flaviviruses—ZIKV and DENV—inhibit human STAT2 through NS5-hSTAT2 interaction. Together with the structural data presented in Ch. 3, the data presented here elucidates the mechanistic details and the importance of the ZIKV NS5-hSTAT2 interaction. We have shown that this interaction is required for efficient hSTAT2 degradation and downstream type I IFN suppression. Importantly, in the absence of this host antagonism, ZIKV replication is severely attenuated in the presence of IFN.

Prior to this work, it was known that the ZIKV NS5 protein interacted with human STAT2, and that the presence of NS5 resulted in the degradation of hSTAT2[9,13]. However, a causal relationship between the NS5-hSTAT2 association and hSTAT2 degradation had not been established. In Ch. 3 of this thesis, guided by the crystal and cryoEM structures of the NS5-hSTAT2 complex, we disrupted the association between these two proteins by mutagenizing key interacting residues within NS5 (Ch. 3, Fig. 10). Here, we used our NS5 mutants as tools to interrogate the functional consequences of the NS5-hSTAT2 interaction. NS5 mutants that are deficient in hSTAT2 interaction are also unable to efficiently degrade hSTAT2 (Fig. 16a) or suppress IFN production (Fig. 16b,c). The NS5 mutations that inhibit hSTAT2 association were shown to be specific to IFN

production downstream of hSTAT2, as they have no effect on the ability of NS5 to suppress upstream RIG-I-mediated IFN production (Fig. 17a). *Flavivirus* NS5 proteins can antagonize both the initiation (RIG-I-mediated) and amplification (ISGF3-mediated) phases of type I IFN production at multiple steps in the pathways[15-20]. Thus, it is not surprising that interruption of the hSTAT2 association only partially restores ISG transcription in NS5-transfected cells (Fig. 16b).

For productive infection, viruses must inhibit the type I IFN response of the infected host cell. We have shown here that without efficient hSTAT2 interaction and degradation, ZIKV is severely attenuated in the presence of IFN (Fig. 18b). In Vero cells, which are deficient in IFN production[22], the growth kinetics of rWT, R327A and G338E/D734A viruses are nearly identical. However, at 12 hpi, rWT yields a titer that is a full log lower than the mutant viruses, but by 48 hpi, all viruses have similar titers (Fig. 16a). This is surprising given the deficiencies in RdRp activity observed for NS5 Mut$_R$ and Mut$_{GD}$ in the *in vitro* enzymatic assay (Fig. 19c). In Ch. 3, however, we demonstrated that hSTAT2 may be competing with viral RNA binding to NS5 (Appendix B, Supplementary Fig. 10e). Given the reduced hSTAT2 interaction exhibited by NS5 Mut$_R$ and Mut$_{GD}$ (Fig. 17a), it is possible that more NS5 in the early infection stages is available for RNA-binding and replication, accounting for the increased viral titer at these time points (Fig. 17c).

We were unable to generate ZIKV containing the NS5 Y25A or H855A mutations alone or in combination with other changes. These residues have not been implicated in the NS5 enzymatic MTase or RdRp mechanisms and our *in vitro* RdRp assay shows no

difference in RdRp activity between wildtype NS5, NS5 Mut$_Y$ or NS5 Mut$_H$ (Fig. 20a). NS5 Y25 has been reported to be essential for NS5 dimerization *in vitro*[23], although dimerization of NS5 has not been shown to be physiologically relevant, so it is unclear whether the Y25A mutation would impact ZIKV viability. It remains a possibility that Y25 and H855 are essential for NS5-mediated hSTAT2 suppression, such that viruses containing changes at these residues are unviable. In attempts to rescue ZIKV containing a single D734A mutation we recovered only viruses that had both D734A and G338E mutations, which were stable through passage in Vero cells. How the G338E change complements D734A to produce virus is unclear. Structurally, G338 is close to D734, and a change to glutamate could theoretically compensate for the loss of the polar, charged D734 residue, potentially restoring interaction with the hSTAT2 R176 residue (Appendix B, Supplementary Fig. 5c). However, our co-IP analysis did not show any difference in hSTAT2 binding between NS5 Mut$_D$ and Mut$_{GD}$ (Fig. 17a). The G338E change also does not appear to restore RdRp activity to the NS5 D734A protein in our *in vitro* RdRp assay (Fig. 20c). Further investigation into the function of G338E in the ZIKV NS5 G338E/D734A virus is warranted.

In summary, we have demonstrated here the essential function of the ZIKV NS5-hSTAT2 interaction for efficient NS5-mediated ISGF3 suppression and ZIKV infection. This detailed mechanistic understanding of this interaction provides at least two opportunities for translational research. First, recombinant viruses that incorporate loss-of-function mutations in NS5 are attractive candidates for live-attenuated vaccine strains. Second, antivirals that target the NS5-hSTAT2 interaction would inhibit an early step

common to these flaviviruses, despite divergent downstream mechanisms employed by the NS5s. The work presented here will contribute to the development of these critical tools in combating ZIKV.

Materials and Methods

Cell lines and viruses.

293T, Vero and A549 cells were purchased from ATCC and cultured in high glucose Dulbecco's modified Eagle's medium (DMEM) supplemented with 5 mM L-glutamine and 10% fetal bovine serum (FBS). All cells were tested mycoplasma negative using the PlasmoTest™ kit (InvivoGen) following the standard protocol. The sub-cultures were validated by morphological evaluation under light microscope regularly. Zika virus (ZIKV/Macaca mulatta/UGA/MR-766/1947: GenBank: KX601169.1) and VSV-GFP were grown in Vero cells. Virus titers were determined by plaque assay with Vero cells.

Plasmids and transfections.

ZIKV NS5 and NS5 mutants were amplified by RT-PCR from total viral RNA and cloned into the pCAGGS vector. C-terminal HA or FLAG tags for these constructs were encoded in the reverse primer sequences. STAT1 and STAT2 mutants were cloned into pCAGGS by RT-PCR from RNA isolated from 293T cells, with C-terminal FLAG tags encoded in the reverse primer sequences. Transfections were done in 293T cells using polyethylenimine (PEI).

To generate recombinant MR766 ZIKV viruses, we generated a panel of mutants in DNA-ZIKV-MR766, the rescue system that carried the indicated mutations in the NS5 gene[21]. Subsequently, we rescued the ZIKV mutants following a procedure reported previously[21]. Briefly, we transfected 293T cells with the different rescue constructs and

subsequently transferred the supernatant to incubate with Vero cells for viral amplification.

hSTAT2 degradation assay.

To investigate degradation of endogenous hSTAT2 in the presence of over-expressed NS5 mutants, 5 x 10_5 293T cells were PEI-transfected with increasing amounts (200 ng, 400 ng, 800 ng) of pCAGGS encoding HA-tagged NS5 variants. Cells were cultured with or without 10 nM proteasome inhibitor MG132 (Catalog # HY-13259C, Medchemexpress Llc). At 36 hpt, the cells were harvested in 1X Laemmli buffer and analyzed by SDS-PAGE followed by immunoblotting with anti-GAPDH, anti-HA, and rabbit anti-STAT2 primary antibodies (Catalog #72604S, Cell Signaling) followed by anti-mouse or goat anti-mouse secondary IgG antibodies (H+L) HRP-linked (Catalog #31460, Thermo-Fisher).

VSV-GFP assay.

To determine the overall levels of IFN influenced by NS5 or NS5 mutants, 2.5x10_5 293T cells were transfected with pCAGGS encoding HA-tagged NS5 and NS5 Mut$_{YRDH}$. At 30 hpt, the transfected cells were primed with 2 μg poly(I:C) transfection. 18 hours later serial 1:2 dilutions of the supernatants from cultures transfected with the NS5 variants were used to treat A549 cells. 24 hours after supernatant treatment, A549 cells were infected with VSV-GFP (gift from Dr. Dusan Bogunovic) at MOI=1. Infected

cells were visualized 24 hpi for GFP expression by the Nikon Eclipse te2000-U fluorescent microscope.

Quantitative RT-PCR.

To quantitate ISG54 mRNA levels in the presence of NS5 or NS5 mutants, $5x10^5$ 293T cells were PEI-transfected with increasing amounts of pCAGGS encoding HA-tagged NS5 variants (NS5: 200 ng, 500 ng and 1000 ng; NS5 Mut^{YRDH}: 200 ng, 400 ng and 800 ng). At 30 hpt, the transfected cells were treated with 1,000 U/mL universal type I interferon (PBL, 11200-1) for 18 hours. After IFN treatment, cells were harvested in PBS and split into two equal-volume samples. One sample was re-suspended in Laemmli buffer and analyzed by SDS-PAGE followed by immunoblotting with anti-GAPDH and anti-HA antibodies. The second sample was used to isolate total RNA for qRT-PCR using Trizol (Catalog # N8080127, Fisher). 1 μg of RNA was reverse transcribed using random hexamer (Catalog # N8080127, Fisher). qRT-PCR was performed using iQ™ SYBR Green Supermix (Catalog # 1708880, BioRad). The ΔCt values were calculated using β-actin mRNA as the internal control. The ΔΔCt values were determined using control samples (non-transfected non-IFN-treated) as the reference value. Relative levels of transcripts were calculated using the formula $2^{(-\Delta\Delta Ct)}$.

Multi-cycle growth curve experiment.

To compare the replication kinetics of our mutant viruses to rWT ZIKV, we performed multi-cycle growth curve experiments, in which IFN-competent A549 cells or

IFN-deficient Vero cells were infected (MOI of 1) for 1 hr. with either the rescued mutant virus or the rescued WT virus. Supernatants were collected daily up to 4 days post infection, and then titers of the supernatants were determined by plaque assays in Vero cell.

IFN-β promoter-driven luciferase activity assay.

293T cells were transfected with the plasmids encoding IFN-β promoter firefly luciferase reporter, renilla luciferase (for normalization), ZIKV NS5-HA (wild type or mutant) or controls, and stimulating factors RIG-I (2CARD), TBK1 or IRF3, respectively, 0.25 μg of each. Cells were harvested at 24 h post-transfection and subjected to the Dual-Luciferase Assay System (Promega) based on manufacturer's instructions. Data were normalized first by renilla luciferase values, and then normalized by non-stimulated samples to obtain fold induction. Empty vector samples were set as 100% fold-induction. Error bars represent mean ± SD. Results are representative of three independent experiments with each one in triplicate.

Statistics and Reproducibility.

Data are presented as the mean ± s.d. of at least three independent experiments. For analysis of the qRT-PCR results, two-tailed Student's t-test was used with a CI of 95% (the degrees of freedom is 4). For the analysis of the growth curves, the two-way ANOVA test with Tukey's multiple comparisons test was used to evaluate significant differences (for comparison of viruses in Vero cells, degrees of freedom (DF) is 2 and F

value is 1.849; for comparison of viruses in A549 cells, degrees of freedom (DF) is 2 and F value is 55.84). For both analyses, a p-value of less than 0.05 was considered significant. All biochemical and cellular assays were performed three or more times with similar results, unless indicated otherwise.

Co-immunoprecipitation.

Using PEI, $1x10_6$ 293T cells were co-transfected with 0.5 μg each of pCAGGS encoding STAT1- or STAT2-FLAG and ZIKV NS5-HA or mutants. Cells were harvested 30 hours post-transfection (hpt) in NP-40 buffer (0.25% NP-40, 50 mM Tris (pH 7.4), 150 mM NaCl, 5 mM EDTA, 10% glycerol, and 1 mM PMSF). Transfected cells were subsequently lysed by rotating end-over-end at 4°C for 15 minutes, followed by centrifugation at 15,000 rpm in 4°C for 15 minutes. To evaluate the interaction between ZIKV NS5 and the endogenous hSTAT2 proteins, $1x10_6$ 293T cells were transfected with 0.5 μg each of pCAGGS encoding ZIKV NS5-HA, WT or mutant. Cells were harvested 30 hpt and lysed. To minimize the variation of the level of endogenous hSTAT2 proteins in the immunoprecipitation procedure, we supplied the lysate of $2x10_6$ 293T cells to each lysate sample transfected with ZIKV NS5-HA, WT or mutant. Immunoprecipitation was performed on the whole cell extract (WCE) by rotating end-over-end at 4°C for 1 hour with 1 μg mAb anti-FLAG antibody (F1804, Sigma) or 1 μg mAb anti-HA antibody (Catalog #26183, Thermo-Fisher) followed by rotating end-over-end at 4°C for 1 hour with recombinant protein G Sepharose 4B beads (Catalog #101243, Thermo-Fisher) pre-blocked with 5% bovine serum albumin (BSA). The beads were pelleted and washed 2

times with PBS, and bound protein was eluted by boiling in Laemmli buffer. Co-IPs and WCE were analyzed by SDS-PAGE followed by immunoblotting with mouse anti-GAPDH (Catalog #10087-384, VWR), anti-HA, and anti-FLAG primary antibodies followed by goat anti-mouse IgG (H+L) HRP-linked secondary antibody (Catalog #31160, Thermo-Fisher).

Confocal immunofluorescence microscopy.

To analyze the co-localization of over-expressed hSTAT2 and NS5 mutants, 293T cells grown on glass coverslips were co-transfected using PEI with 0.25 μg each of pCAGGS encoding hSTAT2-FLAG and ZIKV NS5-HA or mutants. About 48 hpt, cells were fixed and permeabilized with methanol for 20 minutes at -20°C, and then blocked with 3% BSA/0.2% Tween-20/PBS at 30°C for 1 hour. The cells were incubated with mAb anti-HA and rabbit anti-FLAG primary antibodies (Catalog #14793S, Cell Signaling) for 1 hour at 30°C, followed by two 5-minute washes with PBS+0.2% Tween-20 (PBS-T). Alexa Fluor 555-conjugated anti-mouse and Alexa Fluor 488-conjugated anti-rabbit secondary antibodies were added to the cells for 1 hour at 30°C. After two additional washes with PBS, the coverslips were mounted onto slides with Vectashield (Vector Laboratories) containing DAPI. Images were captured using a Leica SP5 confocal microscope. Confocal laser scanning was performed using a Zeiss LSM 880 Meta (Carl Zeiss Microimaging, Thornwood, NY) fitted with a Plan Apochromatic X63/1.4 or X40/1.4 oil objective lens. Images were collected at 16 bits and at a resolution

of 1024 by 1024 pixels. A total of 100 cells per condition were counted and analyzed by microscopy. Image processing and analysis were carried out using Fiji/ImageJ software.

Protein expression and purification.

The DNA sequence encoding full-length ZIKV NS5 or ZIKV NS3-Hel (residues 171–617) was amplified from the cDNA of ZIKV/Macaca mulatta/UGA/MR-766/1947 and inserted into a modified pRSFDuet-1 vector (Novagen) (see Appendix A, Supplementary Table 1 for primer sequences), in which the NS5 or NS3-Hel gene was preceded by an N-terminal His_6-SUMO tag and ULP1 (ubiquitin-like protease 1) cleavage site. The obtained plasmids were then transformed into BL21 (DE3) RIL cell strain (Agilent Technologies) for expression. The cells were first grown at 37°C and then shifted to room temperature when A_{600} reached 1.0, followed by the addition of 0.4 mM isopropyl b-D-galactoside for induction. After another 18h of cell growth, the cells were collected and the His_6- SUMO-tagged ZIKV NS5 or ZIKV NS3-Hel was purified using a Ni-NTA affinity column. ZIKV NS5 was further purified on a Phenyl Sepharose column (GE Healthcare) for separation from degraded protein products, followed by removal of the His_6-SUMO tag through ULP1 cleavage and size-exclusion chromatography on a Superdex 200 16/600 column (GE Healthcare) pre-equilibrated in buffer containing 25 mM Tris, pH 7.5, 500 mM NaCl, 5 mM DTT (dithiothreitol) and 5% glycerol. The ZIKV NS3-Hel fusion protein was first subject to ULP1 cleavage, and subsequently purified on a Phenyl Sepherase column and a Superdex 200 16/600 column preequilibrated in buffer containing 25 mM Tris, pH 7.5, 250 mM NaCl, 5 mM DTT and 5% glycerol.

De novo RdRp assay.

The *de novo* RdRp reaction (20 µl) contained 50 mM Tris (pH 8.0), 10 mM NaCl, 5 mM $MgCl_2$, 2 mM $MnCl_2$, 10 mM DTT, 0.5 mM ATP, 0.5 mM UTP, 0.5 mM GTP, 5 mM CTP, 15 µCi of [α-^{32}P] (10 µCi µl^{-1}, 3,000 Ci mmol^{-1}; Perkin-Elmer), 1 µg of RNA template and 2 µg of ZIKV NS5 protein or ZIKV NS3-Hel. The RNA template was *in vitro* transcribed from a PCR product using T7 polymerase (New England BioLabs). The PCR product contained a T7 promoter, followed by a cDNA fragment representing a ZIKV subgenome with deletion of nucleotides 171–10,343 (GenBank accession no. KU963573.2). The *de novo* RdRp reaction mixtures were incubated at 33°C for 15 and 90 min. 2X denaturing gel loading dye was added to the reactions and samples were loaded onto a 10% denaturing polyacrylamide gel with 7M urea. ^{32}P-labelled RNA results were detected via the autoradiograph of the PAGE gel.

References

1. Hoffmann, H.-H. *et al*. Interferons and viruses: an evolutionary arms race of molecular interactions. *Trends Immunol.* **36,** 124–138 (2015).

2. Sadler, A. J. & Williams, B. R. G. Interferon-inducible antiviral effectors. *Nat. Rev. Immunol.* **8,** 559–568 (2008).

3. Chowdhury, F. Z. & Farrar, J. D. STAT2: A shape-shifting anti-viral super STAT. *JAK-STAT* **2,** e23633 (2013).

4. Blaszczyk, K. *et al.* The unique role of STAT2 in constitutive and IFN-induced transcription and antiviral responses. *Cytokine Growth Factor Rev.* **29,** 71–81 (2016).

5. Fu, X. Y. *et al*. ISGF3, the transcriptional activator induced by interferon alpha, consists of multiple interacting polypeptide chains. *Proc. Natl. Acad. Sci. USA* **87,** 8555–8559 (1990).

6. Platanitis, E. *et al.* A molecular switch from STAT2-IRF9 to ISGF3 underlies interferon-induced gene transcription. *Nat. Commun.* **10,** 2921 (2019).

7. Brierley, M. M. & Fish, E. N. Stats: multifaceted regulators of transcription. *J. Interferon Cytokine Res.* **25,** 733–744 (2005).

8. Ashour, J. *et al*. NS5 of dengue virus mediates STAT2 binding and degradation. *J. Virol.* **83,** 5408–5418 (2009).

9. Grant, A. *et al.* Zika virus targets human STAT2 to inhibit type I interferon signaling. *Cell Host Microbe* **19,** 882–890 (2016).

10. Morrison, J. *et al.* Dengue virus co-opts UBR4 to degrade STAT2 and antagonize type I interferon signaling. *PLoS Pathog.* **9,** e1003265 (2013).

11. Davidson, A. D. Chapter 2. New insights into flavivirus nonstructural protein 5. *Adv. Virus Res.* **74,** 41–101 (2009).

12. Chaudhary, V. *et al.* Selective activation of type II interferon signaling by Zika virus NS5 protein. *J. Virol.* **91,** (2017).

13. Kumar, A. *et al.* Zika virus inhibits type-I interferon production and downstream signaling. *EMBO Rep.* **17,** 1766–1775 (2016).

14. Speer, S. D. *et al.* ISG15 deficiency and increased viral resistance in humans but not mice. *Nat. Commun.* **7,** 11496 (2016).

15. Xia, H. *et al.* An evolutionary NS1 mutation enhances Zika virus evasion of host interferon induction. *Nat. Commun.* **9,** 414–13 (2018).

16. Hertzog, J. *et al.* Infection with a Brazilian isolate of Zika virus generates RIG-I stimulatory RNA and the viral NS5 protein blocks type I IFN induction and signaling. *Eur. J. Immunol.* **48,** 1120–1136 (2018).

17. Lin, S. *et al.* Zika virus NS5 protein antagonizes type I interferon production via blocking TBK1 activation. *Virology* **527,** 180–187 (2019).

18. Zhao, Z. *et al.* Nuclear localization of Zika virus NS5 contributes to suppression of type I interferon production and response. *J. Gen. Virol.*10.1099/jgv.0.001376. DOI:10.1099/jgv.0.001376 (2019).

19. Lundberg, R. *et al.* Zika virus non-structural protein NS5 inhibits the RIG-I pathway and interferon lambda 1 promoter activation by targeting IKK epsilon. *Viruses* **11,** (2019).

20. Li, A. *et al.* NS5 conservative site is required for Zika virus to restrict the RIG-I signaling. *Front. Immunol.* **11,** 51 (2020).

21. Schwarz, M. C. *et al.* Rescue of the 1947 Zika virus prototype strain with a cytomegalovirus promoter-driven cDNA clone. *mSphere* **1,** (2016).

22. Emeny, J. M. & Morgan, M. J. Regulation of the interferon system: evidence that Vero cells have a genetic defect in interferon production. *J. Gen. Virol.* **43,** 247–252 (1979).

23. Ferrero, D. S. *et al.* Supramolecular arrangement of the full-length Zika virus NS5. *PLoS Pathog.* **15,** e1007656–26 (2019).

Appendix A

Supplementary Figures 1-3, Supplementary Table 1

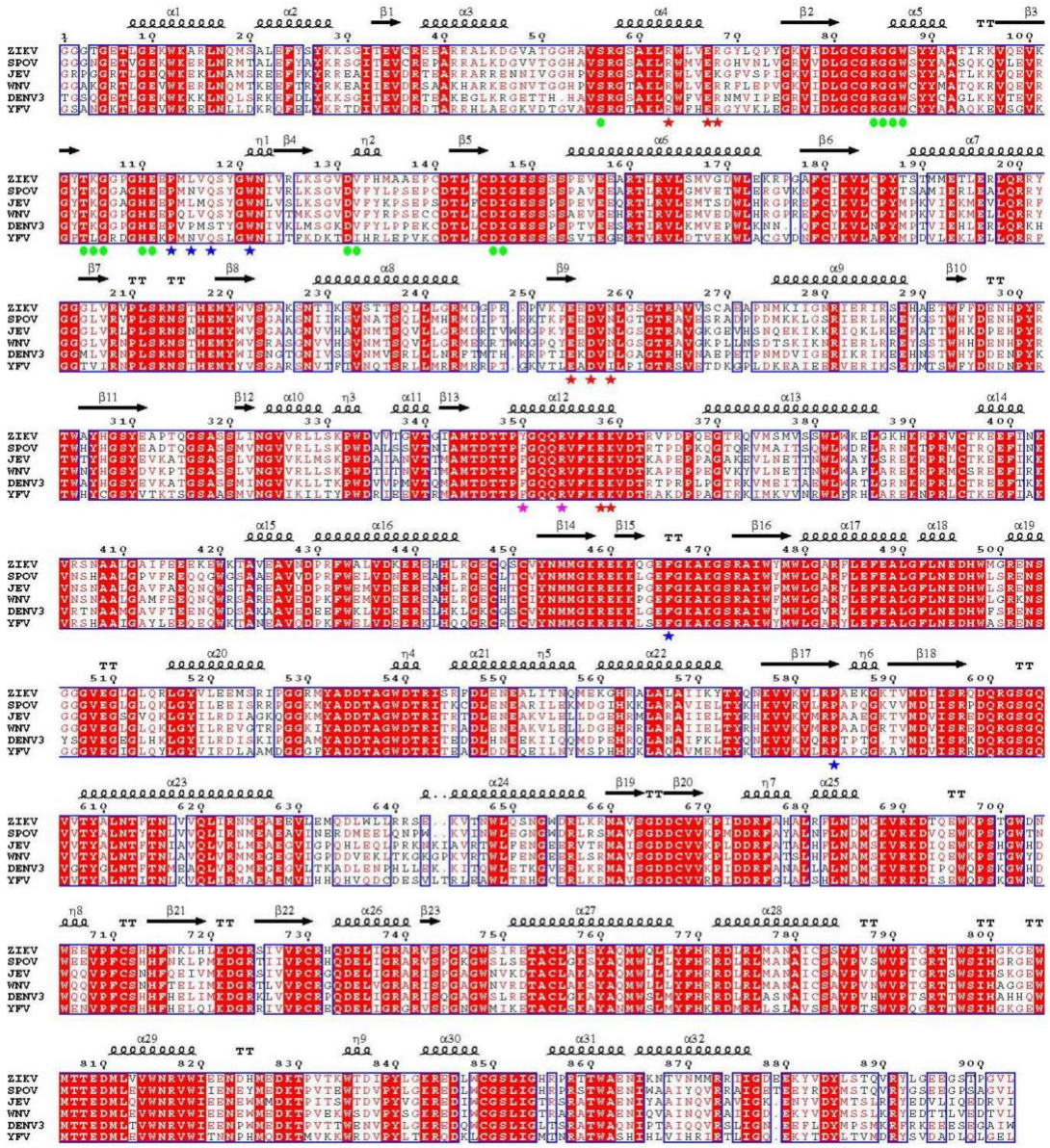

Supplementary Figure 1. **Structure-based sequence alignment of selected flavivirus NS5 proteins**. Identical or similar residues are colored in red. Completely conserved residues are colored in white and highlighted in red. Secondary structure elements are shown above the aligned sequences. Below the aligned sequences: the residues mediating SAH binding, interdomain contact of ZIKV/JEV NS5, and interdomain contact of DENV3 NS5 are marked by green spheres, blue asterisks and red asterisks, respectively. Note that the residues corresponding to Y350 and R354 of ZIKV NS5 (magenta asterisks) are involved in the domain interactions of both ZIKV/JEV NS5 and DENV3 NS5.

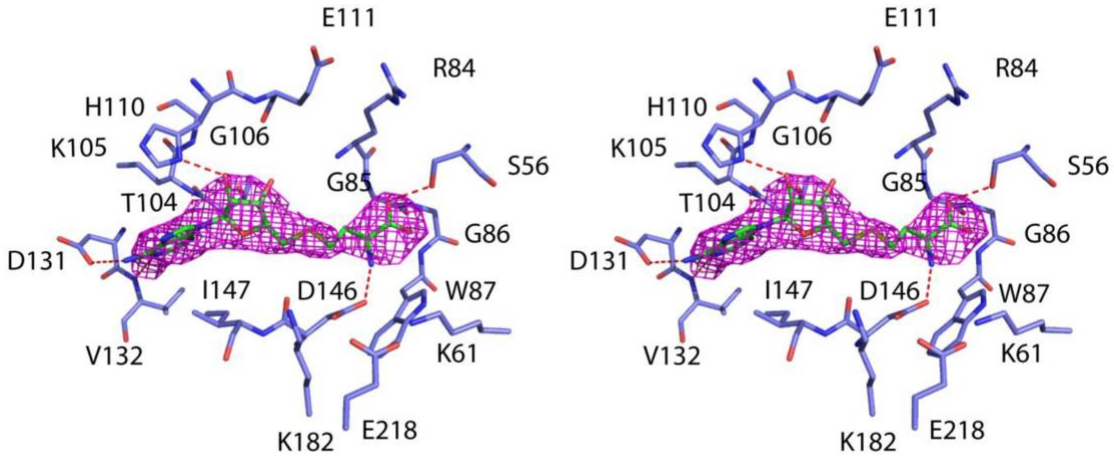

Supplementary Figure 2. **Stereo view of SAH binding.** FO-FC omit map of SAH is colored in magenta and contoured at 3σ level. ZIKV NS5 residues and the bound SAH molecule are shown in blue and green sticks, respectively. The hydrogen bonding interactions are depicted as dashed lines. The catalytic tetrad (K61-D146-K182-E217) is in close proximity with the SAH molecule.

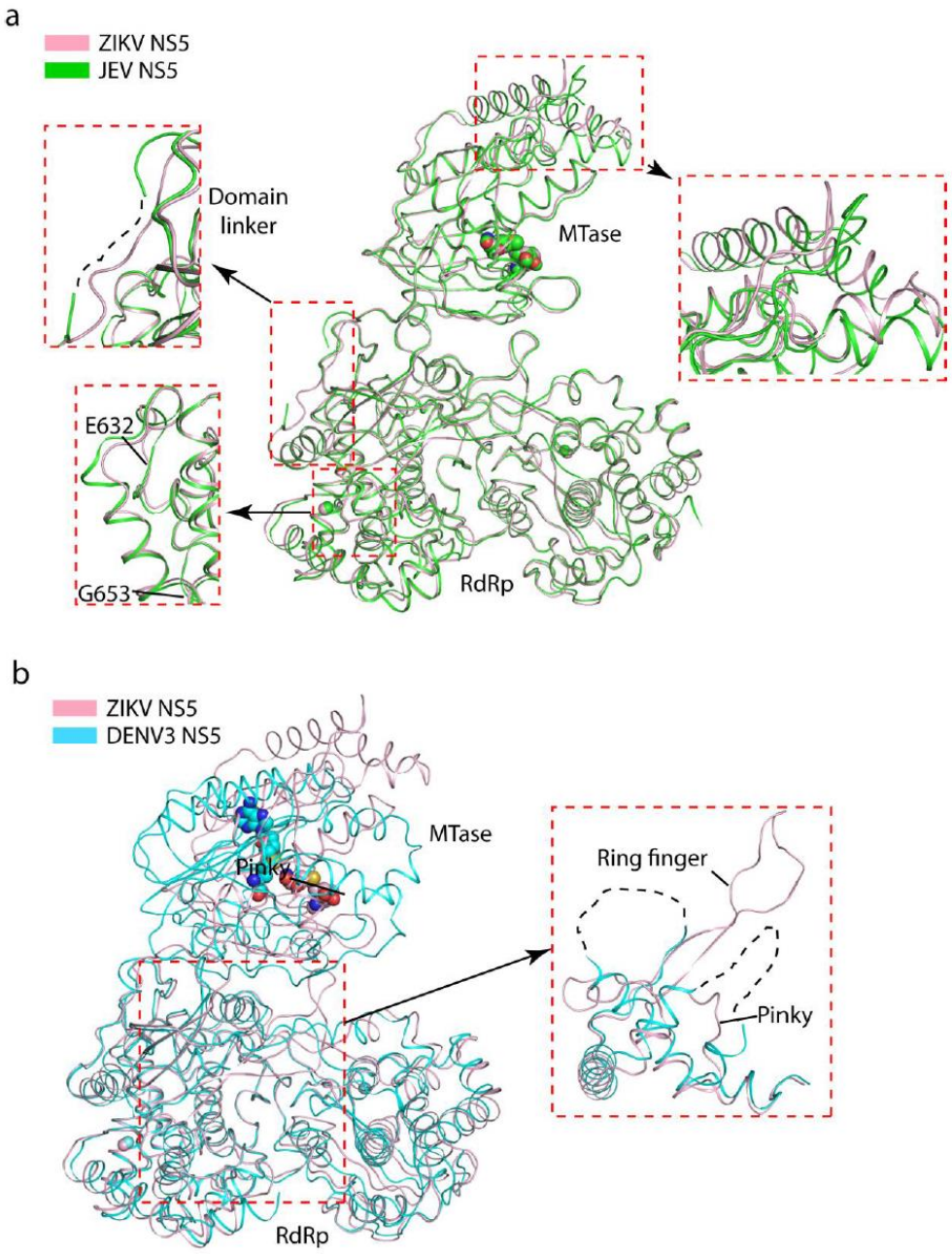

Supplementary Figure 3. **Structural comparison ZIKV NS5 with JEV NS5 and DENV3 NS5.** a) Structural alignment of ZIKV NS5 and JEV NS5 (PDB 4K6M), with structural divergent regions shown in expanded view. b) Structural alignment of ZIKV NS5 and DENV3 NS5 (PDB 4V0Q), with structural divergent regions shown in expanded view. The disordered loops in (a) and (b) are shown as dashed lines.

Primers	Primer sequences (5'->3')	Description
		Generation of protein expression plasmids
1	ACAGATTGGTGGATCCGGAG GTGGGACGGGAGAG	Forward primer for cloning of ZIKV NS5 into pRSF Duet-1 vector
2	CTTTACCAGACTCGAGTTACA ACACTCCGGGTGTGGAC	Reverse primer for cloning of ZIKV NS5 into pRSF Duet-1 vector
3	ACAGATTGGTGGATCCAGGA AGAGACTCCTGTTGAGTGC	Forward primer for cloning of ZIKV NS3 helicase into pRSF Duet-1 vector
4	CTTTACCAGACTCGAGTTATC TTTTCCCAGCGGCAAAC	Reverse primer for cloning of ZIKV NS3 helicase into pRSF Duet-1 vector
		Generation of subgenomic ZIKV RNA template. The subgenomic ZIKV RNA template contains two regions: The 5'- region is comprised of T7 promoter fused to ZIKV genome sequence 1-171, and the 3'-region is comprised of ZIKV genome sequence 10343-10787. These two sequences were first generated separately, followed by ligation into one ZIKV RNA template sequence.
5	TAATACGACTCACTATAGGGA GTTGTTGATCTGTGTGA	Forward primer for ZIKV RNA template 5'-region
6	GGTGCTTACAACACTCCGGG TTACACGGGCTACTCCGCG	Reverse primer for ZIKV RNA template 5'-region
7	CGCGGAGTAGCCCGTGTAAC CCGGAGTGTTGTAAGCACC	Forward primer for ZIKV RNA template 3'-region
8	TCTTGAGAATTCAGAAACCAT GGATTTCCCC	Reverse primer for ZIKV RNA template 3'-region

Supplementary Table 1. Primer list for protein expression plasmids and ZIKV RNA template.

Appendix B

Supplementary Figures 4-11

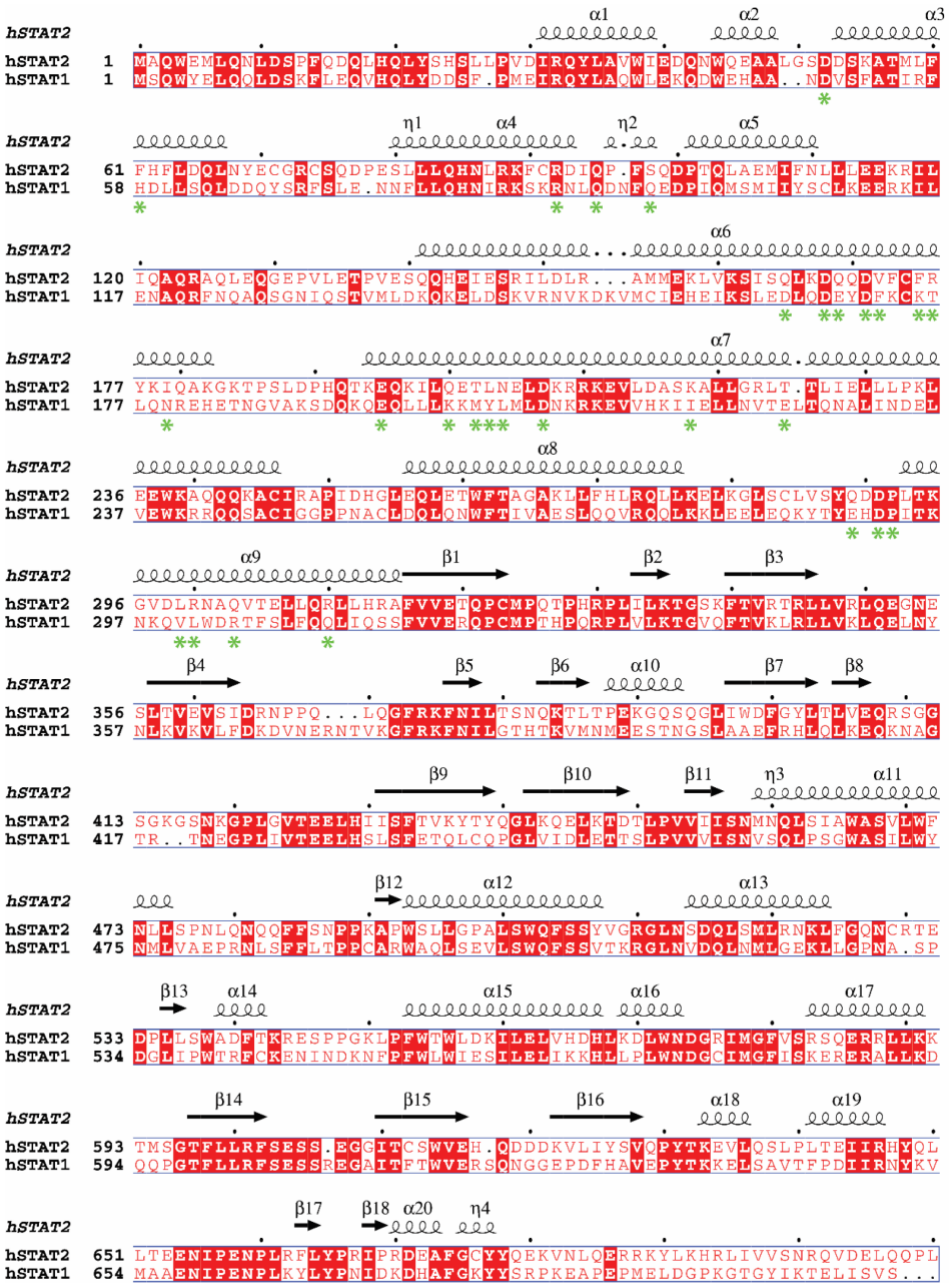

Supplementary Figure 4. Structure-based sequence alignment of hSTAT2 and hSTAT1. The aligned sequences encompass the ND and CF of hSTAT2 and hSTAT1, with the secondary structures of hSTAT2 indicated above. The ZIKV NS5-interacting residues of hSTAT2 are marked with green asterisks.

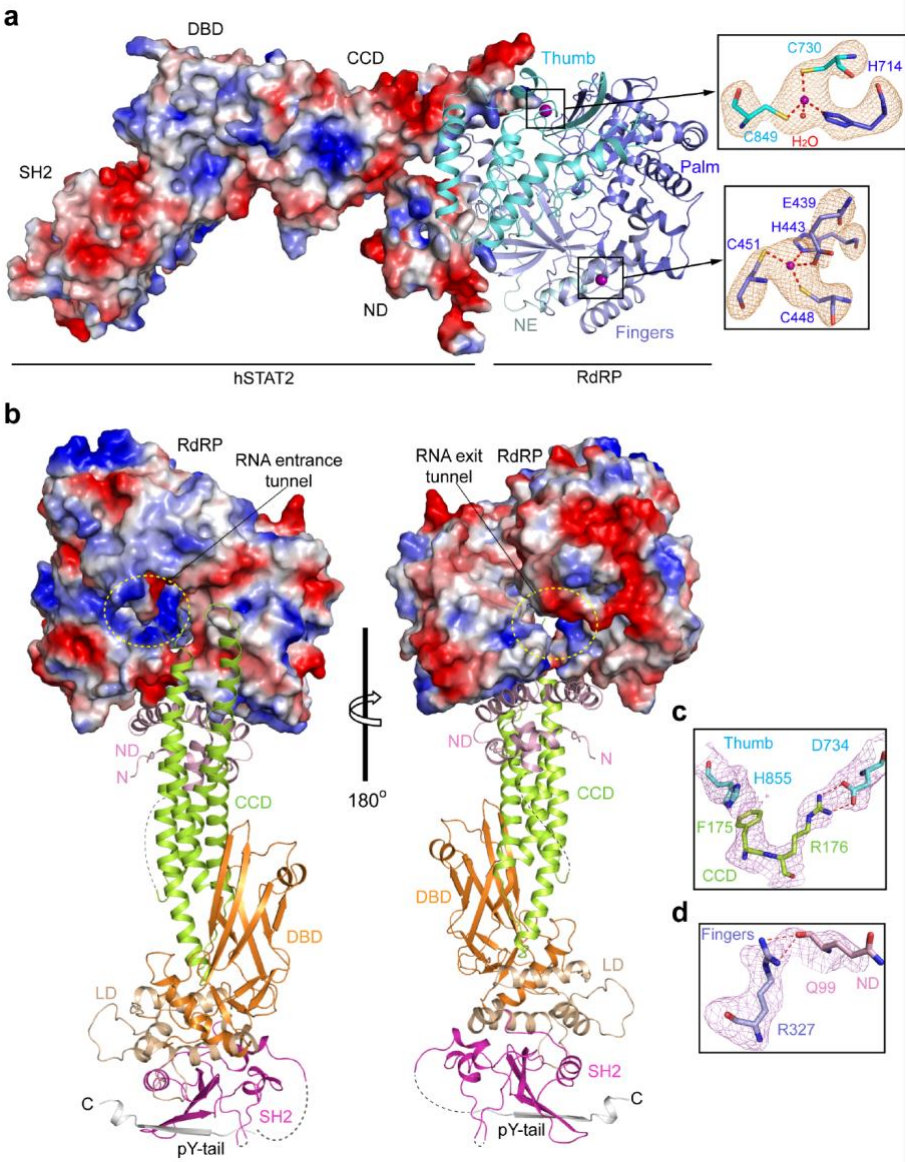

Supplementary Figure 5. Structural analysis of the RdRp domain of ZIKV NS5 in complex with hSTAT2$_{1-713}$. a) The structure of the NS5 RdRp-hSTAT2$_{1-713}$ complex, with hSTAT2$_{1-713}$ shown as electrostatic surface and RdRp shown as ribbon diagram. The two zinc clusters of NS5 RdRp are shown in expanded views, surrounded with Fo-Fc omit map (orange) contoured at 2.0 σ level. b) Two opposite views of the structure of the NS5 RdRp- hSTAT2$_{1-713}$ complex, with hSTAT2$_{1-713}$ shown as ribbon diagram and RdRp shown as electrostatic surface. The RNA entrance and exit tunnels of NS5 RdRp are marked with dashed circles (yellow). The disordered linkers of hSTAT2$_{1-713}$ are depicted as dashed lines. N- and C-termini are indicated by letters 'N' and 'C'. c,d) Fo-Fc omit maps (violet) of selected residues for intermolecular interactions at the RdRp-CCD (c) and RdRp-ND (d) interfaces, contoured at 2.0 σ level. The color schemes for the RdRp and hSTAT2 are the same as that in Figure 8.

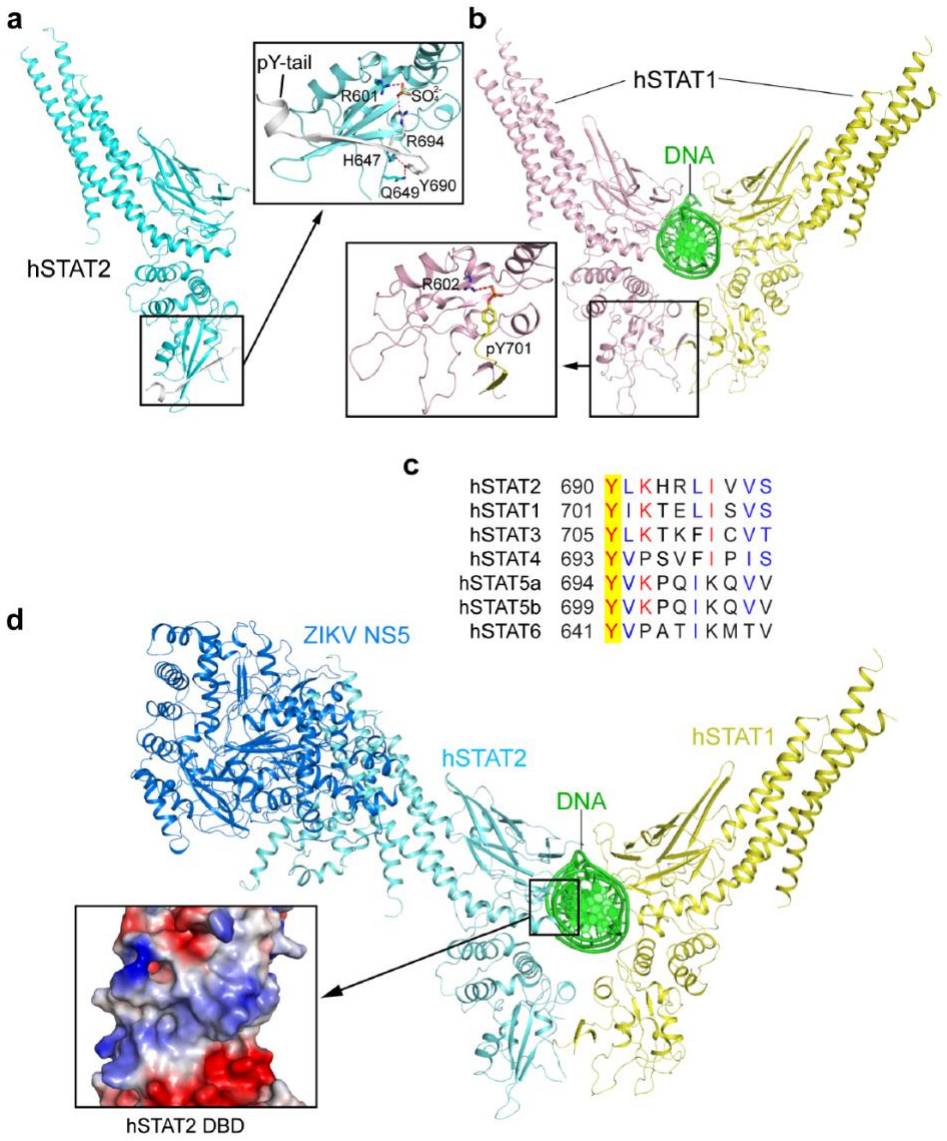

Supplementary Figure 6. Structural comparison of hSTAT2 and hSTAT1. a) Ribbon representations of the CF of hSTAT2 (cyan) in association with its pYtail segment (grey). The intramolecular interaction between the SH2 domain and the unphosphorylated pY-tail segment of hSTAT2 is highlighted in the expanded view. The hydrogen bonds are depicted as dashed lines. b) Ribbon representation of homodimeric hSTAT1 in complex with DNA, with the intermolecular interaction between the hSTAT1 SH2 domain (light pink) and the phosphorylated pY-tail segment from the other monomer (yellow) of the hSTAT1 homodimer shown in the expanded view. c) Sequence alignment of the pY-tail segments of human STAT proteins. Identical and similar residues are marked in red and blue, respectively. The target tyrosine is shaded in yellow. d) Structural model of the ZIKV NS5–hSTAT2–hSTAT1–DNA complex, with the surface electrostatic view of the hSTAT2 DBD shown in the expanded view.

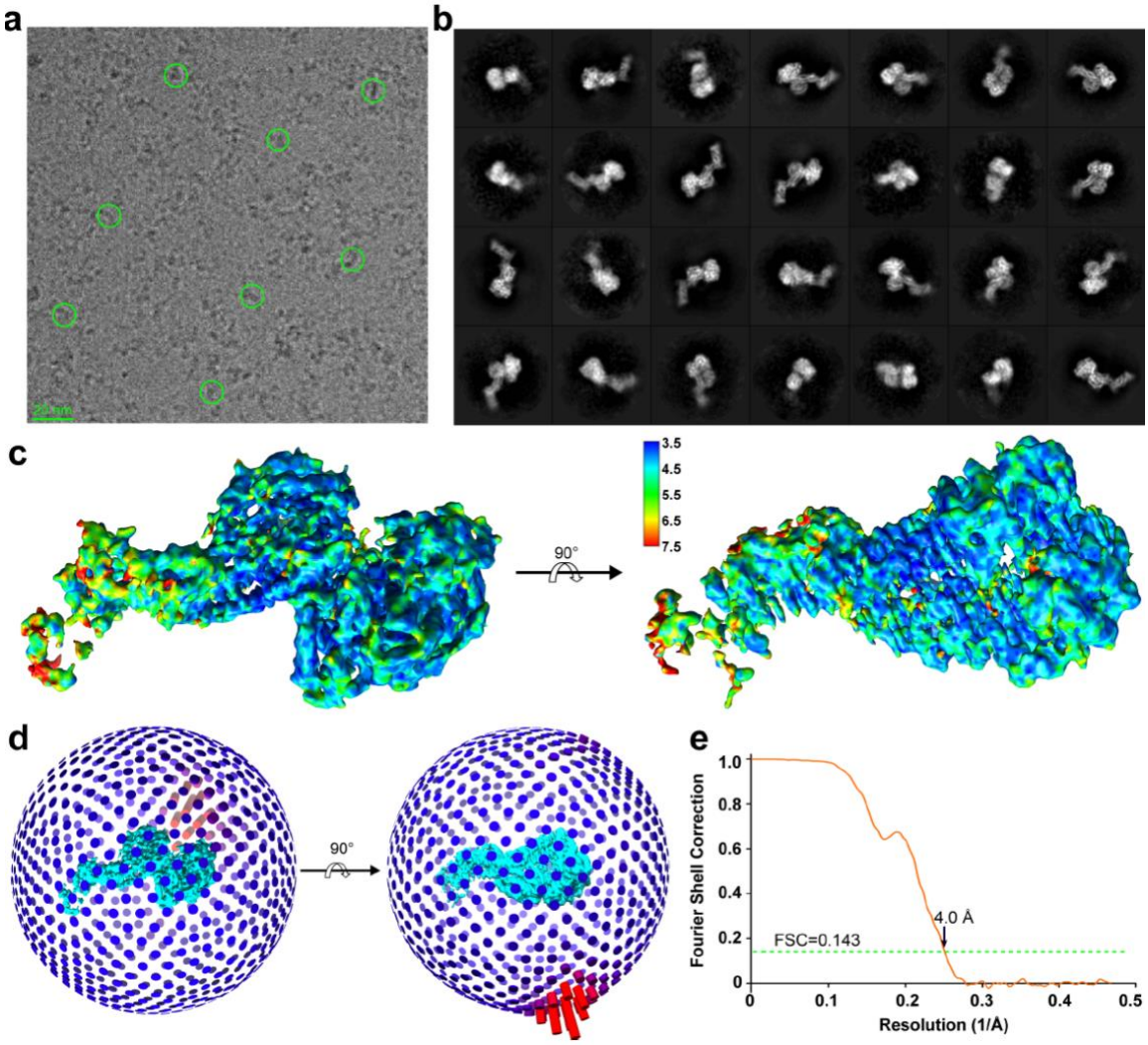

Supplementary Figure 7. Cryo-EM analysis of the ZIKV NS5–hSTAT2 complex. a) A representative cryo-EM micrograph with select particles circled. b) 2D class averages used to generate the model. c) Local resolution evaluation of the reconstructed map by Resmap. d,e) Angular distribution (d) and global resolution evaluation based on "goldstandard" Fourier shell correction (FSC) (e), both generated by RELION.

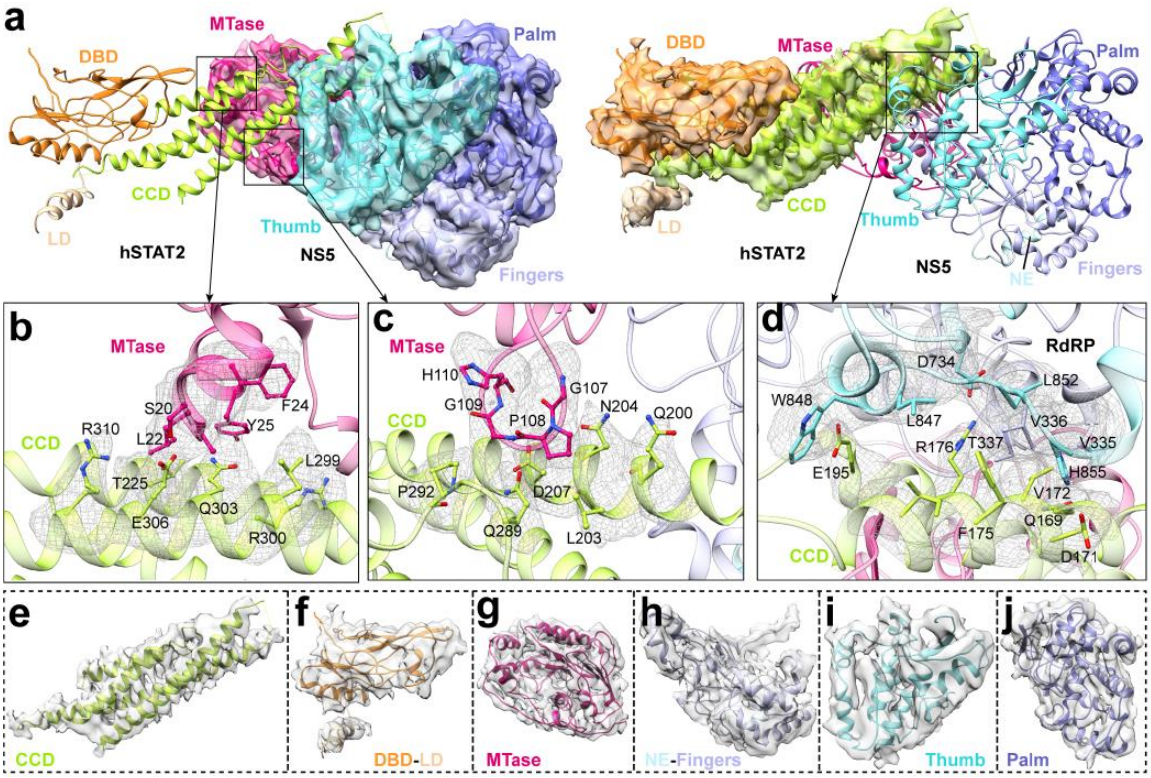

Supplementary Figure 8. Details of the cryo-EM densities overlaid with their atomic models (ribbon) of the domains in ZIKV NS5–hSTAT2 complex. a) Ribbon representations of the atomic model of NS5–hSTAT2, with NS5 (left) and hSTAT2 (right) overlaid with their respective density maps. b,c) Details for the MTase–CCD interaction, with densities of interacting residues shown as mesh. d) Details for the RdRp–CCD interaction, with densities of interacting residues shown as mesh. e,f) CCD, DBD and LD domains in hSTAT2. g-j) MTase, NE and fingers, thumb, and palm domains in NS5.

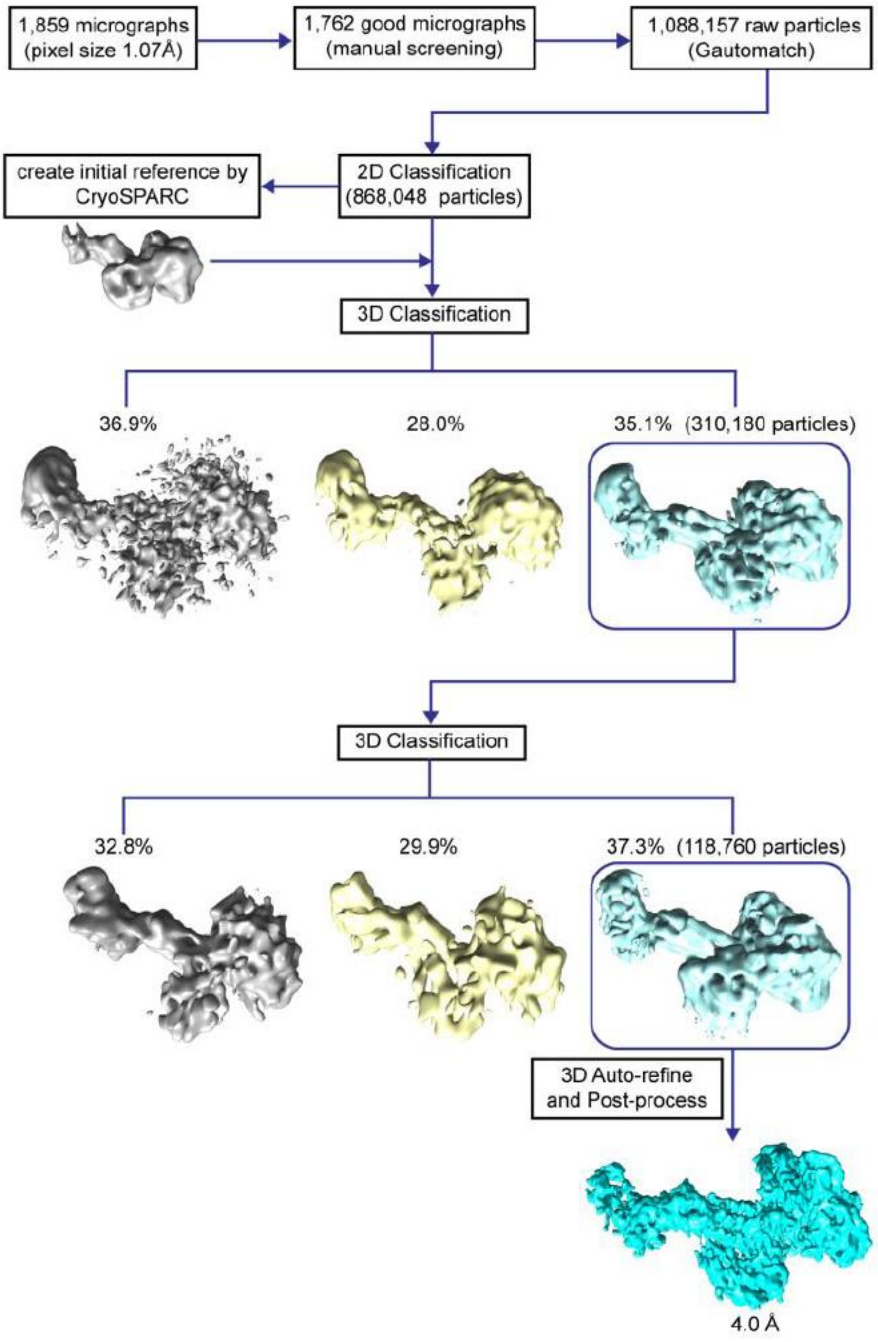

Supplementary Figure 9. Data processing workflow used for cryo-EM reconstruction of the ZIKV NS5 - hSTAT2 complex. Note that 2x2 binning of original movies during motion correction yielded a pixel size of 1.07 Å.

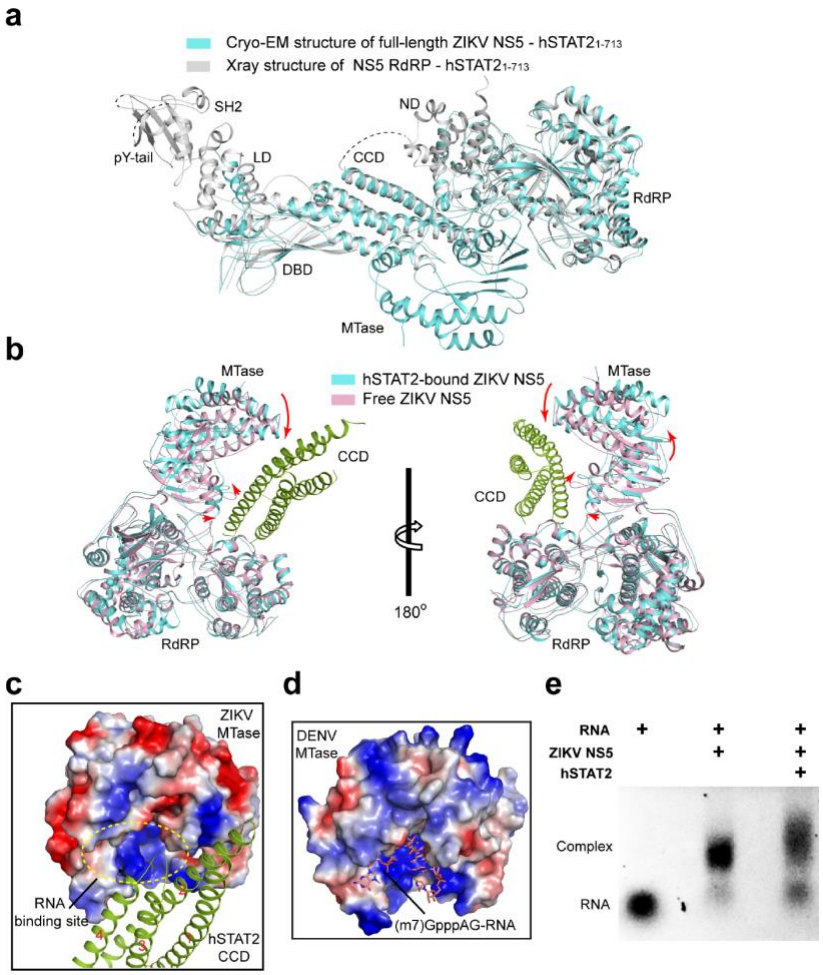

Supplementary Figure 10. Structural analysis of the ZIKV NS5–hSTAT2 interaction. a) Superposition of the crystal structure of NS5 RdRp–hSTAT2$_{1-713}$ (grey) and the cryo-EM structure of full-length NS5–hSTAT2$_{1-713}$ (cyan). While the cryo-EM structure contains the MTase domain, there is no change in the relative orientations of different domains between the two structures. b) Structural superposition of free (PDB 5TMH) and hSTAT2-bound ZIKV NS5. The conformational transition of the MTase domain of ZIKV NS5 from free state to the hSTAT2-bound state is indicated by arrows. For clarity, all the hSTAT2 domains, except for the CCD, were removed. c) Surface view of the MTase domain of ZIKV NS5 bound to hSTAT2 CCD (green ribbon). The four helices of the CCD are sequentially numbered from '1' to '4'. The potential RNA binding site is indicated by dashed circle. d) Surface of the DENV-3 MTase bound to viral cap-0 RNA (PDB 5DTO). e) hSTAT2 inhibition of ZIKV NS5–RNA binding assayed by electrophoretic mobility shift. Addition of NS5 to a cap-1 (m7GpppG2′OMe) yeast mRNA (YLR164W, 749 nt) resulted in a shift of the RNA band. Further addition of STAT2 resulted in release of RNA from the NS5–RNA complex, with concomitant accumulation of free RNA.

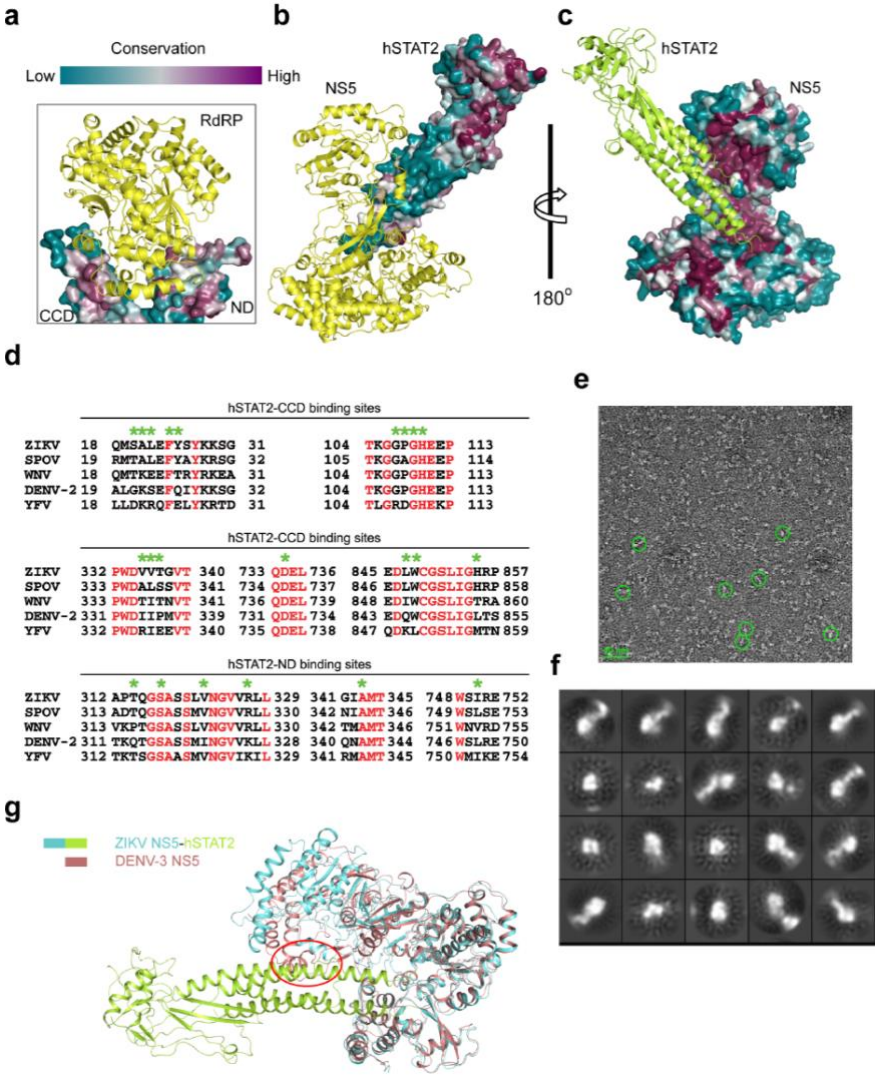

Supplementary Figure 11. Sequence and structural analyses of the DENV NS5-hSTAT2 interaction. a-c) Sequence conservation analysis of the ZIKV NS5–hSTAT2 interaction using the ConSurf server (https://consurf.tau.ac.il/). The sequence conservation of hSTAT2 and ZIKV NS5 residues are color-coded and mapped onto the crystal structure of ZIKV RdRp–hSTAT2 (a) and cyro-EM structure of ZIKV NS5–hSTAT2 (b,c). d) Sequence alignment of the NS5 proteins from members of the *Flaviviridae* family, with the identical residues colored in red and the hSTAT2-binding sites of ZIKV NS5 marked by green asterisks. e) Representative negative-stain EM image of DENV NS5-hSTAT21-713. Bar: 40 nm. f) Characteristic 2D class averages with CTF correction. g) Structural overlay of DENV-3 NS5 and hSTAT2-bound ZIKV NS5. The potential steric clash between the "closed" conformation of DENV-3 NS5 (PDB 4V0Q) and hSTAT2 is marked by a red circle.